Biomechanical assessment of extracellular matrix in native and tissue engineered cartilage across length scales

Inauguraldissertation

zur

Erlangen der Würde eines Doktors der Philosophie

vorgelegt der

Philosophisch-Naturwissenschaftlichen Faklutät

der Universität Basel

von

Marko Loparic

Aus Gorican in Medimurje, Kroatien

Basel, 2012

Genehmigt von der Philosophisch-Naturwisenschaftlichen Fakultät

auf Antrag von

Herrn Prof. Ueli Aebi, Herrn Prof. Ivan Martin,

Herrn Prof. Dr. med. Niklaus F. Friederich

Basel, den 22. Juni 2010   Prof. Dr. Eberhard Parlow

Dekan der Philosophisch Naturwissen-

Schaftlichen Fakultät

*This thesis is dedicated
to my wife Marija and my daughter Jana
for their unfailing love and support*

Table of contents

Chapter 7: Conclusions and Perspectives

Chapter 8: Acknowledgments

Chapter 9: Curriculum vitae

On the cover: Artistic view by Verena Grieder (Photolab, Biozentrum, University of Basel, Basel, Switzerland) and Martin Stolz (nCATS (National Centre for Advanced Tribology at Southampton, University of Southampton, Southampton, UK)) of collagen meshworks as can be found in diverse parts of the body. Collagen from tendon and various types of cartilage were imaged at different magnifications by atomic force microscopy. The image in the middle shows two cartilage cells (chondrocytes) that are expressing the surrounding extracellular matrix. Closer view demonstrates the typical 67 nm D-periodicity of cartilage collagen fibrils. Cartoon of the skeleton by permission, copyright of Medical Multimedia Group, Missoula, MT. See chapter 2 for more details.

Chapter 1

Introduction

Musculoskeletal diseases (MSD) and related disorders account for the largest fraction of temporary and permanent disabilities, and are often considered to be an inevitable consequence of aging. In developed countries, these diseases are responsible for more than half of all chronic conditions suffered by people over the age of 50. In particular, osteoarthritis (OA) is among the leading causes of chronic MSD and the most common joint disorder in the EU. To maintain a normal active lifestyle for patients suffering from OA, the associated costs and the need for effective treatments are very high. For example, more than 45 million people in the US currently have osteoarthritis and it is also the most common joint disorder in EU societies. To date, there is no optimal diagnostic procedure and no permanent cure. OA is usually detected at the level where treatment options are very limited. Thus, the management of OA largely relies on controlling the pain and symptoms through medical therapy that involves medication and rehabilitation exercises. However, if such treatments are inadequate, surgical procedures are necessary e.g. osteotomy or joint replacement to relieve pain and increase joint functions in patients with OA. One promising option involves the implantation of functional cartilage grafts. These are engineered using autologous cells harvested from a small cartilage biopsy and cultured into porous biodegradable scaffolds. Nevertheless, tissue engineered cartilage (TEC) is not used in routine clinical practice because of the variability of the tissue properties (e.g. using cells from different donors) and lack of reliable quality controls. The above mentioned issues generally stem from a limited mechanistic understanding of cartilage function. This has been driving impetus of this work to seek deeper fundamental insight into the functional properties of cartilage and the development of OA. By integrating state-of-the-art technologies, the overarching objective of this MD-PhD is to obtain a biomechanical assessment of the extracellular matrix in native and TEC spanning from the molecular length scale to the tissue level.

1.1 Articular Cartilage Structure and Composition

Hyaline articular cartilage (AC) is a 1-3mm thick connective tissue covering the end of the long bones in diarthrodial joints. In general, cartilage is a complex structure composed from fluid and a solid phase. The fluid phase, which is composed of water and electrolytes as the most prevalent components, accounts for 60-80% of the cartilage structure measured by wet weight. The solid phase is extracellular matrix that consists primarily of collagen II fibrils (~15-20% by wet weight), proteoglycans (PG) (~10% by wet weight) and chondrocytes (1-

5%). The arrangement and distribution of these components across/within the cartilage depth is not uniform. Depending on the specific pattern of collagen orientation and amount of collagen, PG and water, cartilage can be divided into four zones: superficial, intermediate, radiate and calcified. The superficial zone which accounts for 20% of the full cartilage thickness is characterized by a high concentration of densely packed collagen fibrils that are oriented parallel to the joint surface, flattened chondrocytes (Figure 1.1) and relatively low amounts of PG. Therefore, the superficial zone exhibits the highest tensile and shear strength of the cartilage. The direct contact of the superficial zone with the synovial fluid has a significant impact on cartilage function and maintenance. Deterioration of the superficial zone considerably alters cartilage mechanical properties which may result in the development of osteoarthritis (OA). This zone has a unique function in filtering large proinflammatory macromolecules present in the synovial fluid, thus protecting the cartilage from immune reactions [1]. The intermediate zone (40-60% of cartilage thickness) has the highest amount of PG, randomly orientated collagen fibrils and round chondrocytes, while in the radiate zone (20-30% of cartilage thickness) collagen fibrils are oriented perpendicular to the underlying bone. Finally, the calcified zone is partially mineralized and acts as transition between cartilage and subchondral bone [2, 3]. The distribution of the fluid phase depends mainly on the PG concentration which determines the swelling pressure and collagen network strength and organization. In this manner, specific and complex architecture of articular cartilage ensures its durability and optimal function over long period of time and activity.

1.1.1 Collagen

Cartilage consists of specific sets of collagen such as collagen II, collagen IX and collagen XI [4]. The most prevalent is collagen type II which accounts for 90-95% of collagen in cartilage [5]. The highest concentrations of collagen IX and collagen XI are associated with thin collagen II. There is evidence that collagen XI acts as a template to constrain the lateral growth of collagen II fibrils [6] and therefore plays a role in regulating the collagen fibril diameter. Collagen IX decorates the surface of collagen II and plays a role in the covalent binding between collagen II fibrils, collagen IX and PGs. Both collagen IX and XI contribute significantly to the compressive properties and long term stability of articular cartilage [7]. Collagen type II, together with collagen type XI are designated as fibril-forming collagens. Synthesis of collagen II fibers originates in chondrocytes from collagen precursor procollagen, which is a homotrimeric molecule composed of three distinct domains: a N-teminal propeptide, a central triple-helical collagenous domain and a C-terminal propeptide.
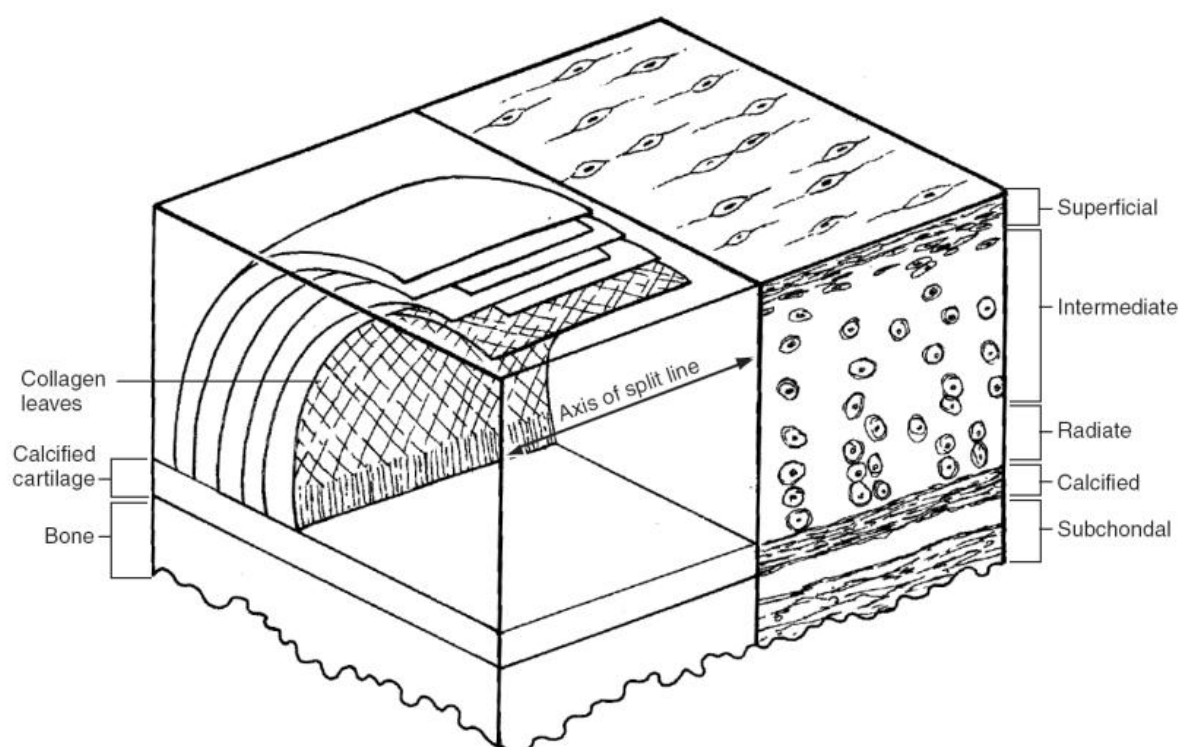
Figure 1.1: Cross section cut through the cartilage thickness. The foreground illustrates orientation of collagen fibrils "leaves" across the thickness. The background shows four distinct zones through the depth of cartilage, From Mansou, 2003.

During the later phase of collagen maturation, procollagen matrix metalloproteinases cleave N- and C-terminal propeptide of procollagen (Figure 1.2) which results in the formation of 280nm long and 1.3nm in diameter, rod-like structure known as tropocollagen. Each tropocollagen molecule is stabilized through intra and intermolecular crosslinking. However, these bonds are at this stage immature and weak.

In the process of fibrillogenesis, tropocollagen sub-units arrange into a staggered array of structures with distinct 67nm banded axial repeat as observed by the electron microscope [8] through lateral and longitudinal interactions At this stage of fibrillogenesis, collagen microfibrils of up to approx. 50nm of diameter are formed. Finally, in the slow process of cross-linkage, collagen fibrils assemble into the collagen fibers which exhibit large diameter (up to 500nm) and increased tensile strength. An important role of collagen XI, collagen IX, decorin and other factors in collagen II fibrillogenesis has been reported [9, 10]. However, an alignment, undulation and twist which are present at a suprafibrillar level of *in vivo* collagen II fibrillogenesis is still not possible to engineer *in vitro* since the underlying complex mechanisms are not yet well understood.

11
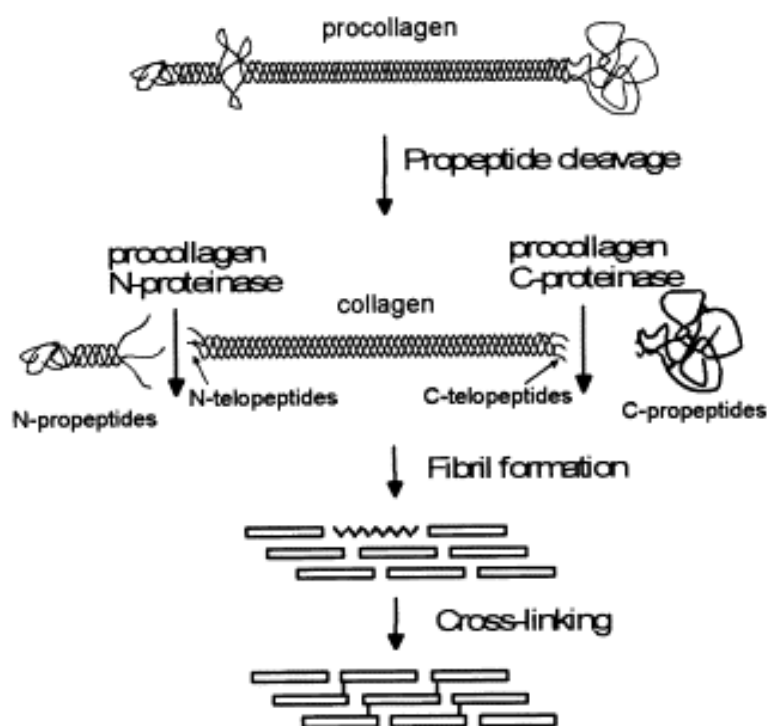
Figure 1.2: Collagen fibrillogenesis. From Holmes, 2001

For this reason, tissue engineered cartilage grafts primarily contains an immature form of collagen II, usually at the stage of microfibrils (Loparic et at. *unpublished*).

Interestingly, the diameter of collagen fibers significantly increases from superficial zone towards the radial zone of cartilage. From an engineering point of view, a firm collagen network exhibits high tensile and shear strength but poor compression resistance properties [11, 12]. It functions as a natural scaffold in the cartilage where it regulates the shape and the bulk mechanical properties of cartilage. Chondrocytes are cells responsible for maintaining of the collagen meshwork. It is important to note, that once skeletal growth ceases, collagen is synthesised at a very low rate (e.g. estimated turnover time is 400 years for human femoral head cartilage) [13]. This has a *tremendous* impact on the healing capacity of the cartilage in the case of a degenerative disease or injury. Moreover, quantitative and qualitative changes in the collagen occur with age due to the higher crosslinking by advanced glycation end products and formation of the stabilized form of collagen [14, 15]. These changes result in increased mechanical strength, brittleness, denaturing temperature and higher conversion of soluble to insoluble forms of collagen which make the cartilage more prone to develop osteoarthritis (OA) [16]. In the early phase of OA the collagen network is not significantly affected as the PGs whilst with further development of OA, concentration of collagen

degrading enzymes (e.g. matrix metalloproteinase - MMP or collagenase) is increased, particularly MMP-1 and MMP-13. These enzymes start to extensively disrupt collagen molecules and overall meshwork and this is considered as the beginning of advanced or irreversible phase of OA. Then the healing capacity of cartilage as well as medical treatment is very limited. Altered mechanical properties of collagen tremendously affect the cartilage shape, integrity and function. Numerous techniques have been employed to measure the mechanical properties of macroscopic collagen fibers (e.g. diameter of few hundred of nm) [17-19] and tropocollagen molecules (diameter approx 1.33nm) [20, 21]. However, the mechanical properties of both microfibrilar and fibrilar collagen (e.g. diameter from 20 nm to over 100 nm) are beyond the scope of these techniques. The introduction of the Atomic Force Microscope (AFM) bridges this gap to assess the mechanical properties of collagen at microfibrilar, fibrilar but also fiber structural levels [22] Moreover, since microfibrilar collagen is produced in engineered cartilage, the AFM provides a better understanding of the collagen and TEC mechanics. In this way, AFM is also a valuable quality control tool.

1.1.2 Proteoglycans

The major structural component of PG is an aggrecan monomer. It has a bottle-brush architecture and consists of a core protein (CP) with many covalently bonded glycosaminoglycans (GAGs) side chains, predominantly chondroitin (CS) and keratane sulphate (KS) (Figure 1.3). Multiple aggrecan monomers are non-covalently bound to hyaluronic acid (hyaluronan) which form a concentrated space-filling gel that ensures aggrecan retention within the collagen network [23]. The binding between the aggrecan and hyaluronan is additionally stabilized by a link protein [24, 25].

PG concentration is not uniform across cartilage tissue and increases towards the cartilage bone interface. The low concentration of PG on the cartilage surface is more permeable to fluid flow which plays an important role in a cartilage compression resistance**.** One distinct property of the aggrecans is the high fixed negative charge density which originates from numerous anionic sulphate (SO_3^-) and carboxyl (COO^-) groups across GAG side chains. The fixed negative charges contribute to the polyelectrolytic character of the aggrecans where he charged state of anionic groups is regulated according to the pH and salt concentration of the surrounding solution. In high salt concentrations, the fixed negative charges are saturated with counter ions that reduce the repulsive electrostatic force between charged side chains and tend to a collapse of the whole aggrecan monomer (Figure 1.4.).
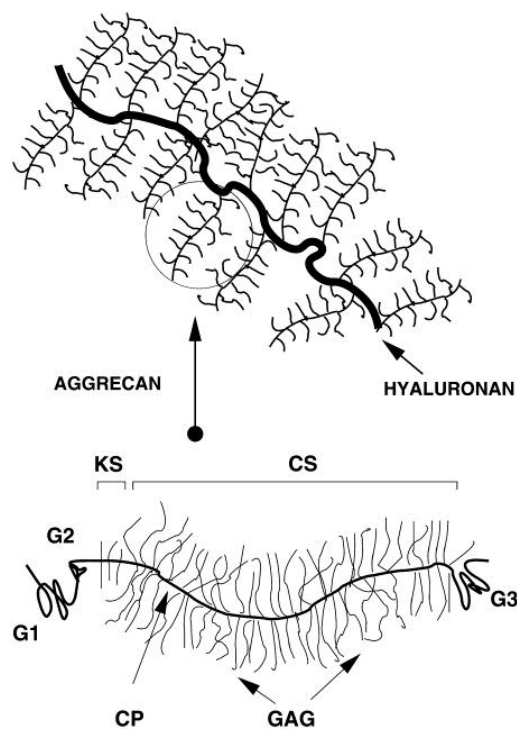
Figure 1.3: Scheme of aggrecan molecule and the proteoglycan aggregates of aggrecan and hyaluronic acid. CP: core protein, CS: chondroitin sulfate, and KS: keratan sulfate. The G1, G2, and G3 are globular domains. From Ng,. 2003

In contrast, in low salt concentrations most of the fixed negative charges are exposed and the repulsive forces between them drive the whole aggrecan monomer to become fully extended (Figure 1.4). Moreover, the fixed negative charges cause in the counter ions imbalance that finally results in the high osmotic pressure within the PG. The resulting swelling of the PG gel is counteracted by the firm collagen network that, together with the high concentration of aggrecan aggregates, is responsible for the low permeability of the ECM.
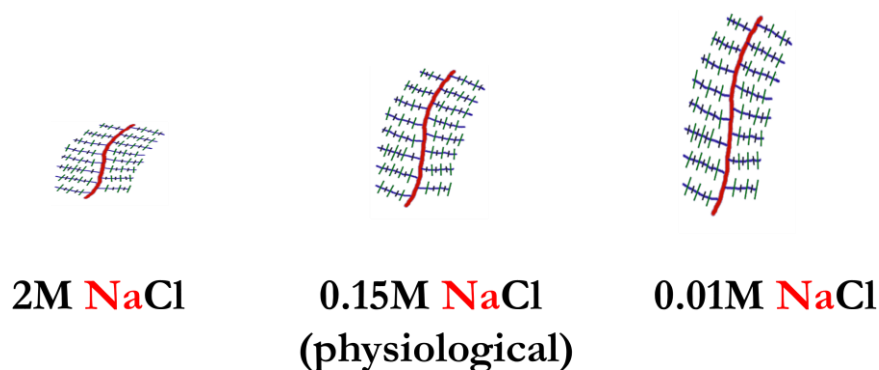
Figure 1.4: Influence of a buffer ionic strength on PGs morphology and mechanics

The resistance to fluid flow (friction drag), is a result of the low permeability which is a crucial component in dissipating energy from the loaded cartilage explained below.

Another class of PGs includes smaller molecules like decorin, biglycan and fibromodulin [26]. Aggrecan is synthesised and secreted by chondrocytes but at much higher rates compared to the collagen thus improving its healing capacity in case of injury or degenerative disease. However, a loss of cellularity of chondrocytes together with non-enzymatic age related modifications has a significant impact on the aggrecan performance in the mechanical function of cartilage [15].

During aging and degeneration PGs undergo significant alterations in composition and organization with respect to both core protein and aggrecan size, sulphate pattern modification and to the length of CS and KS side chains [27-29]. Two different mechanisms are involved in the age-related modifications of PGs. In the first, different glycosyltransferases and sulfotransferases are involved in modifications of GAG chains and are major factors in determining the size and composition of GAGs [30]. For example, significant changes during aging are found in the increase of 6-sulphated form of CS (C6S) in comparison to the 4-sulphated form (C4S). The ratio C6S to C4S dramatically raises from the stage of fetal, immature cartilage (<1) to the adult, mature cartilage (>20) [31]. Moreover, it was found that a disulphate form of the CS, chondrotitin-4,6-sulphate, plays an important role in chain length control by reducing its synthetic activity in chondrocytes [32]. KS chains are becoming longer and the CS shorter during lifetime what may be the results of an avascular nature of cartilage and consequently impaired oxidation of glucose to glucuronic acid needed for CS synthesis [33]. However, its effects on altering cartilage function are still under debate. A second key mechanism of the age related GAGs modification stems from the shortening of the aggrecan monomers due to the proteolytic cleavage at its both ends [34]. This process is modulated by chondrocytes and executed predominantly by ADAMTS-4/5 and MMP activity where after release, the specific fragments of the aggrecan monomers are accumulated. Moreover, those fragments are in competition with *de novo* synthesised intact aggrecan monomers, which has an impact on the overall aggrecan concentration. A relative slow turnover of the fragments prolongs the effect on the ordered assembly and stability of the aggrecan with aging. In case of injury an involvement of the different proinflammatory factors (e.g. IL-1β, TNF-α, TNF-β) enhance the proteolytic cleavage of aggrecan and tends to a dramatic deterioration of the aggrecans and the whole cartilage.

Interestingly, aggrecans are not as stable as the firm collagen network and are more easily affected by degenerative diseases. A degradation of aggrecans at the onset of the degenerative diseases results in a decrease of cartilage stiffness. This can be potentially used as a new biomarker in detecting the degeneration of cartilage. Nevertheless, a reduction of aggrecans and subsequently cartilage stiffness can be overshadowed by the higher stiffness of the surrounding collagen network. In this regard, the Atomic Force Microscopy represents a valuable tool with sufficiently high sensitivity, at the nanometer scale stiffness measurement, to determine the contribution of aggrecans, typically located in-between collagen fibers, to cartilage stiffness. Conventional methods such as histology, immunohistochemistry and western blot require more demanding preparation protocols and yet lack the sensitivity and/or specificity to discriminate between each component.

1.2 Cartilage function

AC forms a mechanically resilient tissue exhibiting remarkable load-bearing properties - it withstands compressive forces that can be several times the weight of the body without damage over several decades of life. In addition to its resistance to compression, a cartilage surface exhibits excellent tribology properties which together with synovial fluid promote the joint motion with minimal friction and wear [3].

1.2.1 Load-bearing properties of cartilage

The remarkable load-bearing properties of cartilage result from the poroviscoelastic nature of ECM which stores and dissipate energy. Cartilage is considered as a biphasic composite material composed from a solid matrix and an interstitial fluid phase. The main viscoelastic response of the cartilage comes from the friction drag which is occurs as the interstitial fluid phase is squeezed phase and flows through the low permeable solid phase (flow dependant viscoelasticity) [35]. Interestingly, under impact loads cartilage behaves as a single-phase, incompressible, elastic material where interstitial fluid comprising of water, electrolytes and nutrients can withstanding over 90% of the load support [36]. Another minor contribution originates from the intrinsic viscoelasticity of the solid matrix (flow independent viscoelasticity) [37] based on the formation and breaking of temporary bonds between solid phase molecules [38]. The porous solid phase is composed from the fibrilar collagen II network, highly negatively charged proteoglycan gel and the chondrocytes [39]. Aggrecans, major PGs in cartilage, are incorporated into a dense collagen meshwork. Large anionic GAG

side chains of aggrecans attract counter-ions (e.g. Na^+, Ca^+) which generates an extremely high osmotic pressure known as the Donnan effect [40]. Finally, the high osmotic pressure creates a large flow of water into the ECM of cartilage thus maintaining the cartilage hydration. The addition of water generates swelling and expansion of the aggrecans within the firm collagen network. An equilibrium state is achieved when the swelling force is insufficient for further stretching of the collagen network (Figure 1.3). This gives cartilage an excellent compression resistance property since loading "squeezes" aggrecans which increase the repulsive forces in-between fixed negative charges and places collagen network under further tension. A subsequential removal of the load leads to a redistribution of water and restitution of pre-load equilibrium state [41]. Thus, articular cartilage is a tough but compliant load-bearing tissue with mechanical characteristics that depend on the integrity of the collagen network and the concentration of embedded PGs.
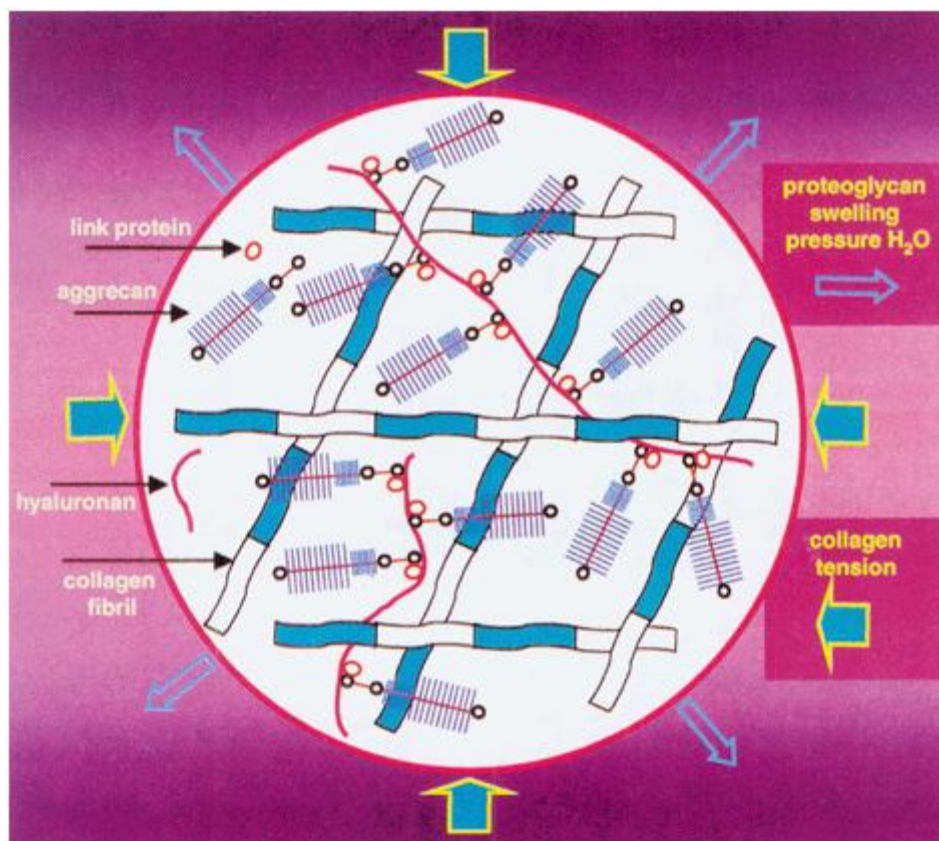

Figure 1.5: Compression resistance mechanism of the collagen/aggrecan network. From Mow, 1994

1.2.2   Frictionless Articulation

Various physiochemical mechanisms have been proposed to explain the superb lubrication and wear characteristics of cartilage. These include fluid-film lubrication[42], boundary lubrication [43, 44], mixed lubrication (e.g. weeping lubrication[45], boosted lubrication[46], and the interstitial fluid pressurization[47]). Fluid-film lubrication considers the presence of a thick layer of synovial fluid in between the opposing surfaces [48]. The fluid in this confined layer is pressurized by an applied load which prevents a direct contact of bearing surfaces so as to minimize friction and wear are minimized. However, this theory is in contradiction with experiments conducted by McCutchen [45, 49] who observed that the friction coefficient of the cartilage did not return to the initial value within one second after unloading as it is expected in the case of a fluid-film regime in a confined space. Therefore, McCutchen proposed the mechanism of mixed lubrication, more precisely weeping lubrication theory as a better explanation of cartilage lubrication mechanism. In the weeping lubrication theory, under the loading condition a pressurized interstitial fluid flows out into the space between opposing load bearing surfaces and forms a thick film of lubricant. A "weeping" of the interstitial fluid through the porous wall supplies enough liquid to maintain the film [49]. Interestingly, the opposing bearing surface layers within the joint create the contact over a 10% of the total area where a direct surface-to-surface friction occurs [50]. Thereby, a boundary lubrication regime is present here and it involves several molecules, such as hyaluronan [51] **,** PRG4 (i.e. lubricin, superficial zone protein, and megakaryocyte-stimulating factor) [52] and surface-active phospholipids [53]. These molecules are present in both the synovial fluid and on the cartilage surface in order to protect and maintain the cartilage surface. Moreover, a fluid film at the cartilage surface can contribute to bearing up the load [54]. Consequently, disturbances of the lubrication molecules clearly have a significant impact on both lubricative and load-bearing properties of the cartilage which could result in the onset of cartilage diseases, including osteoarthritis.
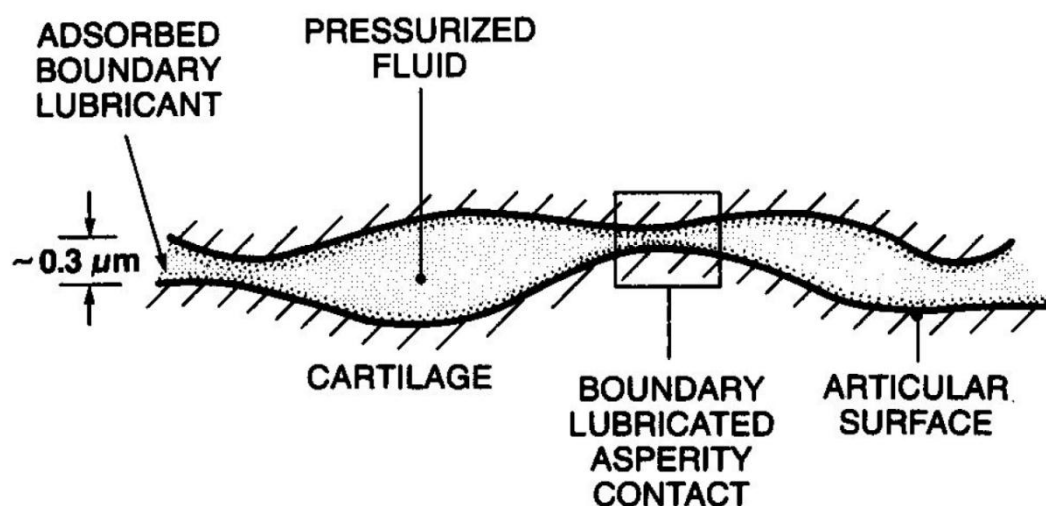
Figure 1.6: Concept of mixed lubrication regime. From Kelly, 1998

1.3 The Pathophysiology of Articular Cartilage

Cartilage is an avascular, aneural and alymphatic tissue [26]. An oxygen gradient from the synovial surface towards hypoxic deep zone (pO2 ~ 2–5%) [55] is present. Synovial fluid and subchondral capillaries provide the nutrition for the chondrocytes. The diffusion of interstitial fluid through the matrix during cyclic loading of the cartilage tissue supplies the nutritions and removes waste products from chondrocytes. Chondrocytes maintain ECM integrity in a low-turnover anabolic/catabolic state of equilibrium which is altered in case of aging and trauma in favour of catabolic activity responsible for cartilage degradation. The absence of blood vessels and small amount of chondrocytes (1-5%), whose number and metabolic activity declines with age [56, 57] can cause the limited healing capacity of cartilage in the event of injury or degenerative diseases. Moreover, once initiated, this damage tends to mark the onset of degenerative diseases such as OA, which is affecting 80% of the elderly population. In the advanced stage cartilage is thinned, and eventually completely worn out with bones rubbing directly against each other. Furthermore, OA is characterised by a subchondral bone sclerosis, formation of osteophytes and modification of the synovial fluid composition. The quality of life is significantly reduced due to the resulting pain, reduced mobility and working disability. Unfortunately, OA disables two to three times more workers than all other chronic conditions. Currently, there is a variety of treatments in clinical use for the repair and regeneration of chondral and osteochondral defects in the knee or hip joints (e.g. microfractures, autologous chondrocyte transplantation, biodegradable scaffolds) [58-60], but none of these is able to durably restore the complex hyaline structure and function of

native cartilage [61]. One of the reasons why TEC has not yet been introduced in the routine clinical practice is related to the variability of the tissue properties achieved using different protocols and the lack of reliable quality controls. Another major issue related to the onset of osteoarthritis is a lack of the early diagnostic tool which will be able to detect inception of the OA, at the level where treatment options are much more efficient than in a more advanced stage of the disease. Currently available diagnostic techniques (e.g. X-ray, MRI, arthroscopy, ultrasound) lack both the sensitivity and specificity for early detection of the OA. For development of early diagnostic methods and design of a functional engineered cartilage constructs it is essential to first understand the structure-function relationships of natural articular cartilage. Since cartilage mechanics is primarily determined at the molecular level, emerging field of cartilage nanomechanics is offering a great potential to revel new scientific information about the cartilage tissue mechanics and in particularly the structure-function relationship. The origin of cartilage nanomechanical properties can be traced to the molecular scale, thus providing the link between OA and the molecular origins of cartilage deformation and degeneration. This is important since the morphological and biomechanical changes (mechanical properties including stiffness, dynamic load etc) at the onset of the disease are accurately detectable at the nanometer (molecular) scale and can be used as a powerful tool to validate simulation results in terms of predicting the progression stages of OA disease.

1.4 Assessment of Articular Cartilage

The traditional approach involves visual inspection and histology [37-38], optical microscopy [39] and allow for direct in vitro observation of cartilage. Applying electron microscopy [40-41] reveals ultra-structural details at molecular resolution. Visual inspection, histology and optical microscopy are limited in terms of spatial resolution (i.e. ~200 nm) to resolve nanometer scale features. Electron microscopy requires chemical fixation and dehydration of the cartilage, followed by metal staining or sputtering, so the specimen is no longer in its native state. Other disadvantages of electron microscopy are the complexity and prolonged time requirements of the sample preparation procedures. Moreover, neither light nor electron microscopy can directly measure the cartilage's mechanical properties. Another imaging method is the MRI – a non-invasive method capable of directly visualizing the articular cartilage macro-morphology i.e. volume and thickness *in situ*. However, cartilage due to the relatively short transverse relaxation time (T2) and broad range of potential sources of

artefacts presents a significant challenge for imaging when using MR technique [45]. Moreover, even state-of-the-art MRI modes e.g. the 3D water-excitation true FISP MRI allows assessment of the knee`s articular cartilage abnormalities with moderate-to-high specificity and low-to-moderate sensitivity [46]. The most direct method for measuring cartilage stiffness is by compression testing. This requires specimens to be precisely oriented in parallel (opposing top and bottom surfaces), what can be only achieved by cutting the cartilage off the bone and trimming the specimens. Since indentation testing avoids cutting, numerous indentation testing devices have been employed to measure the quality of "healthy vs. diseased" articular cartilage [42-43]. These devices employ indenters with typically 1-2 millimetre tip diameter. However these are unable to resolve molecular-level differences in the cartilage specimen.

1.4.1 Nanomechanics of Cartilage

Nanomechanics of cartilage is an emerging filed based on applying the atomic force microscopy to determine the mechanical properties of cartilage at the molecular level. In contrast to other indentation testing devices, AFM has the ability to assess the biomechanical properties of cartilage across length scales in close to native conditions (Chapter 2). Over the last decade AFM has been established as a powerful tool capable of simultaneously imaging, manipulating and measuring the mechanical properties of native biological tissues at the micrometer to nanometer scale [47]. An unprecedented advantage of the AFM over other indentation testing devices is that very small biological specimens (radius 500µm or more), ranging from tissues to cells and molecules, can be investigated in near physiologic conditions (e.g. 37° C, physiological buffer, gas controlled environment, non fixed or stained sample) [48].

The other advantage of the AFM as compared to the MRI is that it is sensitive to surface changes at the nanometer scale. This is where matrix degeneration generally begins in the superficial cartilage and then progresses to the deeper regions of the tissue [49]. Two methods can be applied for measuring mechanical properties by AFM. IT AFM which is used to examine structure–function relationships of cartilage at both micrometer and nanometer scales [49]. Micrometer scale measurements are limited to revealing only the chondrocytes and the surrounding ECM (Loparic et al. in preparation). This results in a unimodal distribution of the stiffness since the bulk elastic property of the ECM is probed. In contrast, nanometer scale measurements give rise to a bimodal distribution of the measured stiffness.

These two peaks correspond to the stiffness of the molecular constituents of cartilage (collagen II and proteoglycans) [62]**.** Clearly, IT AFM provides a good basis for assessing the structure–function relationships of normal, diseased and tissue engineered cartilage. Moreover, when compared to the MRI technique, IT AFM is able to resolve all grades of the cartilage osteoarthritis disease (Outerbridge scale system) in the human knee joint [33]. As compared to the sensitivity of AFM to the cartilage surface region, MRI has a spatial resolution of ~ 200 μm (e.g. for 7T MRI resolution) which limits its access to regions close to the cartilage surface (thickness ~ 100μm). Thus, AFM studies are particularly important in early detection of abnormalities of cartilage since matrix degeneration generally begins in superficial cartilage. Second method, the FF AFM measurement targets the lubricin-friction relationships in the cartilage [51] which is of particular importance in understanding the onset and progression of the OA. Lubricin is the main protein responsible for regulating the friction properties of cartilage and has important role in the development of the OA [52]. Additionally, by applying the AFM for nanometer scale imaging of the native cartilage it is possible to reveal fine structural details (e.g. collagen fibrils orientation and surrounding proteoglycans moiety) not resolved by other techniques [62]. Finally AFM techniques have great potential for the understanding the molecular mechanisms driving the onset of OA and thus to predict, the patient-specific characteristics of articular cartilage, specifically after osteotomy surgery.

In this thesis, biomechanical properties of ECM matrix and its major components from native and tissue engineered cartilage have been measured. Nanoscale resolution of AFM-based technique allows us for the first time measurement of the individual mechanical properties of cartilage's soft PG gel and the collagen fibrils and their contribution to cartilage stiffness measured at the micrometer scale (Chapter 2). Next we proposed and validated a quantitative AFM-based functional analysis to evaluate the influence of various biomechanical stimuli on quality of engineered cartilage grafts (Chapter 3). In particular, we demonstrated that the sliding-type biomechanical stimulus, similar to physiological articulation, plays an essential role in superior tribological and load bearing properties of engineered cartilage grafts. In addition, we measured the mechanical properties of cartilage grafts obtained from animal donors undergoing gene therapy procedure where genetically modified bone marrow clots were used to repair defect sites with or without the presence of growth factors. (Chapter 4). We indentified different amounts and spatial orientation of newly synthesized extracellular components and/or water content within the repaired tissue and compare these values to ones

measured in the native cartilage. In the next work, we proved that the application of more physiologic oxygen percentage (5 % O2) during specific phases of differentiation culture of HAC enhanced the biosynthetic activity and reduced the activity of catabolic enzymes implicated in cartilage breakdown (Chapter 5). Last but not least, by operating AFM in the torsional mode on individual collagen fibers isolated from native cartilage we measured mechanical response at the molecular level directly related to their fundamental physical characteristics: persistence and contour length, adsorption strength (Chapter 6). Overall, work presented in this thesis demonstrates the potential use of cartilage nanomechanics as a valuable marker for assessing the functionality of native and tissue engineered cartilage thereby fostering pre-symptomatic diagnostics and treatment.

1.5 Abbreviations

ECM: extracellular matrix; EM: electronic microscopy; GAG: glycosaminoglycans; HAC: human articular chondrocytes; MMP: metalloproteinase; OA: osteoarthritis; PBS: phosphate buffered saline; SEM: scanning electron microscopy; TEM: transmission electron microscopy; TGFβ1: transforming growth factor beta-1. AFM: Atomic Force Microscopy; PG: Proteoglycan; FF AFM: Friction Force AFM; IT AFM: Indentation-type AFM; MRI: magnetic resonance imaging; FISP MRI: fast imaging with steady state precession magnetic resonance imaging; IL-1β: interleukin-1β; TNF-α: tumor necrosis factor alpha, TNF-β: tumor necrosis factor beta; ADAMTS: a disintegrin and metalloproteinase with a thrombospondin; CS: chondroitin; KS: keratane sulphate;

1.6 References

1.   Bhosale, A.M. and J.B. Richardson, Articular cartilage: structure, injuries and review of management. Br Med Bull, 2008. 87: p. 77-95.

2.   Aspden, R.M. and D.W.L. Hukins, Collagen Organization in Articular-Cartilage, Determined by X-Ray-Diffraction, and Its Relationship to Tissue Function. Proceedings of the Royal Society of London Series B-Biological Sciences, 1981. 212(1188): p. 299-304.

3.   Mow, V.C., A. Ratcliffe, and A.R. Poole, Cartilage and Diarthrodial Joints as Paradigms for Hierarchical Materials and Structures. Biomaterials, 1992. 13(2): p. 67-97.

4.   Miller, E.J. and S. Gay, The Collagens - an Overview and Update. Methods in Enzymology, 1987. 144: p. 3-41.

5.   Yasuda, T., et al., Peptides of type II collagen can induce the cleavage of type II collagen and aggrecan in articular cartilage. Matrix Biology, 2006. 25(7): p. 419-429.

6.   Blaschke, U.K., et al., Collagen XI nucleates self-assembly and limits lateral growth of cartilage fibrils. Journal of Biological Chemistry, 2000. 275(14): p. 10370-10378.

7.   Bruckner, P. and M. van der Rest, Structure and function of cartilage collagens. Microsc Res Tech, 1994. 28(5): p. 378-84.

8.   Prockop, D.J., et al., Biosynthesis of Collagen and Its Disorders .1. New England Journal of Medicine, 1979. 301(1): p. 13-23.

9.   Hansen, U., D.G. Seidler, and P. Bruckner, Supramolecular organization of heterotypic fibrils by decorin. Matrix Biology, 2006. 25: p. S73-S73.

10.   Hansen, U. and P. Bruckner, Macromolecular specificity of collagen fibrillogenesis - Fibrils of collagens I and XI contain a heterotypic alloyed core and a collagen I sheath. Journal of Biological Chemistry, 2003. 278(39): p. 37352-37359.

11.   Wu, J.J. and D.R. Eyre, Cartilage Type-Ix Collagen Is Cross-Linked by Hydroxypyridinium Residues. Biochemical and Biophysical Research Communications, 1984. 123(3): p. 1033-1039.

12.   Eyre, D., Collagen of articular cartilage. Arthritis Research, 2002. 4(1): p. 30-35.

13.   Maroudas, A., Physicochemical properties of articular cartilage. In Adult Articular Cartilage, 2nd edition Edited by Freeman MAR London: Pitman Medical, 1979: p. 215–290.

14.   DeGroot, J., The AGE of the matrix: chemistry, consequence and cure. Current Opinion in Pharmacology, 2004. 4(3): p. 301-305.

15.   Bank, R.A., et al., Ageing and zonal variation in post-translational modification of collagen in normal human articular cartilage - The age-related increase in non-enzymatic glycation affects biomechanical properties of cartilage. Biochemical Journal, 1998. 330: p. 345-351.

16.   DeGroot, J., et al., Accumulation of advanced glycation end products as a molecular mechanism for aging as a risk factor in osteoarthritis. Arthritis and Rheumatism, 2004. 50(4): p. 1207-1215.

17.   Sasaki, N. and S. Odajima, Elongation mechanism of collagen fibrils and force-strain relations of tendon at each level of structural hierarchy. Journal of Biomechanics, 1996. 29(9): p. 1131-1136.

18.   Sasaki, N. and S. Odajima, Stress-strain curve and Young's modulus of a collagen molecule as determined by the X-ray diffraction technique. Journal of Biomechanics, 1996. 29(5): p. 655-658.

19.   Breen, E.C., Mechanical strain increases type I collagen expression in pulmonary fibroblasts in vitro. Journal of Applied Physiology, 2000. 88(1): p. 203-209.

20.   Sun, Y.L., et al., Stretching type II collagen with optical tweezers. Journal of Biomechanics, 2004. 37(11): p. 1665-1669.

21.   Luo, Z.P., et al., Single molecule mechanical properties of type II collagen and hyaluronan measured by optical tweezers. Biorheology, 2004. 41(3-4): p. 247-254.

22.   Staple, D.B., et al., Stretching, Unfolding, and Deforming Protein Filaments Adsorbed at Solid-Liquid Interfaces Using the Tip of an Atomic-Force Microscope. Physical Review Letters, 2009. 102(12): p. -.

23.   Maroudas, A., et al., Aggrecan turnover in human articular cartilage: Use of aspartic acid racemization as a marker of molecular age. Archives of Biochemistry and Biophysics, 1998. 350(1): p. 61-71.

24.   Hardingham, T.E., The role of link-protein in the structure of cartilage proteoglycan aggregates. Biochem J, 1979. 177(1): p. 237-47.

25.   Heinegard, D. and V.C. Hascall, Aggregation of cartilage proteoglycans. 3. Characteristics of the proteins isolated from trypsin digests of aggregates. J Biol Chem, 1974. 249(13): p. 4250-6.

26.   Buckwalter, J.A. and H.J. Mankin, Articular cartilage .1. Tissue design and chondrocyte-matrix interactions. Journal of Bone and Joint Surgery-American Volume, 1997. 79A(4): p. 600-611.

27.   Bayliss, M.T. and S.Y. Ali, Age-related changes in the composition and structure of human articular-cartilage proteoglycans. Biochem J, 1978. 176(3): p. 683-93.

28.   Bayliss, M.T. and P.J. Roughley, The properties of proteoglycan prepared from human articular cartilage by using associative caesium chloride gradients of high and low starting densities. Biochem J, 1985. 232(1): p. 111-7.

29.   Roughley, P.J. and R.J. White, Age-related changes in the structure of the proteoglycan subunits from human articular cartilage. J Biol Chem, 1980. 255(1): p. 217-24.

30.   Velikii, N.N. and Chagobet.Rv, An Enquiry into Exchangability of Cartilage Sulphate Chondroitin in Control and a-Vitamine Deficient Chickens with Use of Different Labelled Forerunners. Doklady Akademii Nauk Sssr, 1970. 193(6): p. 1409-&.

31.   Plaas, A.H.K., et al., Chemical and immunological assay of the nonreducing terminal residues of chondroitin sulfate from human aggrecan. Journal of Biological Chemistry, 1997. 272(33): p. 20603-20610.

32.   Midura, R.J., et al., Nonreducing End Structures of Chondroitin Sulfate Chains on Aggrecan Isolated from Swarm Rat Chondrosarcoma Cultures. Journal of Biological Chemistry, 1995. 270(14): p. 8009-8015.

33.   Scott, J.E., et al., The chemical morphology of age-related changes in human intervertebral disc glycosaminoglycans from cervical, thoracic and lumbar nucleus pulposus and annulus fibrosus. J Anat, 1994. 184 (Pt 1): p. 73-82.

34.   Bolis, S., C.J. Handley, and W.D. Comper, Passive Loss of Proteoglycan from Articular-Cartilage Explants. Biochimica Et Biophysica Acta, 1989. 993(2-3): p. 157-167.

35.   Mow, V.C., et al., Biphasic Creep and Stress-Relaxation of Articular-Cartilage in Compression - Theory and Experiments. Journal of Biomechanical Engineering-Transactions of the Asme, 1980. 102(1): p. 73-84.

36.   Soltz, M.A. and G.A. Ateshian, Experimental verification and theoretical prediction of cartilage interstitial fluid pressurization at an impermeable contact interface in confined compression. Journal of Biomechanics, 1998. 31(10): p. 927-934.

37.   Mak, A.F., The Apparent Viscoelastic Behavior of Articular-Cartilage - the Contributions from the Intrinsic Matrix Viscoelasticity and Interstitial Fluid-Flows. Journal of Biomechanical Engineering-Transactions of the Asme, 1986. 108(2): p. 123-130.

38.   Ateshian, G.A., The role of interstitial fluid pressurization in articular cartilage lubrication. Journal of Biomechanics, 2009. 42(9): p. 1163-1176.

39.   Morgelin, M., et al., The Cartilage Proteoglycan Aggregate - Assembly through Combined Protein-Carbohydrate and Protein-Protein Interactions. Biophysical Chemistry, 1994. 50(1-2): p. 113-128.

40.   Papagiannopoulos, A., et al., Solution structure and dynamics of cartilage aggrecan. Biomacromolecules, 2006. 7(7): p. 2162-2172.

41. Kiani, C., et al., Structure and function of aggrecan. Cell Research, 2002. 12(1): p. 19-32.

42. Roberts, B.J., A. Unsworth, and N. Mian, Modes of Lubrication in Human Hip Joints. Annals of the Rheumatic Diseases, 1982. 41(3): p. 217-224.

43. Radin, E.L., D.A. Swann, and P.A. Weisser, Separation of a Hyaluronate-Free Lubricating Fraction from Synovial Fluid. Nature, 1970. 228(5269): p. 377-&.

44. Hills, B.A., Oligolamellar Lubrication of Joints by Surface-Active Phospholipid. Journal of Rheumatology, 1989. 16(1): p. 82-91.

45. McCutchen, C.W., The frictional properties of animal joints. Wear. 5(1): p. 1-17.

46. Walker, P.S., et al., Boosted Lubrication in Synovial Joints by Fluid Entrapment and Enrichment. Annals of the Rheumatic Diseases, 1968. 27(6): p. 512-&.

47. Ateshian, G.A., A theoretical formulation for boundary friction in articular cartilage. Journal of Biomechanical Engineering-Transactions of the Asme, 1997. 119(1): p. 81-86.

48. Neu, C.P., K. Komvopoulos, and A.H. Reddi, The interface of functional biotribology and regenerative medicine in synovial joints. Tissue Engineering Part B-Reviews, 2008. 14(3): p. 235-247.

49. Mccutchen, C.W., Sponge-Hydrostatic and Weeping Bearings. Nature, 1959. 184(4695): p. 1284-1285.

50. Morrell, K.C., et al., Corroboration of in vivo cartilage pressures with implications for synovial joint tribology and osteoarthritis causation. Proceedings of the National Academy of Sciences of the United States of America, 2005. 102(41): p. 14819-14824.

51. Noyori, K., T. Takagi, and H.E. Jasin, Characterization of the macromolecular components of the articular cartilage surface. Rheumatology International, 1998. 18(2): p. 71-77.

52. Schumacher, B.L., et al., A Novel Proteoglycan Synthesized and Secreted by Chondrocytes of the Superficial Zone of Articular-Cartilage. Archives of Biochemistry and Biophysics, 1994. 311(1): p. 144-152.

53. Sarma, A.V., G.L. Powell, and M. LaBerge, Phospholipid composition of articular cartilage boundary lubricant. Journal of Orthopaedic Research, 2001. 19(4): p. 671-676.

54. Schmidt, T.A., et al., Boundary lubrication of articular cartilage - Role of synovial fluid constituents. Arthritis and Rheumatism, 2007. 56(3): p. 882-891.

55. Zhou, S., Z. Cui, and J.P. Urban, Factors influencing the oxygen concentration gradient from the synovial surface of articular cartilage to the cartilage-bone interface: a modeling study. Arthritis Rheum, 2004. 50(12): p. 3915-24.

56. Stockwell, R.A., The cell density of human articular and costal cartilage. J Anat, 1967. 101(Pt 4): p. 753-63.

57. Vignon, E., et al., Cell Density of Human Femoral-Head Cartilage. Clinical Orthopaedics and Related Research, 1976(121): p. 303-308.

58. Saris, D.B.F., et al., Characterized chondrocyte implantation results in better structural repair when treating symptomatic cartilage defects of the knee in a randomized controlled trial versus microfracture. American Journal of Sports Medicine, 2008. 36(2): p. 235-246.

59. Robert, H., et al., Treatment of deep cartilage defects in the knee with autologous chondrocyte transplantation: a review of 28 cases. Revue De Chirurgie Orthopedique Et Reparatrice De L Appareil Moteur, 2007. 93(7): p. 701-709.

60. Brittberg, M., et al., Treatment of Deep Cartilage Defects in the Knee with Autologous Chondrocyte Transplantation. New England Journal of Medicine, 1994. 331(14): p. 889-895.

61. Galois, L., et al., [Cartilage tissue engineering: state-of-the-art and future approaches]. Pathol Biol (Paris), 2005. 53(10): p. 590-8.

62. Loparic, M., et al., Micro- and nanomechanical analysis of articular cartilage by indentation-type atomic force microscopy: validation with a gel-microfiber composite. Biophys J, 2010. 98(11): p. 2731-40.

Chapter 2

Micro- and nanomechanical analysis of articular cartilage by indentation-type atomic force microscopy – validation with a gel-microfiber composite

Marko Loparic, Dieter Wirz, A.U. Daniels, Roberto Raiteri,

Mark R. VanLandingham, Geraldine Guex, Ivan Martin,

Ueli Aebi and Martin Stolz

2.1 Abstract

As documented previously, articular cartilage exhibits a scale-dependent dynamic stiffness when probed by indentation-type atomic force microscopy (IT-AFM). In this study, a micrometer-size spherical tip revealed an unimodal stiffness distribution (which we refer to as microstiffness), whereas probing articular cartilage with a nanometer-size pyramidal tip resulted in a bimodal nanostiffness distribution. We concluded that indentation of the cartilage's soft proteoglycan (PG) gel gave rise to the lower nanostiffness peak, whereas deformation of its collagen fibrils yielded the higher nanostiffness peak. To test our hypothesis, we produced a gel-microfiber composite consisting of a chondroitin sulfate-containing agarose gel and a fibrillar poly(ethylene glycol)-terephthalate/poly(butylene)-terephthalate block copolymer. In striking analogy to articular cartilage, the microstiffness distribution of the synthetic composite was unimodal, whereas its nanostiffness exhibited a bimodal distribution. Also, similar to the case with cartilage, addition of the negatively charged chondroitin sulfate rendered the gel-microfiber composite's water content responsive to salt. When the ionic strength of the surrounding buffer solution increased from 0.15 to 2 M NaCl, the cartilage's microstiffness increased by 21%, whereas that of the synthetic biomaterial went up by 31%. When the nanostiffness was measured after the ionic strength was raised by the same amount, the cartilage's lower peak increased by 28%, whereas that of the synthetic biomaterial went up by 34%. Of interest, the higher peak values remained unchanged for both materials. Taken together, these results demonstrate that the nanoscale lower peak is a measure of the soft PG gel, and the nanoscale higher peak measures collagen fibril stiffness. In contrast, the micrometer-scale measurements fail to resolve separate stiffness values for the PG and collagen fibril moieties. Therefore, we propose to use nanostiffness as a new biomarker to analyze structure-function relationships in normal, diseased, and engineered cartilage.

2.2 Introduction

Imaging methods for analyzing articular cartilage structure

Visual inspection and histology [1-3] and optical microscopy [4, 5] allow for direct in vitro observation of fresh cartilage under near-physiological conditions but are limited to a spatial resolution of ~200 nm. In contrast, electron microscopy [6-8] reveals ultrastructural details at molecular resolution but requires chemical fixation and dehydration of the cartilage, followed by metal staining or sputtering, so that the specimen is no longer in its native state. Other disadvantages of electron microscopy are the complexity and prolonged time requirements of the sample preparation procedures. Moreover, neither light nor electron microscopy can directly measure the cartilage's mechanical properties. In contrast, atomic force microscopy (AFM) allows for simultaneous imaging and stiffness measurements on a micrometer–nanometer scale in native samples, and thus can help elucidate the structure and mechanical properties of articular cartilage.

Overview of articular cartilage structure-mechanical property relationships

Aggrecan is the most abundant proteoglycan (PG) in articular cartilage and exhibits a bottle-brush structure. The function of aggrecan is strongly determined by the electrostatic repulsion of its glycosaminoglycan side chains, which carry highly negatively charged carboxyl and sulfate groups that repel each other [9]. In physiological solution, the negative charges are balanced by an influx of positive ions (Na^+ and Ca^{2+}). This influx of ions results in an osmotic balance between the PGs and the surrounding synovial fluid, which in turn leads to the creation of a PG gel that causes cartilage to swell in physiological saline solutions. As a result of this swelling and the low water permeability of cartilage (10^{-15}–10^{-16} m^4/Ns), under applied loads the resulting osmosis-based cartilage structure is poroviscoelastic, which enables the tissue to store and dissipate energy upon mechanical deformation [10-13].

Collagen fibrils are the other principal matrix component in articular cartilage. As a result of extensive covalent cross-linking, they form a very strong three-dimensional (3D) collagen meshwork [14, 15]. Thus, articular cartilage is a composite biomaterial consisting of two interpenetrating 3D components (i.e., a PG gel and a cross-linked collagen meshwork) that can resist compressive, tensile, and shear forces. Each individual component of this tissue exhibits distinct physical and chemical properties. Hence, changes in the relative amounts of

collagen, PGs, and water can affect the mechanical properties of cartilage, as frequently described in studies of cartilage pathology [11,12, 16].

Overview of direct mechanical determination of articular cartilage stiffness

When tested at the micrometer–centimeter scale, articular cartilage behaves as a nonstructured and uniform material. This widely used first approximation allows measurement of the overall cartilage stiffness. Also, since cartilage is poroviscoelastic, any overall stiffness measurement produces an aggregate modulus, E^*, which is the result of both elastic and viscous contributions to stiffness (see Fig. 4). Depending on the experimental loading conditions, the loading geometry employed by the articular cartilage exhibits a wide range of values of E^*, from ~1 MPa when loaded at a low frequency of <0.1 Hz [12, 17] to ~60 MPa at dynamic cyclic loads (40 Hz) [18]. At low loading frequencies, the mobile water moves through the pores in the PG gel in response to the load, resulting in a lowering of the cartilage's stiffness. In contrast, at high loading frequencies, the cartilage's low permeability prevents the incompressible water from being displaced, resulting in the cartilage exhibiting a higher stiffness.

Articular cartilage millimeter-scale stiffness measurements

The most direct method for measuring cartilage stiffness is compression testing; however, this approach requires specimens with highly parallel top and bottom surfaces, which can only be achieved by cutting the cartilage off the bone and trimming the specimens. In compression tests, one must also decide which constraints best simulate the situation in vivo (e.g., lateral confinement) and whether the support plate and lateral confinement should be porous to allow movement of water out of the cartilage at low deformation rates. Since indentation testing avoids the need for cutting, numerous indentation testing devices have been employed to measure the quality or health/disease state of articular cartilage [19-21]. These devices employ indenters, typically with a 1–2 mm tip diameter, to quantify the resistance to indentation (stiffness) in a manner similar to that used by the surgeon with a simple hand-held probe. Unfortunately, several investigators have reported that millimeter-scale indenter stiffness measurements are not sensitive to even substantial changes in cartilage structure associated with aging or early-stage osteoarthritis [20, 22].

Choosing articular cartilage dynamic loading conditions

Stiffness tests of cartilage are often performed under displacement control. For example, a series of submillimeter-scale step compression or indentation displacements are applied [23]. In such experiments, each displacement is maintained until the resultant force decays to an equilibrium value. An equilibrium modulus is then determined from the slope of the resultant set of force/displacement values. The force decay is a viscous stress relaxation in response to the imposed 3D structural change, where the relaxation results from slow movement of water through and out of the cartilage. These measurements can take hours to accomplish. The equilibrium modulus is thus related to the cartilage's permeability. In contrast, during gait, the articular cartilage needs to respond to a much faster cyclic loading through deformation. Even though the loads applied to cartilage are not technically controlled by the use of feedback steering to maintain a constant load function, the mechanical behavior of cartilage is best mimicked by load-controlled cyclic deformation. Under such conditions, the low permeability of cartilage significantly restricts the water's mobility through the tissue. Of most importance for diagnostic applications in a clinical environment, the measurements need to be fast. Therefore, we performed indentation testing at a rate of three indentations per second, corresponding to loading rates similar to gait [24, 25].

In the context of exploring novel treatment modalities for osteoarthritis, we recently made the significant observation that all morphological and biomechanical changes that occur at the onset of this disease can solely be depicted on the nanometer scale [25]. In particular, when we employed micrometer-size spherical tips for indentation-type (IT)-AFM, the microstiffness values of articular cartilage exhibited a Gaussian distribution with a peak at $E^*_{micro} = 1.3 \pm 0.4$ MPa [25], in good agreement with previously reported values of macroscopic compressive stiffness measurements obtained at similar loading frequencies (12). In contrast, when we mapped a cartilage surface by employing nanometer-size IT-AFM tips, the measured stiffness exhibited a bimodal distribution, with one peak exhibiting higher stiffness and one peak exhibiting lower stiffness. We assumed that the lower stiffness peak with values of E^*_{PG} ~20 kPa reflected the stiffness of the PG gel, whereas the higher stiffness peak with values of E^*_{Col} ~400 kPa reflected the stiffness of the collagen fibrils [24, 25]. In the study presented here, we modeled the composite nature of cartilage by creating a simple poly(ethylene glycol)-terephthalate (PEGT)/poly(butylene)-terephthalate (PBT)-fibril/agarose/chondroitin sulfate model with a cartilage-like structure, and compared the bimodality of its nanometer-scale stiffness with that of articular cartilage.

2.3 Materials and Methods

Cartilage sample preparation and IT-AFM measurements

Cartilage specimens were prepared as described previously [24]. Briefly, porcine articular cartilage from freshly slaughtered pigs (within 1–2 h postmortem) was harvested from the femoral heads by cutting samples off the underlying bone with a sharp razor blade, yielding ~5 mm × 5 mm pieces that were ~2 mm thick. The specimens were stored in phosphate-buffered saline (PBS; 2.6 mM NaH_2PO_4, 3 mM Na_2HPO_4, 155 mM NaCl, 0.01% NaN_3 w/v, pH 7.2) supplemented with a protease inhibitor cocktail (Complete, Boehringer Mannheim, Mannheim, Germany). The samples were covered with the buffer solution and stored on ice. After the articular cartilage topography was imaged by contact-mode AFM at a scanning rate of ~0.7 Hz, stiffness measurements were obtained by IT-AFM in the same buffer solution. Samples from three different pigs and from three different locations each were analyzed.

Osmotic loading of cartilage

The isotonic PBS solution contained 2.6 mM NaH_2PO_4, 3 mM Na_2HPO_4, 155 mM NaCl, 0.01% NaN_3 w/v, pH 7.2. The hypertonic PBS contained 2.6 mM NaH_2PO_4, 3 mM Na_2HPO_4, 2 M NaCl, 0.01% NaN_3 w/v, pH 7.2. Three cartilage samples each were tested separately.

Preparation of agarose and agarose/chondroitin sulfate gels

For exploratory calibration testing, agarose gels were prepared with 0.5%, 1.0%, 2.25%, and 3.5% (w/w) agarose (AGAR Noble; DIFCO Laboratories, Detroit, MI) in water. For the model material used here, 50 mg of agarose were stirred in 10 mL of PBS, heated up until the solution started to boil, and then cooled down to ~50°C. Next, 200 mg chondroitin sulfate (chondroitin sulfate A from bovine trachea, C9819-5G; Sigma) was added and properly mixed, resulting in a concentration of 20 mg/mL of chondroitin sulfate in the gel. The melted agarose/chondroitin sulfate solution was used to prepare the specimens described below and to perform the swelling tests. Three gel samples were then tested in isotonic and hypertonic PBS.

PEGT/PBT-fibril/agarose/chondroitin sulfate gel model material

PolyActive (PEGT/PBT block copolymer; CellCoTech, Bilthoven, The Netherlands) fibrils were produced by means of the electro-spinning (ESP) technique [26, 27]. Briefly, the PEGT/PBT copolymer (1000 MW PEGT, 70% PEGT, 30% PBT) was dissolved in a mixture

of 10 mL dichloromethane and 10 μL distilled water, and stirred at room temperature for 24 h. The ESP device consisted of a syringe pump (Harvard Apparatus, South Natick, MA), a high-voltage generator (0–30 kV; Brandenburg Ltd., South Croydon, Surrey, England) connected to a syringe (10 mL, 1.6 mm steel needle; Becton Dickinson, Franklin Lakes, NJ) containing the polymer solution, and a stainless-steel plate. An electrical field was applied between the needle (positive pole) and the stainless-steel plate (negative pole). A polymer jet from the spinneret (needle) was then collected as a nonwoven mesh of fibers onto glass microscopy slides (76 × 26 mm; Menzel, Braunschweig, Germany) placed on the stainless-steel plate. ESP resulted in the production of PEGT/PBT fibers of 2.9 ± 0.19 μm thickness, as measured based on scanning electron microscopy images.

A plastic ring (~3 mm inner diameter, ~0.2 mm thick, ~1 mm high) was used to mix the PEGT/PBT-fibrils with the agarose/chondroitin sulfate gel for testing by AFM. This ring was placed onto a PEGT/PBT-fiber-coated glass slide. The fibril coating around the ring was removed with a scalpel. Then, a droplet of ~50 μL of melted 1.0% (w/w) agarose gel was placed into the ring on top of the fibril mesh. For the swelling tests in this work, a droplet of the melted agarose/chondroitin sulfate was used instead. After solidification was achieved, the slide was kept in a cold room (4°C) for ~15 min. The specimen was then removed from the glass slide by moving the ring laterally until it and the specimen were free of the slide. The specimen surrounded by the ring was then glued upside down onto a 10-mm-diameter Teflon disk with a 5-min curing epoxy (Devcon epoxy; ITW Brands, Wood Dale, IL). The upside-down orientation of the specimen ensured that the surface to be evaluated by AFM was populated with fibrils. To prevent drying, the specimen was covered with a droplet of PBS. Three samples were inspected per experimental condition.

AFM and indenter tips

AFM experiments were carried out with a MultiMode AFM and NanoScope IIIa controller (Veeco Metrology, Santa Barbara, CA). AFM tips of different diameters were selected and prepared as follows: For micrometer-scale measurements, hard borosilicate glass spheres (9000 series glass particle size standards 2–2000 μm; Thermo Fisher Scientific, Fremont, CA), diameter $d = 10$ μm, were glued onto tipless rectangular cantilevers (type NSC12; NT-MDT, Moscow, Russia) with nominal spring constants k in the following ranges: 6.5 N/m ≤ k ≤ 27.5 N/m for probing cartilage, and 0.2 N/m ≤ k ≤ 0.7 N/m for probing the model material (Fig. 2.1 *A*). For nanometer-scale experiments, pyramidal tips with a nominal tip radius ≤ 20 nm on V-shaped cantilevers with a nominal spring constant of 0.06 N/m (type NPS; Veeco)

were employed (Fig. 2.1 *B*). The spring constant was measured for each cantilever by means of the thermal noise method [28]. The actual diameter of each micrometer-size tip was determined with the use of scanning electron microscopy images.
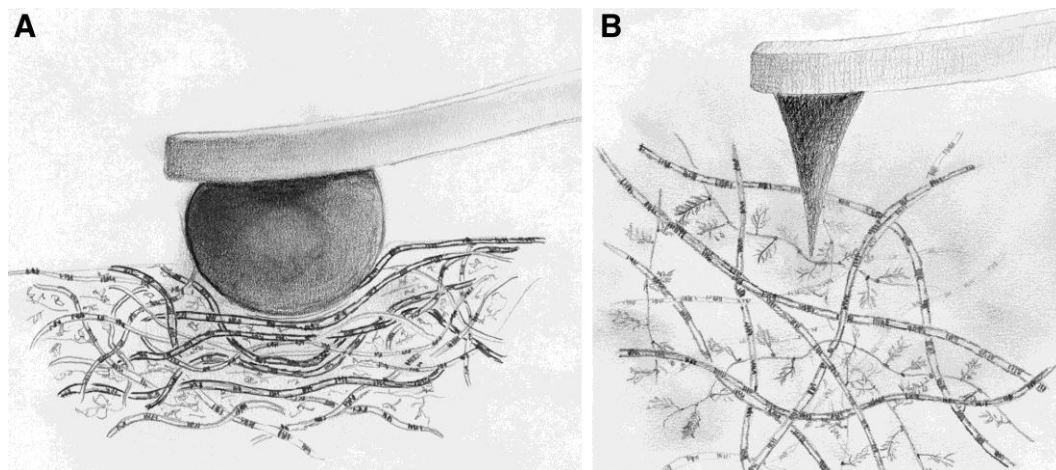
Figure 2.1: Cartoon showing the interaction of a micrometer-size spherical tip (A) and a nanometer-size pyramidal (B) AFM cantilever tip with cartilage.

Stiffness measurements obtained by IT-AFM

Measurements of micro- and nanostiffness (dynamic aggregate modulus, E^*) were obtained by IT-AFM as described previously [24]. Briefly, maps of load-displacement curves were recorded in a regular grid over the sample surface by employing the force-volume mode. An individual set of data consisted of 4096 load-displacement curves obtained at a rate of three full loading cycles per second in a 64×64 curve grid covering sample areas of ~15 μm $\times$ 15 μm. Each force curve consisted of 512 data points. For microscale measurements, a maximum deflection of 150 nm was chosen, which corresponded to a maximum applied load of ~2.0 μN for the cartilage measurements (with k = 13.5 N/m) and a maximum applied load of ~105 nN for the model material (with k = 0.7 N/m; d = 7.7 μm). For nanoscale measurements, a maximum deflection value of 30 nm was set, resulting in a maximum applied load of ~1.8 nN (with k = 0.06 N/m) to probe both authentic articular cartilage and the model material.

**Stiffness data acquisition and calculations**

Stiffness values for cartilage and the model material were obtained from IT-AFM unloading curves. The use of data from unloading (rather than loading) curves ensures that the

displacement data do not contain any irreversible (e.g., plastic) deformation or other extraneous displacement effects. The fundamental IT-AFM stiffness values obtained were force-displacement slopes. A slope was defined as the mean ratio of cantilever deflection (an expression of force) to piezoelectric displacement in the initial unloading part of the load-displacement curve, as described in our previous work [24]. We set the maximum value for nanostiffness to one (corresponding to a slope of one) and displayed all other values at the nanoscale relative to one. The value for microstiffness obtained on articular cartilage (0.15 M NaCl) was set to 0.5. The bin width was set by dividing the maximum value = 1×50 (bars), yielding a dimensionless bin width of 0.02. Slope values alone are sufficient to determine and compare micro- and nanostiffness distributions of IT-AFM measurements. The slopes from a given square grid of IT-AFM measurements were then used to create a slope histogram. The subsequent calculation of microstiffness aggregate modulus (E^*) values from the slope data was performed as previously described [24] (see also Appendix I). To calculate the nanostiffness aggregate modulus (E^* values), the functional relationship $y(x) = (21/(1 - x)) - 21$ was derived from a calibration curve using agarose gels [24] (see also Appendix I).

2.4 Results

Articular cartilage exhibits a scale-dependent mechanical behavior: micro- versus nanostiffness

As documented in Fig. 2.2 *A*, when articular cartilage is imaged with a ~10-μm-diameter spherical tip (see Fig. 2.1 *A*), the sample surface appears relatively uniform and flat. However, to demonstrate that recording the image and the force map of the same specimen area is meaningful, we show a location that exhibits some coarse surface irregularities. Although such a micrometer-size AFM tip cannot resolve the cartilage's fine structural elements, such as individual collagen fibrils, the force map displayed in Fig. 2 *B*, which is derived from 64×64 (i.e., 4096) IT-AFM curves, clearly correlates with the surface irregularities observed in the AFM height image shown in Fig. 2.2 *A*. Fig. 2.2 *C* reveals that the unloading slope histogram for the 4096 force curves in Fig. 2.2 *B* exhibits a narrow Gaussian distribution centered about a slope of 0.53. Fig. 2.2 *D* displays an averaged curve, giving a calculated microstiffness of $E_{\text{micro}} = 1.3 \pm 0.4$ MPa.
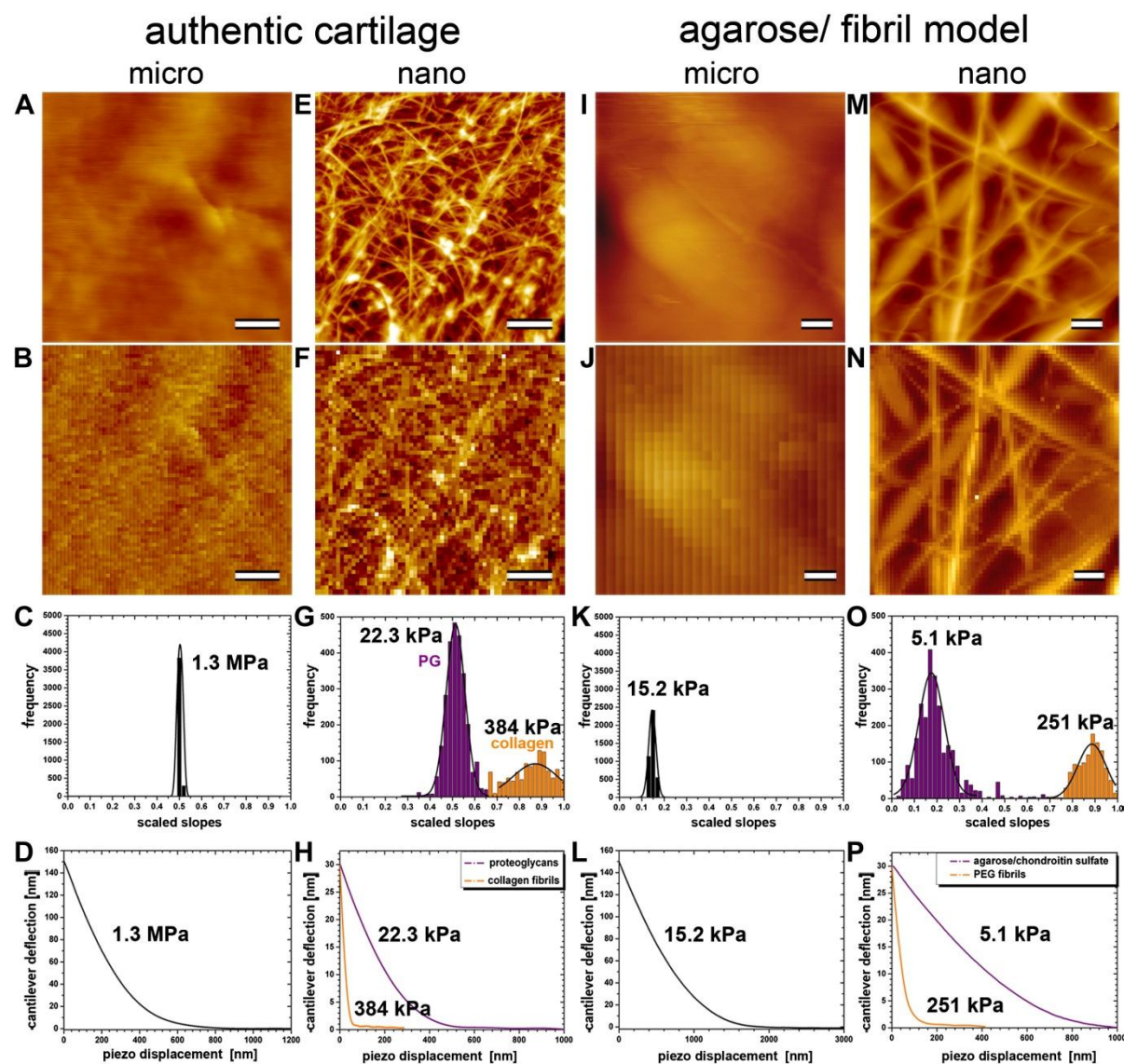
Figure 2.2: Images and IT-AFM measurements of stiffness of articular cartilage and a PEGT/PBT-fibril/agarose/chondroitin sulfate gel composite at the micro- and nanometer scales. Images and force maps on cartilage are scaled to a height of 400 nm, whereas images and force maps on the model material are scaled to a height of 2000 nm. All scale bars correspond to 2 μm. (*A–D, first column*) Micrometer-scale information for cartilage. (*A* and *B*) The corresponding nanometer scale data. (*C*) Distribution of raw stiffness values (scaled slopes) obtained from the IT-AFM force/displacement curves. (*D*) Distribution of force curves and the value of E^*. (*E–H, second column*) Analogous information obtained at the nanometer scale. The third and fourth columns show analogous images and data for the model material.

Fig. 2.2 *E* shows the AFM height image of the same articular cartilage surface, but now recorded by a sharp, nanometer-size tip (see Fig. 2.1 *B*). At this resolution, individual collagen fibrils appear as bright filamentous structures that are separated by nonstructured darker areas. The corresponding force map in Fig. 2.2 *F*, which represents a 12 μm × 12 μm specimen area, also shows the locations of the individual collagen fibrils on the articular cartilage surface. Therefore, any two adjacent points in this 64 × 64 pixel force map are

spaced 187.5 nm apart. As documented in Fig. 2.2 *G*, calculation of the slope for each pixel in this force map yielded a histogram with a bimodal distribution, with the two Gaussian fits being centered about slopes of 0.51 and 0.87, respectively. Accordingly, Fig. 2.2 *H* reveals the two averaged force-displacement curves computed from the 2% of curves centered about the peaks of the two Gaussian fits (corresponding to an average of a few hundred curves, depending on the width of the Gaussian fit). From these, nanostiffnesses of 22.3 ± 1.5 kPa and 384 ± 50 kPa, respectively, were calculated and found to be ~100× and ~6× less than the corresponding microstiffness of 1.3 MPa that was determined with a micrometer-size tip (see Fig. 2.2, *C* and *D*).

Comparison of authentic articular cartilage with a model gel-microfiber composite

Next, we wanted to test our hypothesis that the bimodal distribution shown in Fig. 2.2 *G* is caused by an interaction of the sharp, nanometer-size tip with the two different structural components comprising the cartilage (i.e., the collagen fibrils and the PG moiety). For this purpose, we prepared a PEGT/PBT-fibril/agarose/chondroitin sulfate gel composite material to mimic articular cartilage's relatively stiff collagen meshwork and the softer PG gel moiety. Probing the resulting model material by IT-AFM at the micro- and nanometer scale clearly confirmed that its composite structure consisted of stiff fibrils and a soft matrix similar to that of cartilage.

Accordingly, Fig. 2.2 *I* displays an AFM image of the model material recorded by a micrometer-size spherical tip (see Fig. 2.1 *A*). Next, from the same specimen area and using the same spherical tip, 64 × 64 force-displacement curves were recorded. The resulting force map is shown in Fig. 2.2 *J*, and Fig. 2.2 *K* reveals the distribution of microstiffness slope values for the 4096 points from the force map in Fig. 2.2 *J*. Fig. 2.2 *L* displays the averaged force-displacement curve computed from the 2% of curves centered about the peak of the Gaussian fit (see Fig. 2.2 *K*), from which a microstiffness of 15.2 ± 0.5 kPa was calculated. Compared to cartilage (see Fig. 2.2 *C*), the Gaussian distribution is slightly wider and centered about a much lower slope value (0.15 vs. 0.54 for cartilage). The corresponding E^* value calculated from the slope data (15.2 ± 0.5 kPa) shows that the microstiffness of the model material amounted to only 0.66% of the stiffness of cartilage (i.e., 1.3 MPa; see Fig. 2.2 *D*).

In contrast to Fig. 2.2 *I*, which was recorded by a micrometer-size spherical tip, Fig. 2.2 *M* displays an AFM height image of the model material registered by a sharp, nanometer-size pyramidal tip (see Fig. 2.1 *B*). At this scale, the PEGT/PBT fibrils can clearly be resolved in

both the AFM height image (Fig. 2.2 *M*) and the corresponding force map recorded by IT-AFM of the same specimen area (Fig. 2.2 *N*). Analogously to the case with cartilage (see Fig. 2.2 *G*), the slope histogram shown in Fig. 2.2 *O* exhibits a bimodal distribution, with the two Gaussian fits being centered about slopes of 0.18 and 0.89, respectively. Accordingly, Fig. 2.2 *P* reveals the two averaged force-displacement curves computed from the 2% of curves centered about the peaks of the two Gaussian fits. From these, the nanostiffnesses of 5.1 ± 1.2 kPa and 251 ± 40 kPa, respectively, were calculated and found to be ~3× smaller and ~6× larger, respectively, than the corresponding microstiffness of 15.2 ± 0.5 kPa that was determined with a micrometer-size tip (see Fig. 2.2, *K* and *L*). Hence, in contrast to its microstiffness, the model material's nanostiffness is within the same order of magnitude as that of articular cartilage for both its hard (i.e., the PEGT/PBT-fibrils) and soft (i.e., the agarose/chondroitin sulfate gel) phases.

Effects of ionic-strength changes on the micro- and nanostiffness of authentic articular cartilage and a model gel-microfiber composite—a comparison

To ascertain the effect of osmotically induced changes in water content and the resultant water pressure within cartilage and the model material, we probed the micro- and nanostiffness of both articular cartilage and the model material in isotonic PBS buffer and hypertonic PBS. We performed measurements by exchanging the buffer in the fluid cell of the AFM without moving the positions of the tip and sample. We expected that, as a result of osmotic effects, an increase in salt concentration would decrease water content and increase the nanostiffness of the gel phase. Also, we wanted to determine how much a decrease in water content in the gel phase would affect the overall microstiffness. As shown in Fig. 2.3 *A*, the change to hypertonic PBS increased the slope of the cartilage microstiffness by 21% but did not affect its unimodal frequency distribution. Fig. 2.3 *B* shows the corresponding effects of the change from isotonic to hypertonic PBS on cartilage nanostiffness. The bimodal distribution of nanostiffness was maintained. However, the slope of the lower peak increased by 28%, whereas the increase in slope of the higher peak was insignificant.
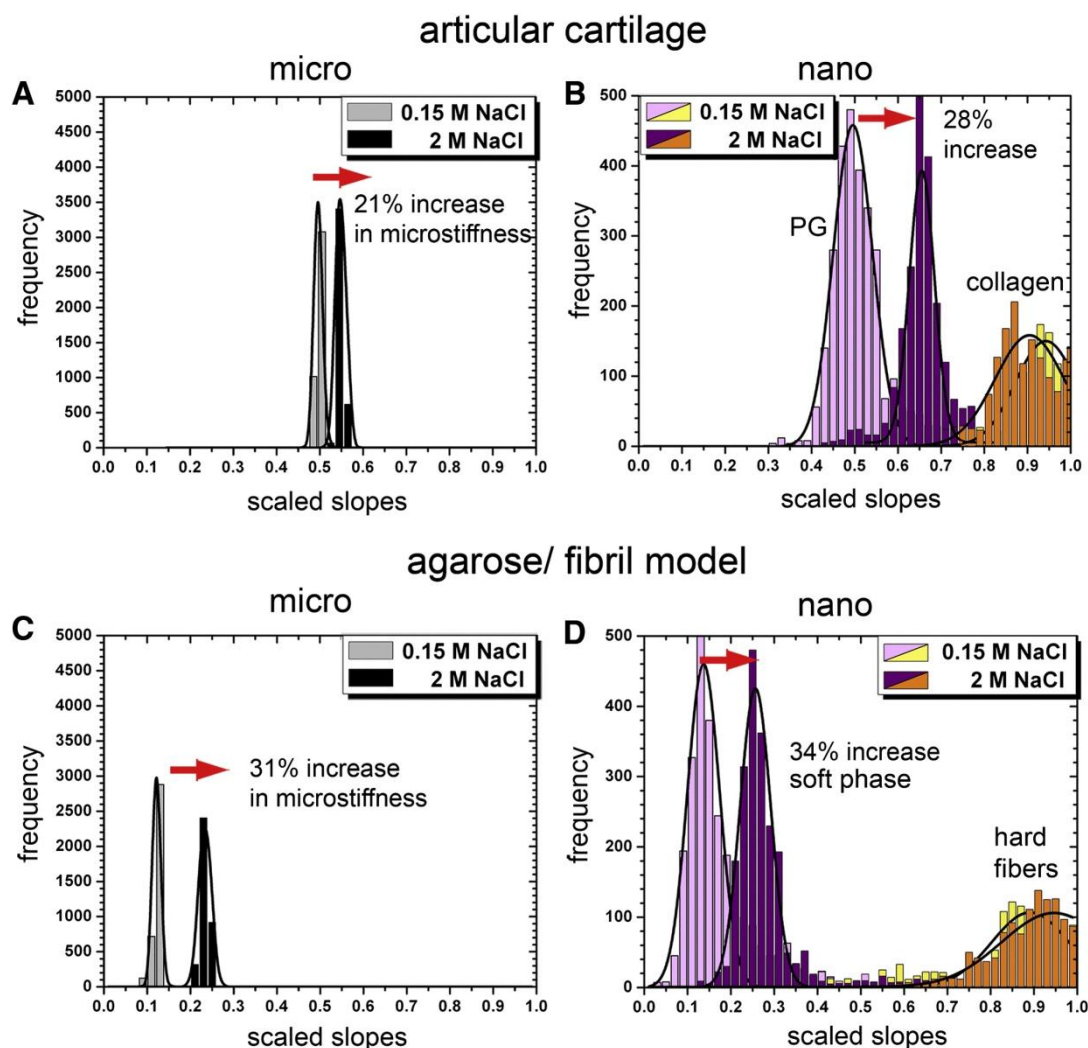
Figure 2.3. Stiffness distributions of cartilage and the model material at the micro- and nanometer scales and at two different ionic strengths of the PBS bathing solution. Stiffness is expressed as the scaled slopes of the IT-AFM unloading curves (see text)

Fig. 2.3, *C* and *D*, reveal the analogous results for the model material. As in cartilage, the microstiffness (Fig. 2.3 *C*) of the model material was also unimodal under both ionic strengths, but hypertonicity increased the stiffness slope by 31%. Again, as in cartilage, the nanostiffness (Fig. 2.3 *D*) was bimodal. Hypertonicity increased the stiffness (slope) of the lower peak by 34%, whereas the increase in slope of the higher peak was again negligible. In contrast, an agarose model material lacking the chondroitin sulfate moiety did not change the stiffness at either scale when exposed to hypertonic PBS (data not shown).

2.5 Discussion

Micro- versus nanometer-scale dynamic stiffness measurements

Fig. 2.1 shows what the indenter "sees" during imaging and what it "feels" in indentation testing when the articular cartilage surface is probed at the (*A*) micrometer or (*B*) nanometer scale. In particular, the micrometer-size tips assess the overall tissue resistance to deformation, where multiple structural elements of the tissue are deformed in concert. In contrast, a nanometer-sized tip can assess the stiffness of cartilage at the level of the fibrils alone and the gel alone. Stiffness changes potentially reveal structural changes, especially in the gel phase. This information is relevant because of the important role played by PGs (in particular the charged glycosaminoglycan chains) in normal cartilage function and the structural changes that occur in aging and osteoarthritis [12, 16, 25, 29, 30].

Source of unimodal microstiffness distributions in articular cartilage

For both cartilage and the model material, indentation stiffness at the micrometer scale, as shown in Fig. 2.2, *A–D*, and *I–L*, reveals a uniform appearance in both images and force maps, and a homogeneous (unimodal) distribution of stiffness values. This homogeneity can be explained by the large size of the IT-AFM tip relative to the molecular-scale structures within the cartilage, i.e., the size of a 10-μm-diameter tip is three orders of magnitude larger than the nanometer-scale PG structures and two orders of magnitude larger than the collagen fibril meshwork of typically $d = 50–150$ nm in articular cartilage.

Source of bimodal nanostiffness distributions in articular cartilage

We hypothesized that the interaction between the nanoindenter and the PG gel in articular cartilage would produce a lower stiffness peak, and the interaction with the resilient collagen fibrils would produce a higher stiffness peak, as shown in Fig. 2.2 *G*. The results obtained at the nanometer-scale with the model material also showed a bimodal distribution of stiffness, as was observed in cartilage. In addition, exposing the model material to hypertonic saline instead of isotonic saline, as shown in Fig. 2.3, shifted the lower stiffness peaks upward while the upper stiffness peak remained unchanged. Since in both cartilage and the model material only the porous gel structure with a high density of negatively charged surface is influenced by changes in ionic strength, these results strongly support our hypothesis that the lower peak represents the stiffness of the PG gel, whereas the upper peak is a measure of the stiffness of the collagen fibrils.

Relative stiffness of cartilage and the model material

The structural and physicochemical differences between cartilage and our model system explain the differences in stiffness at both the micro- and nanometer scales.

1) The collagen fibrils of cartilage form a 3D collagen meshwork with extensive cross-linking by covalent bonds, which provides superior resistance to deformation but also greatly inhibits the movement of the soft PG moiety during loading. Because of its low permeability, the cartilage initially tends to deform rather than decrease in volume, and consequently places the collagen meshwork under tension, resulting in a high initial overall stiffness.

2) In contrast, in the model material, the PEGT/PBT fibrils are neither cross-linked nor spatially stabilized by any strong interactions, and therefore do not offer the same resistance to gel-induced deformation.

Accuracy of calculated values of E^* for collagen and PEGT/PBT fibrils

A spring constant of $k = 0.06$ N/m is optimal for probing the gel phase, but it does not allow one to quantitatively measure the stiffness of the collagen fibrils with the same accuracy. To compute values of nanostiffness from the slopes, we employed the calibration curve established by Stolz et al. [24]: $y(x) = (21/(1 - x)) - 21$. However, this calibration curve exhibits an asymptotic behavior that results in large errors for slopes close to one. Since it is difficult to reliably measure the nanostiffness of hard fibrils using a $k = 0.06$ N/m cantilever, we present the results with large standard deviations (see Appendix II).

Effects of ionic strength on cartilage stiffness

Our measured increase of microstiffness by osmotic loading is in general agreement with previous observations [10, 11, 13, 16, 31-35]. However, we measured a change of microstiffness of only ~21% in hypertonic PBS compared to published values of ~50% in hypertonic PBS and a 1 M NaCl bathing solution [13, 31, 35]. This apparent discrepancy may be explained by major differences between the experimental setups: Eisenberg and Grodzinsky [13] performed confined compression tests by employing a porous indenter (diameter $d = 6.4$ mm) that was capable of taking up and retaining significant amounts of water, whereas we performed indentation tests using a much smaller ($d = 10$ μm) spherical indenter. Furthermore, those authors applied much larger forces to the cartilage, which resulted in substantial indentation depths. Also, they trimmed off the surface and thus probed deeper zones, whereas we tested the intact surface by applying indentation depths on the order of only ~1 μm. Therefore, we tested the superficial zone, where PGs are less dense than

in the deeper zones [35, 36]. Moreover, protocols for compression testing of cartilage typically employ much lower loading rates or use a series of short discrete compressive strains to measure the equilibrium stiffness. We measured the dynamic aggregate modulus E^* at a rate of three indentations per second. Cartilage stiffness is strongly affected by the deformation rate, and therefore the higher stiffness measured in this study may be at least partly the result of the higher rates employed.

Relation of IT-AFM cartilage nanostiffness values to reported values for isolated cartilage structures

In previous studies, single collagen fibrils exhibited stiffness in tension and indentation of a few gigapascals [37, 38]. However, it is difficult to directly compare those results with the IT-AFM-measured nanostiffness of collagen in native cartilage. The IT-AFM values reported here are much lower (e.g., 384 kPa). They are in effect a measure of the dynamic bending stiffness of a collagen fibril that is part of a cross-linked meshwork and embedded in the PG moiety. In contrast, the mechanical behavior of isolated aggrecan gels at physiologically relevant concentrations of 20–80 mg/mL [31, 34] exhibited stiffness of only ~1 kPa [39, 40]. However, measurements of the isolated components do not take into account their behavior within the tissue. In particular, PGs in articular cartilage are cross-linked. Therefore, our higher values of $E_{Pg} = 22.3 \pm 1.5$ kPa for the cartilage gel phase measured in situ reflect the intact cross-links in PG. These results are even more plausible when we consider the contribution made by the dynamically cross-linked meshwork of collagen fibrils to the PG nanostiffness.

Value of nanometer-scale dynamic stiffness measurements

Nanomechanical structures govern the functional behavior and success or failure of engineered cartilage. Our composite model provides a material that can be tuned by adjusting the total PEGT/PBT content, fibril length, fibril diameter distribution, and fibril orientation, and by creating an interfibrillar meshwork by introducing covalent cross-links. In addition, the density and other parameters of the agarose/chondroitin sulfate moiety can be modified by varying the charged groups or the concentration of agarose, or including a low concentration of polyacrylamide. Such a tunable artificial tissue could be valuable for interpreting and even predicting structure-mechanical property relationships on different length scales, and the resultant data could be used to further improve engineered cartilage.

2.6 Conclusions

A primary challenge in evidence-based medicine is the need for early detection of various diseases, such as osteoarthritis [25], artherosclerosis [41], and cancer [42], ideally at the presymptomatic stage. AFM-based indentation testing has yielded some encouraging results in terms of detecting systematic changes in the nanostiffness of articular cartilage during the progression of osteoarthritis [43]. Monitoring scale-dependent changes in tissue plasticity during disease progression or in response to different treatment modalities may lead to the development of novel diagnostic tools [44] and therapeutic interventions. Nevertheless, there still remain a number of technical difficulties involving data collection and analysis that must be overcome before AFM-based indentation testing can be moved from the bench to the patient [42]. In this study, we have attempted to explain the observed scale-dependent stiffness of articular cartilage when measured by IT-AFM, and to rationalize this finding in terms of cartilage biology and pathology [25]. It is hoped that the insights gained will be more generally applicable to scale-dependent analyses, and enhance our understanding of tissue mechanics.

2.7 Acknowledgements

2.8 Appendix I: Deformation Rate-Dependent Mechanical Response of Articular Cartilage

The functional stiffness of articular cartilage is $|E^*|$, the dynamic elastic modulus, as explained in Fig. 2.4. $|E^*|$ is a function of the rate of deformation and can be determined from cyclic load/displacement data. The rate employed should reflect the transient loading-unloading time of normal ambulation (i.e., walking or running). In humans, this is in the range of a few hundred milliseconds [45]. Therefore, we performed indentation measurements at a rate of three complete loading/unloading cycles per second, corresponding to a tip unloading time of ~150 ms. Even after hundreds of loading/unloading cycles, we did not observe any progressive change in the load/displacement behavior, persistent residual indentations (which would be indicative of yield and plastic flow), or effects indicative of material fatigue.
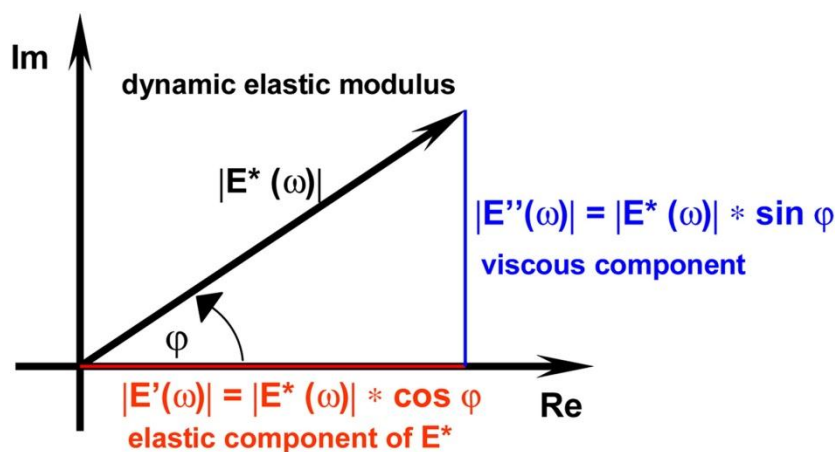
Figure 2.4: Illustration of stiffness parameter relationships for a viscoelastic material subjected to a cyclic dynamic force or deformation. At low frequencies, the magnitudes of force and deformation are out of phase, i.e., they do not reach maximum values simultaneously. This is expressed as the phase angle, φ, between their maximum values. As frequency is increased, φ decreases. In the limit $\varphi = 0$ and $E^* = E'$, i.e., the material behaves as an elastic solid. The out-of-phase behavior is due to the inability of the viscous portions of the material structure to store energy. Thus φ is a measure of energy loss and is also called the loss angle or loss tangent.

2.9 Appendix II: Calculation of Stiffness Values from Indentation Curves

Indentation tests were originally developed in the field of materials science [46] and more recently have been applied to study soft biological tissues at different scales of architectural organization [24, 25]. Mechanical properties, such as the dynamic elastic modulus, E^* (or stiffness, to use the more general term), can be obtained from unloading load-displacement curves as shown in Fig. 2.5 *A*. E^* $(= E)$ was calculated from the following equation:

$$E = \frac{\sqrt{\pi}}{2}\left(1 - v^2\right)\frac{S}{\sqrt{A}}$$

v = Poisson's ratio, S [N/m] = contact stiffness (slope of the initial part of the unloading regime of the load-indentation curve);

$$S = \frac{dP}{dh}$$

P *[N]* = applied force onto the indenter, h *[m]* = indentation; A *[m²]* = is the projected area of the spherical indenter at depth of indentation;

$$A = \pi \cdot \rho^2$$

ρ = radius of the indenter as measured perpendicular to the tip axis at the depth of contact;

$$\rho = \sqrt{h_c\left(2r - h_c\right)}$$

r = radius of indenter; h_c is depth of contact. To simplify the analysis, $h_c = h$ was assumed, where h is the total depth of indentation.

A

spring constant: k = 13.5 N/m
tip radius: r = 5 μm
Poisson number: υ (cartilage) = 0.5
depth of indentation: h_c = (880 -150) nm = 730 nm

contact stiffness: $S = \dfrac{dp}{dh} = \dfrac{50\,nm \cdot 13.5\,N/m}{75\,nm} = 9.0\ N/m$

$\rho = \sqrt{h_c(2r - h_c)}$

$A = \pi \cdot \rho^2$

$E = \dfrac{\sqrt{\pi}}{2}(1-\upsilon^2)\dfrac{S}{\sqrt{A}} = \dfrac{\sqrt{\pi}}{2} \cdot 0.75 \cdot \dfrac{9.0\ N/m}{\sqrt{2.1 \cdot 10^{-11}\,m^2}} = 1.3\,MPa$

deflection on a hard surface

point of contact (poc) = 880 nm

B

k = 0.06 N/m
ν = 0.5

$E = \dfrac{(1-\nu^2)S}{2h \cdot \tan\Theta}$

- –·– mica
- –·– gel 3.5%
- –·– gel 2.25%
- –·– gel 0.5%

E (3.5%) = 146 kPa
E (2.25%) = 19 kPa
E (0.5%) = 6 kPa

geometry of the pyramidal tip

$L = h \cdot \tan\Theta$
$\Theta = 35°$

~130 nm
~310 nm
poc ~520 nm
0 = 30 nm

Figure 2.5. Graphs illustrating data and calculation of the dynamic elastic modulus (E*) at the (A) microscale (microstiffness) and (B) nanoscale (nanostiffness) from IT-AFM data. A shows a force-displacement curve measured with a spherical indenter on articular cartilage. In addition, the curve of constant compliance (1 (nm/nm)) has been drawn in, and exhibits the force related to deflection of the AFM cantilever when in contact with a hard surface that allows no indentation to take place. *B* shows data and calculations of the dynamic elastic nanoscale modulus (nanostiffness) exemplified on three agarose gels exhibiting strengths of 0.5%, 2.25%, and 3.5%. The graph displays the corresponding averaged force-displacement curves.

For the pyramidal tips as shown in Fig. 2.5 *B*, *E* is calculated as follows:

$$E = \frac{\left(1 - v^2\right)S}{2h \cdot \tan\theta}$$

where *θ* is the half-opening angle of the tip (Fig. 5, *inset*).

The indentation equations are based on Hertz's law, which is only true for linear elastic materials. The rationale for using them in this application is that the measured displacements are small and the displacement rate is high. Further, a Poisson's ratio of 0.5 was assumed, i.e., it was assumed that volume was conserved during deformation. Reported values of Poisson's ratio for cartilage range from 0.0 to 0.4, and also likely depend on deformation rates (see Table 3 in Mankin et al. [47]. Consequently, the values of E^{*} reported here are approximate and to some extent peculiar to the experimental methods and calculation assumptions employed.

2.10 Appendix III: Accuracy of Measuring Stiffness

If the cantilever is much stiffer than the stiffness of the material being indented, it will not deflect much and is thus an insensitive means of measuring force. If it exhibits a too-low spring constant, then too little indentation will occur at a given force. In particular, in IT-AFM on cartilage with a nanometer-size indenter tip, the probe will interact with both the gel phase and the much stiffer collagen fibrils. Therefore, both a well-matched, low-stiffness cantilever (for testing the gel phase) and a higher-stiffness cantilever (for testing the collagen fibrils) are required to prevent errors due to mismatch of the spring constant in stiffness measurements. Unfortunately, the stiffness of the cantilever cannot be adjusted during the measurement and has to be selected in advance. In our work, the selected spring constant value, *k* = 0.06 N/m, was suitable for accurately testing the gel phase; however, it reduced the accuracy of measurements of the collagen fibrils, as expressed as large standard deviations in the calculated stiffness values. Similarly, the spring constant value, *k* = 0.06 N/m, was suitable for accurately testing soft gels (~0.5% agarose), as shown in <u>Appendix II</u> (<u>Fig. 5</u>, *B*), but it gradually overestimated the calculated values of nanostiffness for higher gel strengths. The IT-AFM measurement is most sensitive when the cantilever spring constant, *k*, and the contact stiffness, $S = dP/dh \sim 2rE/(1 - v^2)$, are of similar magnitude.

A calibration curve (sometimes also called blind calibration) was established in a previous study [24] to improve the quantitative capabilities of this method. The main advantage of this approach is that actual knowledge of the tip shape is not required.

2.11 References

1.   Bhosale, A.M. and J.B. Richardson, Articular cartilage: structure, injuries and review of management. Br Med Bull, 2008. **87**: p. 77-95.

2.   Aspden, R.M. and D.W.L. Hukins, Collagen Organization in Articular-Cartilage, Determined by X-Ray-Diffraction, and Its Relationship to Tissue Function. Proceedings of the Royal Society of London Series B-Biological Sciences, 1981. **212**(1188): p. 299-304.

3.   Mow, V.C., A. Ratcliffe, and A.R. Poole, Cartilage and Diarthrodial Joints as Paradigms for Hierarchical Materials and Structures. Biomaterials, 1992. **13**(2): p. 67-97.

4.   Miller, E.J. and S. Gay, The Collagens - an Overview and Update. Methods in Enzymology, 1987. **144**: p. 3-41.

5.   Yasuda, T., et al., Peptides of type II collagen can induce the cleavage of type II collagen and aggrecan in articular cartilage. Matrix Biology, 2006. **25**(7): p. 419-429.

6.   Blaschke, U.K., et al., Collagen XI nucleates self-assembly and limits lateral growth of cartilage fibrils. Journal of Biological Chemistry, 2000. **275**(14): p. 10370-10378.

7.   Bruckner, P. and M. van der Rest, Structure and function of cartilage collagens. Microsc Res Tech, 1994. **28**(5): p. 378-84.

8.   Prockop, D.J., et al., Biosynthesis of Collagen and Its Disorders .1. New England Journal of Medicine, 1979. **301**(1): p. 13-23.

9.   Hansen, U., D.G. Seidler, and P. Bruckner, Supramolecular organization of heterotypic fibrils by decorin. Matrix Biology, 2006. **25**: p. S73-S73.

10.   Hansen, U. and P. Bruckner, Macromolecular specificity of collagen fibrillogenesis - Fibrils of collagens I and XI contain a heterotypic alloyed core and a collagen I sheath. Journal of Biological Chemistry, 2003. **278**(39): p. 37352-37359.

11.   Wu, J.J. and D.R. Eyre, Cartilage Type-Ix Collagen Is Cross-Linked by Hydroxypyridinium Residues. Biochemical and Biophysical Research Communications, 1984. **123**(3): p. 1033-1039.

12.   Eyre, D., Collagen of articular cartilage. Arthritis Research, 2002. **4**(1): p. 30-35.

13.   Maroudas, A., Physicochemical properties of articular cartilage. In Adult Articular Cartilage, 2nd edition Edited by Freeman MAR London: Pitman Medical, 1979: p. 215–290.

14.   DeGroot, J., The AGE of the matrix: chemistry, consequence and cure. Current Opinion in Pharmacology, 2004. **4**(3): p. 301-305.

15.   Bank, R.A., et al., Ageing and zonal variation in post-translational modification of collagen in normal human articular cartilage - The age-related increase in non-

enzymatic glycation affects biomechanical properties of cartilage. Biochemical Journal, 1998. **330**: p. 345-351.

16.   DeGroot, J., et al., Accumulation of advanced glycation end products as a molecular mechanism for aging as a risk factor in osteoarthritis. Arthritis and Rheumatism, 2004. **50**(4): p. 1207-1215.

17.   Sasaki, N. and S. Odajima, Elongation mechanism of collagen fibrils and force-strain relations of tendon at each level of structural hierarchy. Journal of Biomechanics, 1996. **29**(9): p. 1131-1136.

18.   Sasaki, N. and S. Odajima, Stress-strain curve and Young's modulus of a collagen molecule as determined by the X-ray diffraction technique. Journal of Biomechanics, 1996. **29**(5): p. 655-658.

19.   Breen, E.C., Mechanical strain increases type I collagen expression in pulmonary fibroblasts in vitro. Journal of Applied Physiology, 2000. **88**(1): p. 203-209.

20.   Sun, Y.L., et al., Stretching type II collagen with optical tweezers. Journal of Biomechanics, 2004. **37**(11): p. 1665-1669.

21.   Luo, Z.P., et al., Single molecule mechanical properties of type II collagen and hyaluronan measured by optical tweezers. Biorheology, 2004. **41**(3-4): p. 247-254.

22.   Staple, D.B., et al., Stretching, Unfolding, and Deforming Protein Filaments Adsorbed at Solid-Liquid Interfaces Using the Tip of an Atomic-Force Microscope. Physical Review Letters, 2009. **102**(12): p. -.

23.   Maroudas, A., et al., Aggrecan turnover in human articular cartilage: Use of aspartic acid racemization as a marker of molecular age. Archives of Biochemistry and Biophysics, 1998. **350**(1): p. 61-71.

24.   Hardingham, T.E., The role of link-protein in the structure of cartilage proteoglycan aggregates. Biochem J, 1979. **177**(1): p. 237-47.

25.   Heinegard, D. and V.C. Hascall, Aggregation of cartilage proteoglycans. 3. Characteristics of the proteins isolated from trypsin digests of aggregates. J Biol Chem, 1974. **249**(13): p. 4250-6.

26.   Buckwalter, J.A. and H.J. Mankin, Articular cartilage .1. Tissue design and chondrocyte-matrix interactions. Journal of Bone and Joint Surgery-American Volume, 1997. **79A**(4): p. 600-611.

27.   Bayliss, M.T. and S.Y. Ali, Age-related changes in the composition and structure of human articular-cartilage proteoglycans. Biochem J, 1978. **176**(3): p. 683-93.

28.   Bayliss, M.T. and P.J. Roughley, The properties of proteoglycan prepared from human articular cartilage by using associative caesium chloride gradients of high and low starting densities. Biochem J, 1985. **232**(1): p. 111-7.

29.   Roughley, P.J. and R.J. White, Age-related changes in the structure of the proteoglycan subunits from human articular cartilage. J Biol Chem, 1980. **255**(1): p. 217-24.

30.   Velikii, N.N. and Chagobet.Rv, An Enquiry into Exchangability of Cartilage Sulphate Chondroitin in Control and a-Vitamine Deficient Chickens with Use of Different Labelled Forerunners. Doklady Akademii Nauk Sssr, 1970. **193**(6): p. 1409-&.

31.   Plaas, A.H.K., et al., Chemical and immunological assay of the nonreducing terminal residues of chondroitin sulfate from human aggrecan. Journal of Biological Chemistry, 1997. **272**(33): p. 20603-20610.

32.   Midura, R.J., et al., Nonreducing End Structures of Chondroitin Sulfate Chains on Aggrecan Isolated from Swarm Rat Chondrosarcoma Cultures. Journal of Biological Chemistry, 1995. **270**(14): p. 8009-8015.

33.   Scott, J.E., et al., The chemical morphology of age-related changes in human intervertebral disc glycosaminoglycans from cervical, thoracic and lumbar nucleus pulposus and annulus fibrosus. J Anat, 1994. **184 (Pt 1)**: p. 73-82.

34.   Bolis, S., C.J. Handley, and W.D. Comper, Passive Loss of Proteoglycan from Articular-Cartilage Explants. Biochimica Et Biophysica Acta, 1989. **993**(2-3): p. 157-167.

35.   Mow, V.C., et al., Biphasic Creep and Stress-Relaxation of Articular-Cartilage in Compression - Theory and Experiments. Journal of Biomechanical Engineering-Transactions of the Asme, 1980. **102**(1): p. 73-84.

36.   Soltz, M.A. and G.A. Ateshian, Experimental verification and theoretical prediction of cartilage interstitial fluid pressurization at an impermeable contact interface in confined compression. Journal of Biomechanics, 1998. **31**(10): p. 927-934.

37.   Mak, A.F., The Apparent Viscoelastic Behavior of Articular-Cartilage - the Contributions from the Intrinsic Matrix Viscoelasticity and Interstitial Fluid-Flows. Journal of Biomechanical Engineering-Transactions of the Asme, 1986. **108**(2): p. 123-130.

38.   Ateshian, G.A., The role of interstitial fluid pressurization in articular cartilage lubrication. Journal of Biomechanics, 2009. **42**(9): p. 1163-1176.

39.   Morgelin, M., et al., The Cartilage Proteoglycan Aggregate - Assembly through Combined Protein-Carbohydrate and Protein-Protein Interactions. Biophysical Chemistry, 1994. **50**(1-2): p. 113-128.

40.   Papagiannopoulos, A., et al., Solution structure and dynamics of cartilage aggrecan. Biomacromolecules, 2006. **7**(7): p. 2162-2172.

41.   Kiani, C., et al., Structure and function of aggrecan. Cell Research, 2002. **12**(1): p. 19-32.

42.   Roberts, B.J., A. Unsworth, and N. Mian, Modes of Lubrication in Human Hip Joints. Annals of the Rheumatic Diseases, 1982. **41**(3): p. 217-224.

43.   Radin, E.L., D.A. Swann, and P.A. Weisser, Separation of a Hyaluronate-Free Lubricating Fraction from Synovial Fluid. Nature, 1970. **228**(5269): p. 377-&.

44.   Hills, B.A., Oligolamellar Lubrication of Joints by Surface-Active Phospholipid. Journal of Rheumatology, 1989. **16**(1): p. 82-91.

45.   McCutchen, C.W., The frictional properties of animal joints. Wear. **5**(1): p. 1-17.

46.   Walker, P.S., et al., Boosted Lubrication in Synovial Joints by Fluid Entrapment and Enrichment. Annals of the Rheumatic Diseases, 1968. **27**(6): p. 512-&.

47.   Ateshian, G.A., A theoretical formulation for boundary friction in articular cartilage. Journal of Biomechanical Engineering-Transactions of the Asme, 1997. **119**(1): p. 81-86.

48.   Neu, C.P., K. Komvopoulos, and A.H. Reddi, The interface of functional biotribology and regenerative medicine in synovial joints. Tissue Engineering Part B-Reviews, 2008. **14**(3): p. 235-247.

49.   Mccutchen, C.W., Sponge-Hydrostatic and Weeping Bearings. Nature, 1959. **184**(4695): p. 1284-1285.

50.   Morrell, K.C., et al., Corroboration of in vivo cartilage pressures with implications for synovial joint tribology and osteoarthritis causation. Proceedings of the National Academy of Sciences of the United States of America, 2005. **102**(41): p. 14819-14824.

51.   Noyori, K., T. Takagi, and H.E. Jasin, Characterization of the macromolecular components of the articular cartilage surface. Rheumatology International, 1998. **18**(2): p. 71-77.

52.   Schumacher, B.L., et al., A Novel Proteoglycan Synthesized and Secreted by Chondrocytes of the Superficial Zone of Articular-Cartilage. Archives of Biochemistry and Biophysics, 1994. **311**(1): p. 144-152.

53.   Sarma, A.V., G.L. Powell, and M. LaBerge, Phospholipid composition of articular cartilage boundary lubricant. Journal of Orthopaedic Research, 2001. **19**(4): p. 671-676.

54.   Schmidt, T.A., et al., Boundary lubrication of articular cartilage - Role of synovial fluid constituents. Arthritis and Rheumatism, 2007. **56**(3): p. 882-891.

55.   Zhou, S., Z. Cui, and J.P. Urban, Factors influencing the oxygen concentration gradient from the synovial surface of articular cartilage to the cartilage-bone interface: a modeling study. Arthritis Rheum, 2004. **50**(12): p. 3915-24.

56.   Stockwell, R.A., The cell density of human articular and costal cartilage. J Anat, 1967. **101**(Pt 4): p. 753-63.

57.   Vignon, E., et al., Cell Density of Human Femoral-Head Cartilage. Clinical Orthopaedics and Related Research, 1976(121): p. 303-308.

58.   Saris, D.B.F., et al., Characterized chondrocyte implantation results in better structural repair when treating symptomatic cartilage defects of the knee in a randomized controlled trial versus microfracture. American Journal of Sports Medicine, 2008. **36**(2): p. 235-246.

59.   Robert, H., et al., Treatment of deep cartilage defects in the knee with autologous chondrocyte transplantation: a review of 28 cases. Revue De Chirurgie Orthopedique Et Reparatrice De L Appareil Moteur, 2007. **93**(7): p. 701-709.

60.   Brittberg, M., et al., Treatment of Deep Cartilage Defects in the Knee with Autologous Chondrocyte Transplantation. New England Journal of Medicine, 1994. **331**(14): p. 889-895.

61.   Galois, L., et al., [Cartilage tissue engineering: state-of-the-art and future approaches]. Pathol Biol (Paris), 2005. **53**(10): p. 590-8.

62.   Loparic, M., et al., Micro- and nanomechanical analysis of articular cartilage by indentation-type atomic force microscopy: validation with a gel-microfiber composite. Biophys J, 2010. **98**(11): p. 2731-40.

63.   Liu, W.H., K. Bonin, and M. Guthold, Easy and direct method for calibrating atomic force microscopy lateral force measurements. Review of Scientific Instruments, 2007. **78**(6): p. -.

Chapter 3

Sliding motion modulates stiffness and friction coefficient at the surface of tissue engineered cartilage

Marko Loparic*, Sibylle Grad*, Robi Peter, Martin Stolz,

Ueli Aebi, Mauro Alini

*Both authors contributed equally to this study

3.1 Abstract

Objective: Functional cartilage tissue engineering aims to generate grafts with a functional surface, similar to that of authentic cartilage. Bioreactors that stimulate cell-scaffold constructs by simulating natural joint movements hold great potential to generate cartilage with adequate surface properties. In this study two methods based on atomic force microscopy (AFM) were applied to obtain information about the quality of engineered graft surfaces. For better understanding of the molecule–function relationships, AFM was complemented with immunohistochemistry.

Methods: Bovine chondrocytes were seeded into polyurethane scaffolds and subjected to dynamic compression, applied by a ceramic ball, for 1 h daily [loading group 1 (LG1)]. In loading group 2 (LG2), the ball additionally oscillated over the scaffold, generating sliding surface motion. After 3 weeks, the surfaces of the engineered constructs were analyzed by friction force and indentation-type AFM (IT-AFM). Results were complemented and compared to immunohistochemical analyses.

Results: The loading type significantly influenced the mechanical and histological outcomes. Constructs of LG2 exhibited lowest friction coefficient and highest micro- and nanostiffness. Collagen type II and aggrecan staining were readily observed in all constructs and appeared to reach deeper areas in loaded (LG1, LG2) compared to unloaded scaffolds. Lubricin was specifically detected at the top surface of LG2.

Conclusion: This study proposes a quantitative AFM-based functional analysis at the micrometer- and nanometer scale to evaluate the quality of cartilage surfaces. Mechanical testing (load-bearing) combined with friction analysis (gliding) can provide important information. Notably, sliding-type biomechanical stimuli may favor (re-)generation and maintenance of functional articular surfaces and support the development of mechanically competent engineered cartilage.

3.2 Introduction

Articular cartilage is a smooth, wear-resistant tissue that adsorbs impact forces and allows for almost frictionless gliding of the two opposing surfaces within a joint. The articular surface has a unique function in cartilage homeostasis and nutrition, but also in filtering large proinflammatory macromolecules present in the synovial fluid, thus protecting the cartilage from immune reactions [1]. It is characterized by high level of collagen fibrils oriented parallel to the joint surface, lower levels of proteoglycans in comparison to the underlying zones of cartilage, and a high concentration of densely packed lubricin molecules [1] and [2]. Lubricin, also known as cartilage superficial zone protein or proteoglycan-4, is a large, water-soluble and flexible rod-shaped glycoprotein present in both the synovial fluid and on the cartilage surface [3], [4] and [5]. Several studies have shown that lubricin plays a key role in the protection of the surface from friction and wear in articulating joints [4], [6] and [7]. Hence, the intact cartilage surface has a vital role in providing a highly efficient lubrication mechanism with a low coefficient of friction that is mediated by boundary lubricants such as lubricin and hyaluronan [8]. The direct contact of the superficial zone with the synovial fluid is considered to be important for cartilage function and maintenance [8]. Deterioration of the superficial zone considerably alters cartilage homeostasis and mechanical properties, which often result in the development of osteoarthritis (OA) [9] and [10]. Moreover, the cartilaginous matrix is generated by a low density of chondrocytes, which together with their low metabolic activity and the avascular nature of the cartilaginous tissue results in a limited repair capacity of damaged cartilage [2] and [11].

Articular cartilage injuries and degenerative joint diseases affect a considerable proportion of the population. While cartilage injuries are occurring in all age groups, it is estimated that 68% of individuals older than 55 years have radiographic evidence of OA [12]. Established surgical treatment strategies range from debridement, marrow stimulation techniques, a variety of cell and tissue transplantation techniques, to total joint replacement1 [3]. In particular, autologous chondrocyte transplantation (ACT) and matrix induced chondrocyte implantation (MACI) have been frequently applied in orthopedic practice, but there is still a considerable failure rate [14]. An appropriately developed tissue engineered construct may have better chances to withstand the forces that impact the cartilage during daily activities compared to techniques where chondrocytes are directly administered into the cartilage defect. Surface properties of engineered cartilage

that are similar to native cartilage are likely to be beneficial for tissue homeostasis and mechanical function required for a high success rate.

Engineering of cartilaginous tissue implies culturing of either chondrocytes or mesenchymal stem cells within a three-dimensional natural or synthetic biomaterial [15]. Biomechanical cues are increasingly employed to stimulate the development of functional articular cartilage. A variety of different bioreactors and loading devices have been designed that typically apply dynamic compressive load, shear strain, fluid flow, hydrostatic pressure, or a combination of these stimuli [16]. Our custom designed bioreactor system is based on the implementation of motion patterns which approximate the kinematics of physiological joint motion to support the generation of a tissue with properties similar to native articular cartilage [17]. Studies have shown that dynamic compression and sliding surface motion, applied by a ceramic ball, improves the gene expression and the synthesis of cartilage specific matrix molecules in chondrocytes-scaffold constructs [18], [19] and [20].

Quality control, i.e., measuring the mechanical properties of the tissue engineered cartilage and in particular of the surface zone is crucial for generating tissue engineered cartilage constructs that can be used to repair damaged sites in the joints. Notably, the Food and Drug Administration (FDA) recently requested mechanical data for all articular cartilage repair products in their guidance for "Repair or Replace Knee Cartilage" (ucm072952) [21], which additionally emphasizes the importance of mechanical characterization of cartilage constructs. Recently, atomic force microscopy (AFM) has been proposed to assess cartilage integrity at the micro- and nanometer scale [22], [23] and [24]. Owing to its high scale sensitivity AFM has the potential to not only detect early degenerative changes of the articular surface but also to determine the functional characteristics of an immature and still developing tissue.

Here, we characterized the functional surface properties of tissue engineered cartilage by friction force and indentation-type AFM (IT-AFM). Cell-scaffold constructs that were cultured free swelling were compared with constructs stimulated by dynamic axial compressive loading with or without superimposed sliding surface motion. We hypothesized that the mechanical loading regime which includes sliding motion and hence simulates natural joint movements would generate constructs with surface properties closer to authentic articular cartilage.

3.3 Materials and Methods

Polyurethane scaffold

Polyurethane scaffolds (8 mm diameter; 4 mm height) with interconnected pores had an average pore size of 90–300 μm and a pore-to-volume ratio of 85% [25]. The polymers were synthesized with hexamethylene diisocyanate, poly(ε-caprolactone) diol with a molecular mass of 530 Da, and isosorbide diol (1,4:3,6-dianhydro-d-sorbitol) as chain extender [25]. Scaffolds were sterilized in a cold-cycle (37°C) ethylene oxide process and subsequently evacuated at 45°C and 150 mbar for 3–4 days. Before cell seeding, the scaffolds were evacuated in the presence of growth medium for 1 h, in order to wet the hydrophobic polymer.

Chondrocyte isolation, seeding and culture conditions

Chondrocytes were isolated from full thickness metacarpal joint cartilage of 4–8 months old calves using sequential pronase and collagenase digestion [26]. Isolated chondrocytes (5×10^6/scaffold) were suspended in 75 μL fibrinogen solution. Then an equal volume of thrombin solution was added, the suspension was mixed and infiltrated into the pores of the scaffold. This was achieved by pressing the elastic and resilient scaffold into the cell suspension and slowly releasing it, causing the cells to be imbibed. With this method a uniform cell distribution throughout the scaffold is obtained [27]. The fibrin components were provided by Baxter Biosurgery (Vienna, Austria). The final concentrations of the fibrin gel were 17 mg/mL fibrinogen, 0.5 U/mL thrombin, and 665 KIU/mL aprotinin. Constructs were incubated for 1 h (37°C, 5% CO_2, 95% humidity) to permit fibrin gelation before adding growth medium (Dulbecco's Modified Eagle's medium (DMEM) supplemented with antibiotics, 10% fetal calf serum (FCS), 50 μg/mL ascorbic acid, 40 μg/mL l-proline, non-essential amino acids, and 500 KIU/mL aprotinin). Cell-scaffold constructs were placed into the sample holders (Fig. 1), and 3 mL of growth medium were added. Medium was changed every second day, and conditioned medium was collected for analysis of sulfated glycosaminoglycan (sGAG). After 6 days in free swelling culture, the samples were exposed to mechanical loading regimes as described below.
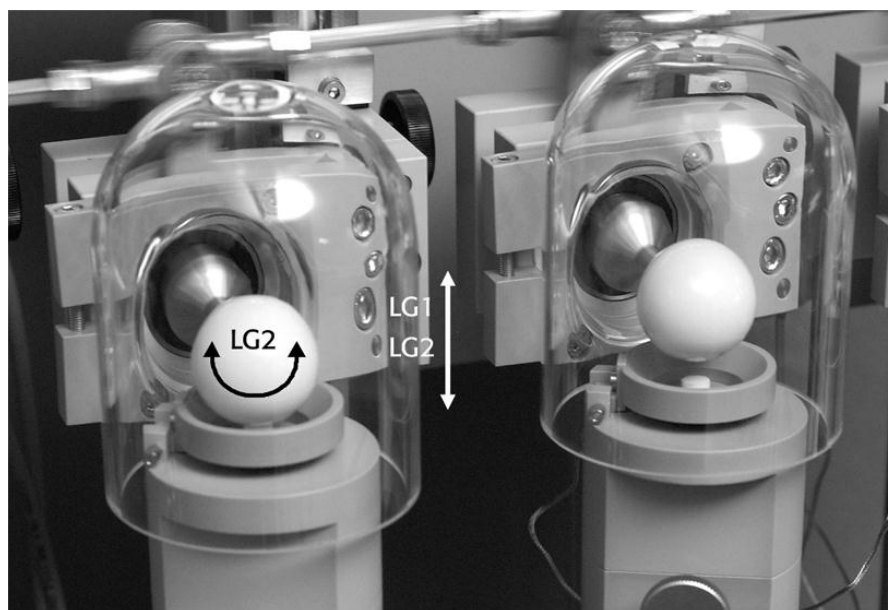
Figure 3.1: Bioreactor used for mechanical conditioning of cell-scaffold constructs. A ceramic ball was pressed onto the cell-seeded scaffold. In scaffolds of LG1 and LG2, the ball oscillated at 1 Hz between 10% and 20% of the scaffold height (in the center of the construct). In scaffolds of LG2, the ball additionally oscillated about an axis perpendicular to the scaffold axis at amplitude of ±25° and 1 Hz.

Mechanical loading

Mechanical conditioning of cell-scaffold constructs was performed using our four-station bioreactor system, which was installed in a CO2 incubator at 37°C, 5% CO2, 85% humidity (Fig. 1) [17]. At each station a commercially available ceramic hip ball (32 mm in diameter) was pressed onto a cell-seeded scaffold to provide a constant displacement of 0.6 mm or 15% of the scaffold height (measured in the construct center). In scaffolds of loading groups 1 and 2 (LG1 and LG2) the ball oscillated in a sinusoidal manner between 0.4 mm and 0.8 mm, i.e., between 10% and 20%, of the scaffold height at a frequency of 1 Hz. In scaffolds of LG2, interface motion was generated in addition to the cyclic compressive loading by reciprocating rotation of the ball about an axis perpendicular to the scaffold axis at amplitude of ±25° and 1 Hz. This regime of dynamic axial compression with superimposed sliding motion is suggested to more closely simulate joint articulation compared to axial compression alone [17].

One hour of mechanical loading was performed daily for 6 days/week. In-between loading cycles constructs were kept in a free swelling condition (without ball contact). Construct analysis was performed after a total culture time of 4 weeks including 3 weeks of mechanical loading. Unloaded scaffolds served as controls.

Sample preparation for friction and stiffness measurement by AFM

The cylindrical cell-scaffold constructs were cut vertically into four equal sections. Each quadrant was glued onto a round Teflon disk with the 5 min Epoxy glue (Devcon, Danvers, Mass., USA). An additional supporting plastic ring around the sample was used in order to ensure full immersion of the sample in phosphate buffered saline (PBS) containing protease inhibitor cocktail (Complete, Boehringer Mannheim). Half of the sample (two quadrants) was used for indentation testing, while the other half was used for friction testing. Articular cartilage was harvested from 4 to 8 months old calves and also tested for indentation and friction as described below.

Indentation testing

Indentation testing was performed using the Nanoscope IIIa AFM (Veeco, Santa Barbara, USA) as described previously [23]. Briefly, stiffness values were measured at the micrometer- and nanometer scale. Micrometer scale measurements were performed using borosilicate glass spheres (r = 5 ± 1 μm, Duke Scientific Corporation, Palo Alto, USA) that were glued onto tip-less cantilevers, lengths l = 350 μm, spring constants of k = 0.3 ± 0.1 N/m (NSC12, MikroMasch, Tallinn, Estonia). For nanometer-scale stiffness measurement, silicon nitride pyramidal tips (height = 20 ± 4 μm, cantilever k = 0.08 ± 0.02 N/m, CSC38/Si3N4/AlBS, MikroMasch, Tallinn, Estonia) were used. Prior to the experiment, the deflection sensitivity and the spring constant were measured for each cantilever. The normal spring constant was experimentally determined by the Sader calibration method [28]. Stiffness was calculated from load-displacement curves recorded on at least eight random locations of the sample surface at two different maximum applied forces, i.e., 2.4 nN (nanometer scale) and 12.5 nN (micrometer scale). Indentation testing was performed at 3 Hz. Stiffness was calculated from the measured raw AFM curves. For the automated analysis of AFM data custom made LABVIEW software (National Instruments, USA) was used. The contact point was determined by applying a polynomial fit to raw force curves according to a published algorithm [29] and [30]. The slope of each data point is calculated by performing a linear fit to the upper 50% of the unloading force curve. Stiffness (elastic modulus) was calculated accordingly as described by Oliver and Pharr [31].

Friction testing

Friction measurements were performed using the Nanowizard I BioAFM (JPK, Berlin, Germany). Tip-less cantilevers (vertical k = 0.2 ± 0.05 N/m) with attached microsphere probes were used. Borosilicate microsphere probes (5 ± 1 μm, Duke Scientific Corporation, Palo Alto, USA) were coated with tetra-ethylene glycol to reduce unspecific adhesion between the probe and sample surface [32] and [33]. Friction was measured by recording the lateral deflection signal as the probe scanned over the samples at a velocity of 40 μm/s and scan angle of 90°. The friction force was calculated by multiplying the half-width of the friction loop (one-half of the voltage difference between mean lateral trace and mean lateral retrace) by the torsional calibration factor (nN/V). The torsional calibration factor was determined by lateral manipulation of small glass fibers as described previously [33]. Friction forces were measured on at least three different sites of the samples and with five different vertical loading forces (10 nN, 20 nN, 30 nN, 40 nN, 50 nN) applied. Finally, the friction forces were plotted as a function of the vertical loading force, with the resulting slope defining the coefficient of friction.

Biochemical analysis

Scaffolds were digested overnight using 0.5 mg/mL proteinase K at 56°C. The DNA content was measured spectrofluorometrically using Hoechst 33258 dye (Polysciences Inc., Warrington, PA, USA) and purified calf thymus DNA as a standard. The amount of sGAG was determined by the dimethylmethylene blue dye method, using bovine chondroitin sulfate as a standard. Total sGAG content of the culture media was also measured to assess the release of matrix molecules from the constructs into the media.

Immunohistochemistry

For immunohistochemical analysis scaffolds were fixed in methanol at 4°C and incubated in 5% d(+)sucrose solution in PBS for 12 h at 4°C before cryo-sectioning at 12 μm. After enzyme pretreatment (0.25 U/mL Chondroitinase AC for aggrecan and 0.5 U/mL Hyaluronidase for collagen types I and II staining), sections were blocked with 5% horse serum. Then the sections were incubated using primary antibodies against collagen type I (Sigma–Aldrich, Inc., Saint Louis, Missouri, USA; 1:2000 dilution), collagen type II (CIICI supernatant; Development Studies Hybridoma Bank (DSHB), University of Iowa, Iowa City; IA, USA; 1:6 dilution), aggrecan (12/21/1-C-6; DSHB; 1:10 dilution) [34] and [35], and lubricin (3A4; 1:400 dilution; kindly provided by Bruce Caterson, Cardiff University, UK). Before detection of aggrecan, a neo-epitope had to be generated by

reduction and alkylation steps [36]. Primary antibody was applied over night at 4°C, followed by biotinylated secondary antibody (30 min, RT) and the preformed avidin–biotin–peroxidase complex [30 min, room temperature (RT)]. All detection reagents were taken from the Vectastain Elite ABC Kit (Vector Laboratories). As a chromogen 3, 3′-diaminobenzidine monomer (DAB) was used. Sections from bovine articular cartilage that were prepared and probed according to the same protocol served as positive controls. For the negative controls, the primary antibody was replaced by PBS.

Statistical analysis

Values are reported as mean ± 95% confidence interval. Stiffness values (n = 5), coefficient of friction (n = 4), and sGAG content (n = 8) were evaluated by analysis of variance (ANOVA) and least significant difference (LSD) post hoc testing using SPSS v.16.0 to reveal differences between loaded and control scaffolds and between loading groups. P < 0.05 was considered as significant.

3.4 Results

Indentation Testing

Both micrometer scale and nanometer-scale stiffness were different between the groups. Lowest stiffness values were measured for the unloaded control group. For constructs from LG1, the average nanostiffness was 15.9 ± 6.4 kPa (P = 0.053 vs control), while microstiffness values of 23.9 ± 9.2 kPa were recorded (P = 0.055 vs control). Constructs of LG2 demonstrated highest stiffness values at both the nanometer scale (33.3 ± 6.5 kPa) and micrometer scale (46.6 ± 10.2 kPa) levels. Stiffness measurements from LG2 were significantly enhanced compared to both unloaded controls and scaffolds of LG1 (Fig. 2). For bovine cartilage nanostiffness values of 45.7 ± 13.6 kPa were measured, while microstiffness is in the range of 0.8 MPa (data not shown).
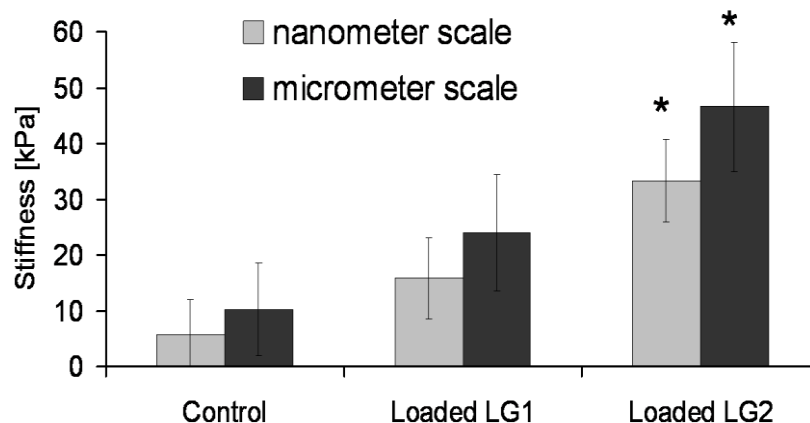
Figure 3.2: Stiffness of cell-scaffold constructs measured by nanoscale and mircoscale indentation type atomic force microscopy. Constructs of LG1 were stimulated by dynamic compression only; constructs of LG2 were stimulated by dynamic compression and sliding surface motion; controls were not loaded. Nanostiffness was significantly higher in LG2 vs control (P < 0.001) and in LG2 vs LG1 (P = 0.003); microstiffness was significantly higher in LG2 vs control (P < 0.001) and in LG2 vs LG1 (P = 0.007). * = significant difference vs control; # = significant difference vs LG1 (mean ± 95% confidence interval; n = 5).

Friction Coefficient

A coefficient of friction of 0.681 ± 0.172 was measured for unloaded control scaffolds. Compared to the unloaded controls, the coefficient of friction was reduced in cell-scaffold constructs stimulated by axial compression alone (LG1) (0.427 ± 0.326). The surface of constructs exposed to cyclic axial compression combined with sliding surface motion (LG2) demonstrated a significantly decreased coefficient of friction compared to controls (0.251 ± 0.183, P = 0.033) (Fig. 3). For bovine cartilage a friction coefficient of 0.121 ± 0.005 was obtained.
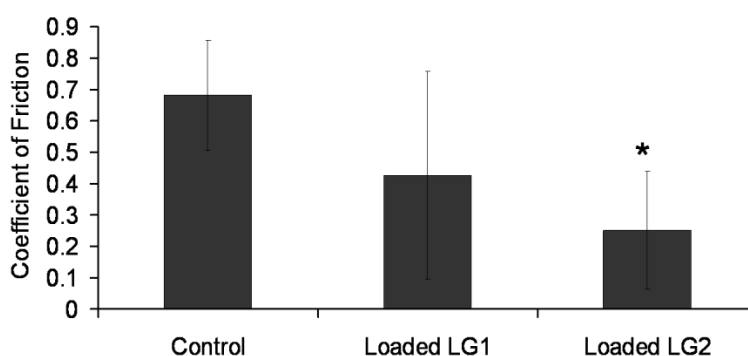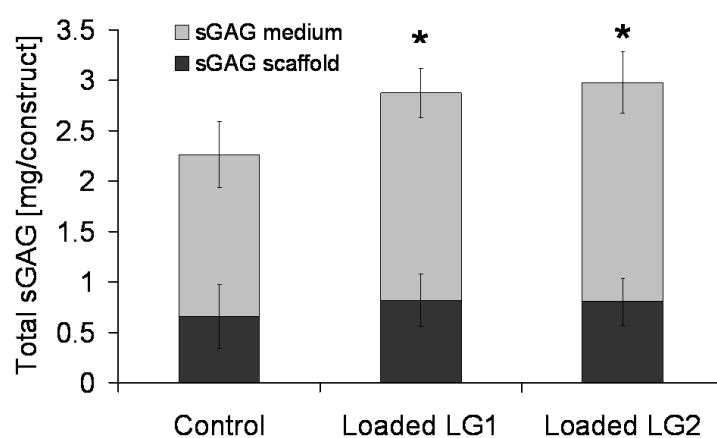

Figure 3.3: Coefficient of friction of the surface of cell-scaffold constructs measured by atomic force microscopy. Constructs of LG1 were stimulated by dynamic compression only; constructs of LG2 were stimulated by dynamic compression and sliding surface motion; controls were not loaded. * = significant difference vs control (P = 0.033) (mean ± 95% confidence interval; n = 4).

Biochemical Analysis

There was no difference in DNA content between the scaffolds of LG1 (35.9 ± 7.7 µg), LG2 (36.5 ± 5.3 µg), and the unloaded controls (34.7 ± 9.5 µg), indicating that mechanical loading had no effect on cell proliferation. Amounts of sGAG retained within the constructs were slightly but not significantly higher in loaded (LG1: 821 ± 181 µg; LG2: 805 ± 163 µg) than in control scaffolds (658 ± 218 µg). However, total amounts of sGAG synthesized by the cells, i.e., sGAG accumulated within scaffolds and released into the medium, were significantly increased in loaded scaffolds (LG1: 2.90 ± 0.29 mg, $P = 0.010$; LG2: 2.96 ± 0.32 mg, $P = 0.006$) compared to unloaded controls (2.23 ± 0.37 mg) (Fig. 4).

Figure 3.4: Total amounts of sulfated glycosaminoglycans (sGAG) retained within cell-scaffold constructs and released into the culture medium. Constructs of LG1 were stimulated by dynamic compression only; constructs of LG2 were stimulated by dynamic compression and sliding surface motion; controls were not loaded. Total amounts of sGAG were significantly higher in LG1 vs control ($P = 0.010$) and in LG2 vs control ($P = 0.006$). * = significant difference vs control (mean ± 95% confidence interval; n = 8).

Immunohistochemistry

While the cell distribution is generally homogeneous after cell seeding, enhanced cell and matrix accumulation at the surface and the edges of the constructs can be noted after longer time in culture. This has often been observed in cell-seeded scaffolds and may be due to increased availability of nutrients at the periphery compared to the center of the constructs [27]. Histochemistry images of tissue engineered constructs and of bovine cartilage are shown in Fig. 5. Pronounced type II collagen staining was observed in both loaded and unloaded constructs over a depth of around 0.3–0.4 mm, while the staining intensity appeared less toward the central areas of the constructs [Fig. 5(a–c)]. In constructs of LG2, the staining appeared more uniform than in constructs of LG1 and in unloaded controls. Collagen type I staining was visible as a thin layer at the surface of loaded constructs, especially from LG2,

which appears similar to the collagen type I distribution in normal articular cartilage [Fig. 5(g, h)]. In non-loaded controls and constructs of LG1, type I collagen staining appeared to reach deeper areas of the scaffolds [Fig. 5(e)]. Aggrecan staining was readily observed in all constructs and appeared to reach deeper areas in loaded (LG1, LG2) compared to unloaded scaffolds, while there was no difference in overall staining intensity [Fig. 5(i–k)].
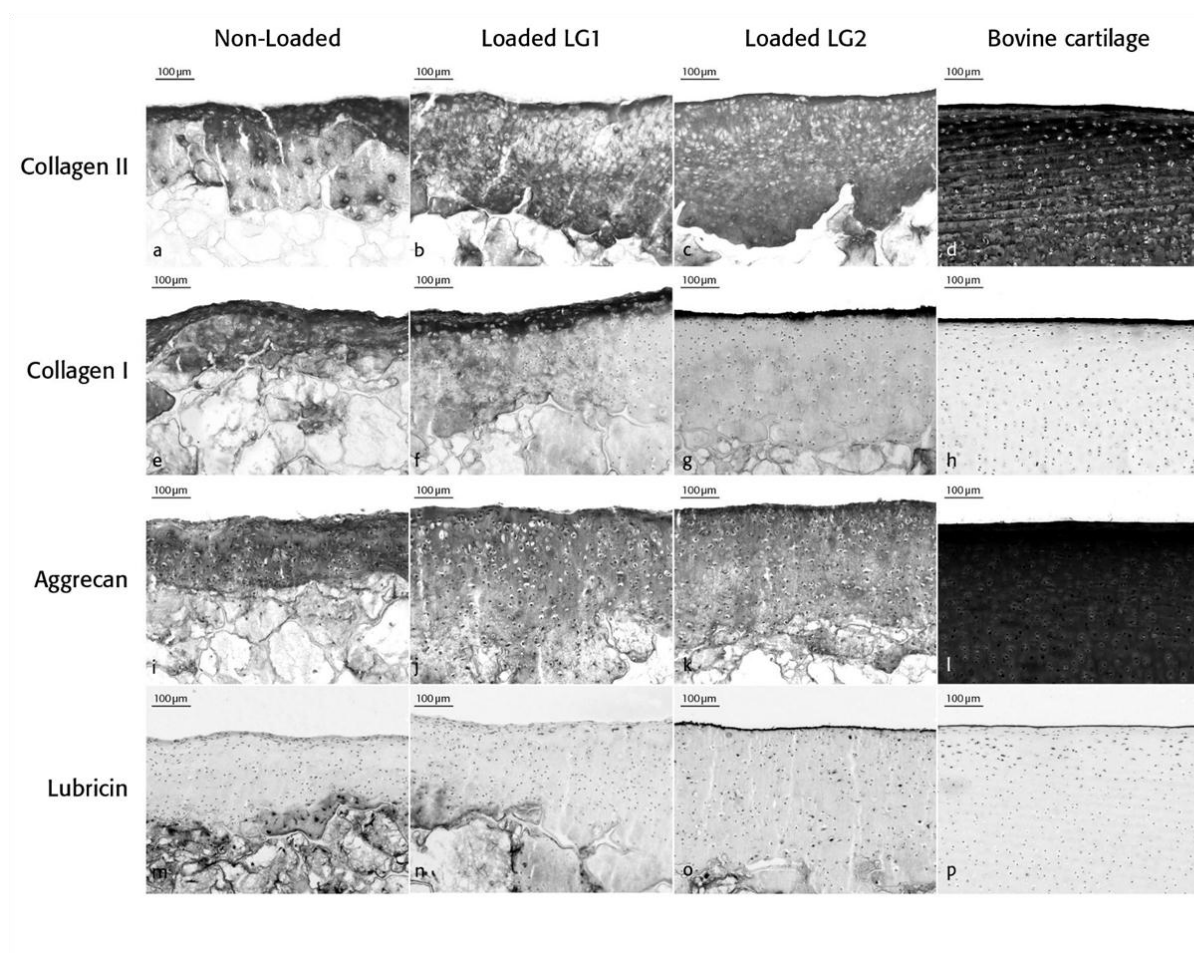
Figure 3.5: Immunolabeling of cell-scaffold constructs for collagen type II, collagen type I, aggrecan, and lubricin. Constructs of LG1 were stimulated by dynamic compression only; constructs of LG2 were stimulated by dynamic compression and sliding surface motion. Immunolabeling characteristics of bovine articular cartilage used as positive control are also shown. Scale bar = 100 μm.

Similar to the appearance of the native articular surface, strong immunoreactivity for lubricin was noticed at the top surface of constructs from LG2. Some positive cells were also visible in deeper zones. In constructs of LG1 and in unloaded controls, the cells at the surface were mostly immunonegative for lubricin. However, interestingly, cells in deeper zones of the LG1 and control scaffolds showed more pronounced lubricin immunoreactivity as compared to

scaffolds from LG2 [Fig. 5(m–p)]. Negative controls did not show any staining throughout all the sections.

3.5 Discussion

While numerous studies have been performed to optimize the quality of tissue engineered cartilage, most conventional cartilage testing devices lack high sensitivity and therefore do not allow for a more distinct inspection of mechanical surface properties. In contrast, AFM has recently been employed to evaluate cartilage ex vivo and in situ at greater detail [22], [23], [37], [38] and [39]. As one specific application, here we utilized a standard commercial AFM to demonstrate that dynamic compressive loading in combination with sliding surface motion, mimicking joint articulation, can considerably affect the surface characteristics of in vitro engineered cartilage in terms of (1) micro- and nanometer-scale stiffness, (2) friction coefficient and (3) histological manifestation.

For constructs that were mechanically stimulated to resemble the natural motion characteristics (LG2), we obtained nanostiffness values similar to the ones measured for native cartilage [22]. Results from a recent study indicate that the nanostiffness values in the range of about 20 kPa reflect the stiffness of the proteoglycan gel present at the articular surface [37]. Thus, the increased nanostiffness in constructs subjected to compressive loading that was further enhanced by additional sliding motion may be attributed to increased proteoglycan content and/or increased cross-linking between the proteoglycan molecules and collagen molecules at the construct surface [9] and [37]. In native cartilage, both enzymatic digestion of cartilage proteoglycans and hyperosmotic challenge resulted in significant stiffening at the nanometer scale as a result of the loss in water content [22] and [37]. While monitoring of nanostiffness values has been proposed as a sensitive tool for detection of early degenerative damage of the cartilage surface [23], this study additionally shows the great potential of nanometer-scale indentation-type AFM (IT-AFM) to determine the functional properties of in vitro engineered cartilage surface already at the very early stages of graft development.

Microstiffness data, although highest in constructs experiencing simulated-physiological loading, were still two orders of magnitude lower compared to values of native articular cartilage. This result is in agreement with other studies demonstrating that stiffness values of

natural cartilage are generally not reached after short to medium-term in vitro culture of engineered cartilaginous tissues [26], [40], [41], [42] and [43]. It is apparent that the elastic response of an immature in vitro developing tissue is significantly different from authentic mature cartilage; this is predominantly due to the early stage of collagen fibrillogenesis, where collagen microfibrils are very thin and without mature (pyridinoline, deoxypyridinoline) cross-link bonds [44] and [45]. Nevertheless, differences in microstiffness were noted between constructs cultured under different loading conditions. Several studies have reported that physical loading can improve the mechanical properties of tissue engineered cartilage [46] and [47], and recent findings have confirmed the benefit of sliding contact loading on the equilibrium modulus of chondrocytes-seeded agarose gels [48]. The superior microstiffness can result from an increased accumulation of extracellular matrix, particularly at the construct surface, in the loaded samples. Histochemical observations contribute to this hypothesis. In all constructs, type II collagen and aggrecan, the main macromolecules responsible for the strength and elasticity of the cartilage extracellular network, were abundant. In loaded constructs, the accumulation of matrix generally appeared to reach deeper areas, which may be related to improved transport of nutrients to the cells inside the scaffold. In contrast, in LG2 collagen type I was produced only in a thin layer at the surface, which has been shown also in natural articular cartilage. Although the presence of type I collagen at the articular surface has been described, its amounts and function remain a matter of debate and its effects on the surface properties will require further investigation [49], [50] and [51].

AFM has increasingly been employed to determine the frictional behavior of cartilaginous surfaces, as it appears particularly appropriate for friction measurements in boundary lubrication systems [32] and [52]. This study emphasizes the value of a sliding-type motion regime to effectively decrease the coefficient of friction at the construct surface, approaching the level of young bovine cartilage. It is suggested that the decrease in friction results from the specific accumulation of lubricin at the construct surface. This distinct layer of lubricin was noted only in the group subjected to sliding motion, adding to previous observations of enhanced gene expression and release of lubricin in cell-scaffold constructs upon application of surface motion [18], [19] and [20].

Lubricin has been proposed to serve as the primary lubricant in articular joints [52], [53], [54] and [55]. Relationship between the presence of lubricin and reduced friction in diarthrodial

joints has been widely documented [7] and [52]. Although in scaffolds that were stimulated by axial compression without surface motion no distinct layer of lubricin was noted at the surface, they showed lower coefficient of friction than the unloaded controls. This suggests that other features such as enhanced deposition of proteoglycans and altered orientation of collagen fibers in the superficial zone might also have contributed to a reduction in the friction coefficient [56] and [57]. The friction lowering effect of sliding contact motion has recently been shown also for chondrocytes-seeded agarose constructs [48]. Here we conclude that the molecular composition of the superficial zone is adapted by the local mechanical stimulus, decreasing friction, which is at least partly due to localized lubricin deposition. The contribution of the fibrin to the stiffness and friction was not assessed, which may be a limitation of this study. However, while fibrin may play a role at the beginning of culture, histological images after 4 weeks show that at least at the surface fibrin is largely replaced by extracellular matrix. Therefore it is suggested that the contribution of the fibrin to the stiffness and friction is minimal at this stage.

The total amounts of sGAG produced by the chondrocytes during culture were enhanced in mechanically stimulated grafts, confirming previous reports of accelerated metabolic activity of chondrocytes exposed to mechanical cues. The retention rate of approximately 30% that was found in all constructs is comparable to previous findings with chondrocytes-seeded scaffolds [27]. Retention might depend on the presence of extracellular matrix before initiation of loading and on the capability of the scaffold to accumulate newly produced matrix molecules. Increased release of sGAG into the medium can be attributed to accelerated pressing out of unincorporated matrix molecules by the cyclic compression. Additional mechanisms may be related to an activation of matrix turnover including degrading enzymes or mechanical disruption as a result of the loading forces58. While aggrecan immunostaining appeared to reach deeper areas in loaded scaffolds, no apparent difference in overall staining intensity was noted. This is in agreement with the merely small differences in the amounts of sGAG measured in the differently cultured scaffolds.

To conclude, while quantitative information on the matrix synthesis can be obtained through biochemical analysis and the type and distribution of matrix molecules can be evaluated through immunolabeling, additional measurements are needed to assess the functional quality of cartilaginous grafts. This study proposes a quantitative AFM-based functional analysis including friction testing (gliding) and multiscale mechanical testing (load-bearing). Such

quality tests are essential to provide reliable mechanical data for "articular cartilage repair products", which is increasingly required by authorities for approval of new products and methods [21]. Moreover, this study emphasizes the functional characterization of superficial layer of cartilage due to its unique role in cartilage homeostasis and mechanical properties. Due to its high sensitivity and multifunctionality (imaging, stiffness and friction measurements) AFM can be useful to evaluate friction and stiffness behavior of the cartilage surface. Finally, our results underline the importance of a sliding-type biomechanical stimulus for the (re)generation and maintenance of an operative articular surface. This has implications for both in vitro tissue engineering as well as in vivo physical regenerative therapy regimes.

3.6 Acknowledgment

3.7 References

1.   Bhosale AM, Richardson JB. Articular cartilage: structure, injuries and review of management. Br Med Bull, 87 (2008), pp. 77–95

2.   Hunziker EB, Quinn TM, Hauselmann HJ. Quantitative structural organization of normal adult human articular cartilage. Osteoarthritis Cartilage, 10 (7) (2002), pp. 564–572

3.   Jay GD, Tantravahi U, Britt DE, Barrach HJ, Cha CJ. Homology of lubricin and superficial zone protein (SZP): products of megakaryocyte stimulating factor (MSF) gene expression by human synovial fibroblasts and articular chondrocytes localized to chromosome 1q25. J Orthop Res, 19 (4) (2001), pp. 677–687

4.   Flannery C.R., Hughes C.E., Schumacher B.L., Tudor D., Aydelotte M.B., Kuettner K.E. *et al.* Articular cartilage superficial zone protein (SZP) is homologous to megakaryocyte stimulating factor precursor and is a multifunctional proteoglycan with potential growth-promoting, cytoprotective, and lubricating properties in cartilage metabolism. Biochem Biophys Res Commun, 254 (3) (1999), pp. 535–541

5.   Ikegawa S, Sano M, Koshizuka Y, Nakamura Y. Isolation, characterization and mapping of the mouse and human PRG4 (proteoglycan 4) genes. Cytogenet Cell Genet, 90 (3–4) (2000), pp. 291–297

6.   Jay GD, Torres JR, Rhee DK, Helminen HJ, Hytinnen MM, Cha CJ *et al.* Association between friction and wear in diarthrodial joints lacking lubricin. Arthritis Rheum, 56 (11) (2007), pp. 3662–3669

7.   Coles JM, Zhang L, Blum JJ, Warman ML, Jay GD, Guilak F. *et al.* Loss of cartilage structure, stiffness, and frictional properties in mice lacking PRG4. Arthritis Rheum, 62 (6) (2010), pp. 1666–1674

8.   Greene GW, Banquy X, Lee DW, Lowrey DD, Yu J, Israelachvili JN. Adaptive mechanically controlled lubrication mechanism found in articular joints. Proc Natl Acad Sci U S A, 108 (13) (2011), pp. 5255–5259

9.   Hedlund H, Hedbom E, Heinegård D, Mengarelli-Widholm S, Reinholt FP, Svensson O. Association of the aggrecan keratan sulfate-rich region with collagen in bovine articular cartilage. J Biol Chem, 274 (9) (1999), pp. 5777–5781

10.   Buckwalter JA, Mankin HJ, Grodzinsky AJ. Articular cartilage and osteoarthritis. Instr Course Lect, 54 (2005), pp. 465–480

11.   Hunziker EB. Articular cartilage repair: basic science and clinical progress. A review of the current status and prospects. Osteoarthritis Cartilage, 10 (6) (2002), pp. 432–463

12.   Elders MJ. The increasing impact of arthritis on public health. J Rheumatol Suppl, 60 (2000), pp. 6–8

13. Simon TM, Jackson DW. Articular cartilage: injury pathways and treatment options. Sports Med Arthrosc, 14 (3) (2006), pp. 146–154

14. Brittberg M, Peterson L, Sjogren-Jansson E, Tallheden T, Lindahl A. Articular cartilage engineering with autologous chondrocyte transplantation. A review of recent developments. J Bone Joint Surg Am, 85-A (Suppl 3) (2003), pp. 109–115

15. Stoddart MJ, Grad S, Eglin D, Alini M. Cells and biomaterials in cartilage tissue engineering. Regen Med, 4 (1) (2009), pp. 81–98

16. Schulz RM, Bader A. Cartilage tissue engineering and bioreactor systems for the cultivation and stimulation of chondrocytes. Eur Biophys J, 36 (4–5) (2007), pp. 539–568

17. Wimmer MA, Grad S, Kaup T, Hanni M, Schneider E, Gogolewski S *et al.* Tribology approach to the engineering and study of articular cartilage. Tissue Eng, 10 (9–10) (2004), pp. 1436–1445

18. Grad S, Lee CR, Gorna K, Gogolewski S, Wimmer MA, Alini M. Surface motion upregulates superficial zone protein and hyaluronan production in chondrocyte-seeded three-dimensional scaffolds. Tissue Eng, 11 (1–2) (2005), pp. 249–256

19. Grad S, Lee CR, Wimmer MA, Alini M. Chondrocyte gene expression under applied surface motion. Biorheology, 43 (3–4) (2006), pp. 259–269

20. Grad S, Gogolewski S, Alini M, Wimmer MA. Effects of simple and complex motion patterns on gene expression of chondrocytes seeded in 3D scaffolds. Tissue Eng, 12 (11) (2006), pp. 3171–3179

21. McFarland R, Kaiser A. Guidance for Industry: Preparation of IDEs and INDs for Products Intended to Repair or Replace Knee Cartilage. Department of Health and Human Services, Rockville, MD, U.S (2007)

22. Stolz M, Raiteri R, Daniels AU, VanLandingham MR, Baschong W, Aebi U. Dynamic elastic modulus of porcine articular cartilage determined at two different levels of tissue organization by indentation-type atomic force microscopy. Biophys J, 86 (5) (2004), pp. 3269–3283

23. Stolz M, Gottardi R, Raiteri R, Miot S, Martin I, Imer R *et al.* Early detection of aging cartilage and osteoarthritis in mice and patient samples using atomic force microscopy. Nat Nanotechnol, 4 (3) (2009), pp. 186–192

24. Park S, Costa KD, Ateshian GA, Hong KS. Mechanical properties of bovine articular cartilage under microscale indentation loading from atomic force microscopy. Proc Inst Mech Eng H, 223 (3) (2009), pp. 339–347

25. Gorna K, Gogolewski S. Biodegradable porous polyurethane scaffolds for tissue repair and regeneration. J Biomed Mater Res A, 79 (1) (2006), pp. 128–138

26. Grad S, Kupcsik L, Gorna K, Gogolewski S, Alini M. The use of biodegradable polyurethane scaffolds for cartilage tissue engineering: potential and limitations. Biomaterials, 24 (28) (2003), pp. 5163–5171

27. Lee CR, Grad S, Gorna K, Gogolewski S, Goessl A, Alini M. Fibrin-polyurethane composites for articular cartilage tissue engineering: a preliminary analysis. Tissue Eng, 11 (9–10) (2005), pp. 1562–1573

28. Green CP, Lioe H, Cleveland JP, Proksch R, Mulvaney P, Sader JE. Normal and torsional spring constants of atomic force microscope cantilevers. Rev Sci Instrum, 75 (6) (2004), p. 1988

29. Plodinec M, Loparic M, Suetterlin R, Herrmann H, Aebi U, Schoenenberger CA. The nanomechanical properties of rat fibroblasts are modulated by interfering with the vimentin intermediate filament system. J Struct Biol, 174 (3) (2011), pp. 476–484

30. Lin DC, Dimitriadis EK, Horkay F. Robust strategies for automated AFM force curve analysis-I. Non-adhesive indentation of soft, inhomogeneous materials. J Biomech Eng, 129 (3) (2007), pp. 430–440

31. Oliver WC, Pharr GM. An improved technique for determining hardness and elastic modulus using load and displacement sensing indentation experiments. J Mater Res, 7 (1992), pp. 1564–1583

32. Coles JM, Blum JJ, Jay GD, Darling EM, Guilak F, Zauscher S. In situ friction measurement on murine cartilage by atomic force microscopy. J Biomech, 41 (3) (2008), pp. 541–548

33. Liu W, Bonin K, Guthold M. Easy and direct method for calibrating atomic force microscopy lateral force measurements. Rev Sci Instrum, 78 (6) (2007), p. 063707

34. Milz S, Aktas T, Putz R, Benjamin M. Expression of extracellular matrix molecules typical of articular cartilage in the human scapholunate interosseous ligament.J Anat, 208 (6) (2006), pp. 671–679

35. Milz S, Sicking B, Sprecher CM, Putz R, Benjamin M. An immunohistochemical study of the triangular fibrocartilage complex of the wrist: regional variations in cartilage phenotype. J Anat, 211 (1) (2007), pp. 1–7

36. Tischer T, Milz S, Maier M, Schieker M, Benjamin M. An immunohistochemical study of the rabbit suprapatella, a sesamoid fibrocartilage in the quadriceps tendon containing aggrecan. J Histochem Cytochem, 50 (7) (2002), pp. 955–960

37. Loparic M, Wirz D, Daniels AU, Raiteri R, VanLandingham MR, Guex G. *et al.* Micro- and nanomechanical analysis of articular cartilage by indentation-type atomic force microscopy: validation with a gel-microfiber composite. Biophys J, 98 (11) (2010), pp. 2731–2740

38. Imer R, Akiyama T, Fd Rooij, Stolz M, Aebi U, Friederich F *et al.* The measurement of biomechanical properties of porcine articular cartilage using atomic force microscopy. Arch Histol Cytol, 72 (4–5) (2009), pp. 251–259

39. Desrochers J, Amrein MA, Matyas JR. Structural and functional changes of the articular surface in a post-traumatic model of early osteoarthritis measured by atomic force microscopy. J Biomech, 43 (16) (2010), pp. 3091–3098

40. Hunter CJ, Mouw JK, Levenston ME. Dynamic compression of chondrocyte-seeded fibrin gels: effects on matrix accumulation and mechanical stiffness. Osteoarthritis Cartilage, 12 (2) (2004), pp. 117–130

41. Kelly TA, Fisher MB, Oswald ES, Tai T, Mauck RL, Ateshian GA et al. Low-serum media and dynamic deformational loading in tissue engineering of articular cartilage. Ann Biomed Eng, 36 (5) (2008), pp. 769–779

42. Bastiaansen-Jenniskens YM, Koevoet W, De Bart AC, van der Linden JC, Zuurmond AM, Weinans H *et al.*Contribution of collagen network features to functional properties of engineered cartilage. Osteoarthritis Cartilage, 16 (3) (2008), pp. 359–366

43. Preiss-Bloom O, Mizrahi J, Elisseeff J, Seliktar D. Real-time monitoring of force response measured in mechanically stimulated tissue-engineered cartilage. Artif Organs, 33 (4) (2009), pp. 318–327

44. Strobel S, Loparic M, Wendt D, Schenk AD, Candrian C, Lindberg RL *et al.*Anabolic and catabolic responses of human articular chondrocytes to varying oxygen percentages. Arthritis Res Ther, 12 (2) (2010), p. R34

45. Fratzl P. Collagen: Structure and Mechanics. Springer, New York (2008)

46. Hung CT, Mauck RL, Wang CC, Lima EG, Ateshian GA. A paradigm for functional tissue engineering of articular cartilage via applied physiologic deformational loading. Ann Biomed Eng, 32 (1) (2004), pp. 35–49

47. Kisiday JD, Jin M, DiMicco MA, Kurz B, Grodzinsky AJ. Effects of dynamic compressive loading on chondrocyte biosynthesis in self-assembling peptide scaffolds. J Biomech, 37 (5) (2004), pp. 595–604

48. Bian L, Fong JV, Lima EG, Stoker AM, Ateshian GA, Cook JL *et al.*Dynamic mechanical loading enhances functional properties of tissue-engineered cartilage using mature canine chondrocytes. Tissue Eng Part A, 16 (5) (2010), pp. 1781–1790

49. Eyre DR. Collagens and cartilage matrix homeostasis. Clin Orthop Relat Res (Suppl 427) (2004), pp. S118–S122

50. Wachsmuth L, Soder S, Fan Z, Finger F, Aigner T. Immunolocalization of matrix proteins in different human cartilage subtypes. Histol Histopathol, 21 (5) (2006), pp. 477–485

51. Roberts S, McCall IW, Darby AJ, Menage J, Evans H, Harrison PE *et al.* Autologous chondrocyte implantation for cartilage repair: monitoring its success by magnetic resonance imaging and histology. Arthritis Res Ther, 5 (1) (2003), pp. R60–R73

52. Chan SM, Neu CP, Duraine G, Komvopoulos K, Reddi AH. Atomic force microscope investigation of the boundary-lubricant layer in articular cartilage. Osteoarthritis Cartilage, 18 (7) (2010), pp. 956–963

53. Jones AR, Gleghorn JP, Hughes CE, Fitz LJ, Zollner R, Wainwright SD *et al.* Binding and localization of recombinant lubricin to articular cartilage surfaces. J Orthop Res, 25 (3) (2007), pp. 283–292

54. Schmidt TA, Gastelum NS, Nguyen QT, Schumacher BL, Sah RL. Boundary lubrication of articular cartilage: role of synovial fluid constituents. Arthritis Rheum, 56 (3) (2007), pp. 882–891

55. Jay D, Torres JR, Warman ML, Laderer MC, Breuer KS. The role of lubricin in the mechanical behavior of synovial fluid. Proc Natl Acad Sci U S A, 104 (15) (2007), pp. 6194–6199

56. Basalo IM, Chen FH, Hung CT, Ateshian GA. Frictional response of bovine articular cartilage under creep loading following proteoglycan digestion with chondroitinase ABC. J Biomech Eng, 128 (1) (2006), pp. 131–134

57. Katta J, Stapleton T, Ingham E, Jin ZM, Fisher J. The effect of glycosaminoglycan depletion on the friction and deformation of articular cartilage. Proc Inst Mech Eng H, 222 (1) (2008), pp. 1–11

58. Blain EJ. Mechanical regulation of matrix metalloproteinases. Front Biosci, 12 (2007), pp. 507–527

Chapter 4

Articular cartilage repair by genetically modified

bone marrow aspirate in sheep

A. Ivkovic, A. Pascher, D. Hudetz, D. Maticic, M. Jelic, S. Dickinson,

M. Loparic, M. Haspl, R. Windhager and M. Pecina

4.1 Abstract

Bone marrow presents an attractive option for the treatment of articular cartilage defects as it is readily accessible, it contains mesenchymal progenitor cells that can undergo chondrogenic differentiation and, once coagulated, it provides a natural scaffold that contains the cells within the defect. This study was performed to test whether an abbreviated *ex vivo* protocol using vector-laden, coagulated bone marrow aspirates for gene delivery to cartilage defects may be feasible for clinical application. Ovine autologous bone marrow was transduced with adenoviral vectors containing cDNA for green fluorescent protein or transforming growth factor (TGF)-β1. The marrow was allowed to clot forming a gene plug and implanted into partial-thickness defects created on the medial condyle. At 6 months, the quality of articular cartilage repair was evaluated using histological, biochemical and biomechanical parameters. Assessment of repair showed that the groups treated with constructs transplantation contained more cartilage-like tissue than untreated controls. Improved cartilage repair was observed in groups treated with unmodified bone marrow plugs and Ad.TGF-β1-transduced plugs, but the repaired tissue from TGF-treated defects showed significantly higher amounts of collagen II ($P<0.001$). The results confirmed that the proposed method is fairly straightforward technique for application in clinical settings. Genetically modified bone marrow clots are sufficient to facilitate articular cartilage repair of partial-thickness defects *in vivo*. Further studies should focus on selection of transgene combinations that promote more natural healing.

4.2 Introduction

Hyaline cartilage is a highly specialized tissue, with a unique three-dimensional structure that enables it to withhold tremendous mechanical forces inflicted during joint movement and a smooth surface allowing nearly frictionless contact between articulating joint surfaces. However, this tissue is also avascular, aneural and alymphatic with a low cell density embedded within the extracellular matrix (ECM). For these reasons, hyaline cartilage has very modest reparative and regenerative capabilities. Articular cartilage defects are very frequent, especially among active young adults and the working population. Such defects do not heal and, with time, often lead to premature osteoarthritis, consequently decreasing quality of life for the patient and adding substantially to health care costs.

The restoration of damaged cartilage remains one of the biggest challenges in modern orthopaedics. There is no pharmacological treatment that promotes the repair of the cartilage. Current treatment modalities include microfracture, transplantation of ostechondral grafts and chondrocytes, use of biodegradable scaffolds or combination of these [1,2]. Although these procedures can produce initially good clinical results in terms of pain relief and improvement of joint function, they typically produce a fibrocartilagenouse repair tissue that is inferior to normal cartilage, such that long-term outcomes are less predictable and satisfactory[3].

New biological approaches to cartilage repair that are based on the use of cells and molecules that promote chondrogenesis or/and inhibit cartilage breakdown offer a promising alternative to current treatment options[4]. Any successful strategy that attempts to repair hyaline cartilage defects must include sufficient number of cells, appropriate signal to modulate cellular response and a scaffold that would contain the cells within the defect. Mesenchymal stromal cells (MSCs) present very attractive option for cell-based strategies as they can be readily isolated, expanded and, under appropriate conditions, differentiated into mesenchymal tissues such as cartilage, bone or muscle[5]. Numerous gene products such as transforming growth factor-β (TGF-β) [6], bone morphogenetic protein-7 (BMP-7) [7], insulin-like growth factor-1 (IGF-1) [8] and BMP-2 [9] have shown potential in regulating the process of growth, repair and regeneration of cartilage in animal models, but their use is limited by delivery problems and rapid clearance from the joint. This issue can be addressed by gene therapy approaches for delivering therapeutic gene products specifically to the site of repair[10,11]. In particular, viral vectors have been used successfully to modify graftable articular chondrocytes, periosteal cells and bone marrow-derived MSCs *ex vivo*, as well as for directly

modifying the synovial lining *in vivo* [12,13]. The use of scaffolds in cartilage repair is often required to contain, deliver and orient cells within their three-dimensional structure. Many different types have been tested in clinical and experimental settings, but the selection of suitable scaffolds for clinical application is still ongoing [14].

Much of the current research into cartilage repair has focused on *ex vivo*, or indirect, approaches to the treatment of defects using genetically modified cells. These typically involve harvesting and expansion of the cells, transduction with a therapeutic gene, seeding onto a scaffold and reimplantation into the defect. While providing the aforementioned components for successful cartilage repair, this general approach is technically demanding, expensive and requires at least two surgical procedures. Pascher *et al.* [15] have recently proposed an abbreviated *ex vivo* protocol that uses vector-laden, coagulated bone marrow aspirates or 'gene plugs', for gene delivery to cartilage defects. This study showed that nucleated cells within fresh autologous bone marrow aspirates may be successfully transduced with adenoviral vectors sufficient to secret transgene products up to 21 days. In theory, this approach also provides all necessary ingredients for successful cartilage repair: transduced mononuclear cells secrete signals that stimulate mesenchymal progenitors to differentiate along the chondrogenic lineage, and the bone marrow clot (BMC) itself provides a natural autologous three-dimensional scaffold to be used for containment of cells and vectors within the defect.

To examine whether direct implantation of gene plugs might be used in situations that closely mimic real-life clinical situations, partial-thickness chondral defects were created on the weight-bearing surface of the femoral condyle in sheep. Fresh autologous bone marrow aspirates were transduced with adenoviral constructs carrying therapeutic or marker genes, and the clots were press-fit within the defects. The three principle objectives of this study were to determine feasibility of the proposed abbreviated *ex vivo* protocol to be used as a novel treatment tool in clinical settings, to determine whether transgene expression of TGF-β1 within the gene plug enhances cartilage repair, and to test whether there is a presence of adenoviral genome within the cells of synovial lining, which would suggest vector leakage from the clots.

4.3 Results

Histological assessment

The mean scores of the histological assessment are shown in Table 4.1, and representative histological sections are shown in Figure 4.1. Six months after the surgical procedure, all groups treated with BMC transplantation were superior to empty control in terms of overall score according to the ICRS Visual Histological Assessment Scale, although statistical significance was not observed (P=0.061) (Table 4.1). Each histological parameter was analysed by Kruskal–Wallis test. A statistically significant difference was observed in one category—columnar cell distribution: TGF and BMC groups had a higher score than the CON group (Table 4.1). Although improved fusion between the repair tissue and the surrounding undamaged tissue had been achieved in TGF-treated groups, the side-to-side integrations were far from optimal.
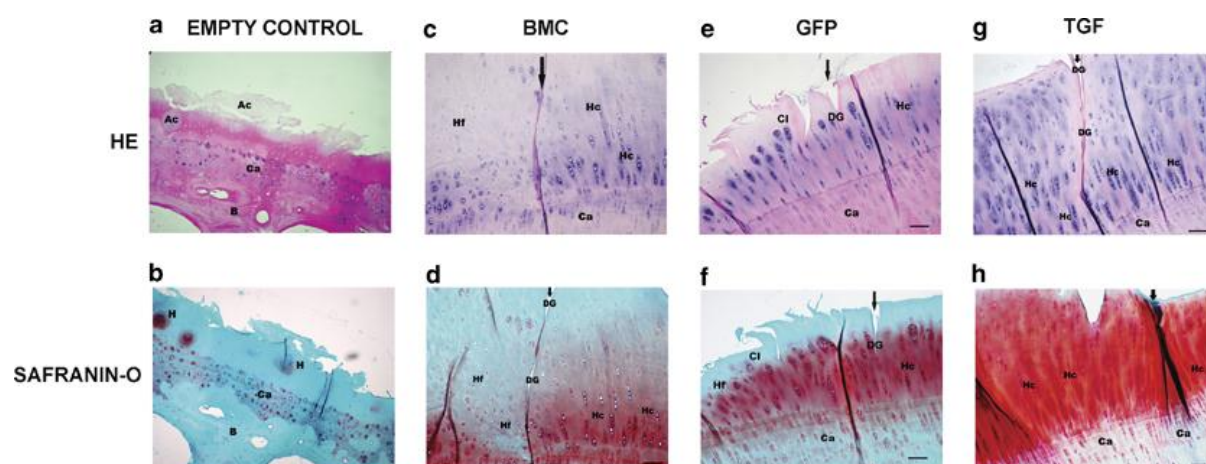
Figure 4.1: Representative histological sections of the repair tissue filling ovine chondral defects, stained with either haematoxylin-eosin (upper row) or safranin-O (lower row). Panel bars: 100 μm. (**a**, **b**) Empty defect group showing acellular tissue (Ac) within the defect with intact calcified layer (Ca) and subchondral bone (B). (**c**, **d**) BMC group. The defect is predominantly filled with fibrocartilage (Hf). There is clear demarcation between native hyaline cartilage (Hc) and fibrocartilage (Hf) separated by a defect gap (DG). Black arrow indicates border of the defect separating newly formed (New) and native (Nat) cartilage. Calcified layer (Ca). (**e**, **f**) GFP group. Irregular filling of the defect with fissures. The defect is filled with mixture of hyaline and fibrocartilage. Clusters of clonal cell division (Cl) are present in upper layers newly formed tissue. Black arrow indicates border of the defect separating newly formed (New) and native (Nat) cartilage. Calcified layer (Ca). (**g**, **h**) TGF group. Improved histological appearance of the repair tissue within the defect. Hyaline cartilage (Hc) and columnar organization of chondrocytes is detected on both sides of the defect gap (DG). Black arrow indicates border of the defect separating newly formed (New) and native (Nat) cartilage. Calcified layer (Ca).

Table 4.1: Histological grading of the repair tissue at 6 months according to ICRS visual histological assessment Scale[a] (medians±interquartile range)

ICRS Score	Treatment group								P[b]
	CON		BMC		GFP		TGF		
	C	Q	C	Q	C	Q	C	Q	
Surface	0.00	0	0.00	0	0.00	0	0.00	0	0.343
Matrix	1.50	2	3.00	1	3.00	2	3.00	0	0.062
Columnar cell distribution	1.00[c]	0	2.00	0	2.00	2	2.00	0	0.016
Cell population viability	0.00	1	1.00	3	0.00	0	0.00	0	0.095
Subchondral bone	2.50	1	3.00	0	3.00	3	3.00	0	0.177
Cartilage mineralization	1.50	3	3.00	0	3.00	3	3.00	0	0.162
Median total score	6.50	6	11.50	4	11.00	9	11.00	0	0.061

Abbreviations: CON, control group; BMC, bone marrow clot group; GFP, green fluorescent protein group; TFG, transforming growth factor-β1 group, C, median; Q, interquartile range.

[a] The table shows the medians from each group for each subcategories, and the total medians for each group.

[b] Kruskal–Wallis test (Mann–Whitney test was used as a *post hoc* procedure when K–W test revealed statistically significant difference).

[c] Significantly lower score from TGF and BMC groups (*P*=0.002 and *P*=0.008, respectively, Mann–Whitney test).

In vitro culturing of genetically modified BMCs

BMCs transduced with green fluorescent protein (Ad.GFP) showed a high number of fluorescent cells throughout the coagulate over 21 days of culture. BMCs formed in the absence of Ad.GFP confirmed the specificity of fluorescence signal.

Biochemical properties

Glycosaminoglycan (GAG) analysis did not reveal any statistical difference between mean values for repaired cartilage in the treatment groups and native cartilage from contralateral knees (*P*>0.050 for all comparisons, paired samples *t*-test; Figure 4.2a). There were no statistically significant differences in GAG mean values for repaired cartilage between the treatment groups ($F_{2,19}$=0.6, *P*=0.581, one-way analysis of variance (ANOVA); Figure 4.2a).
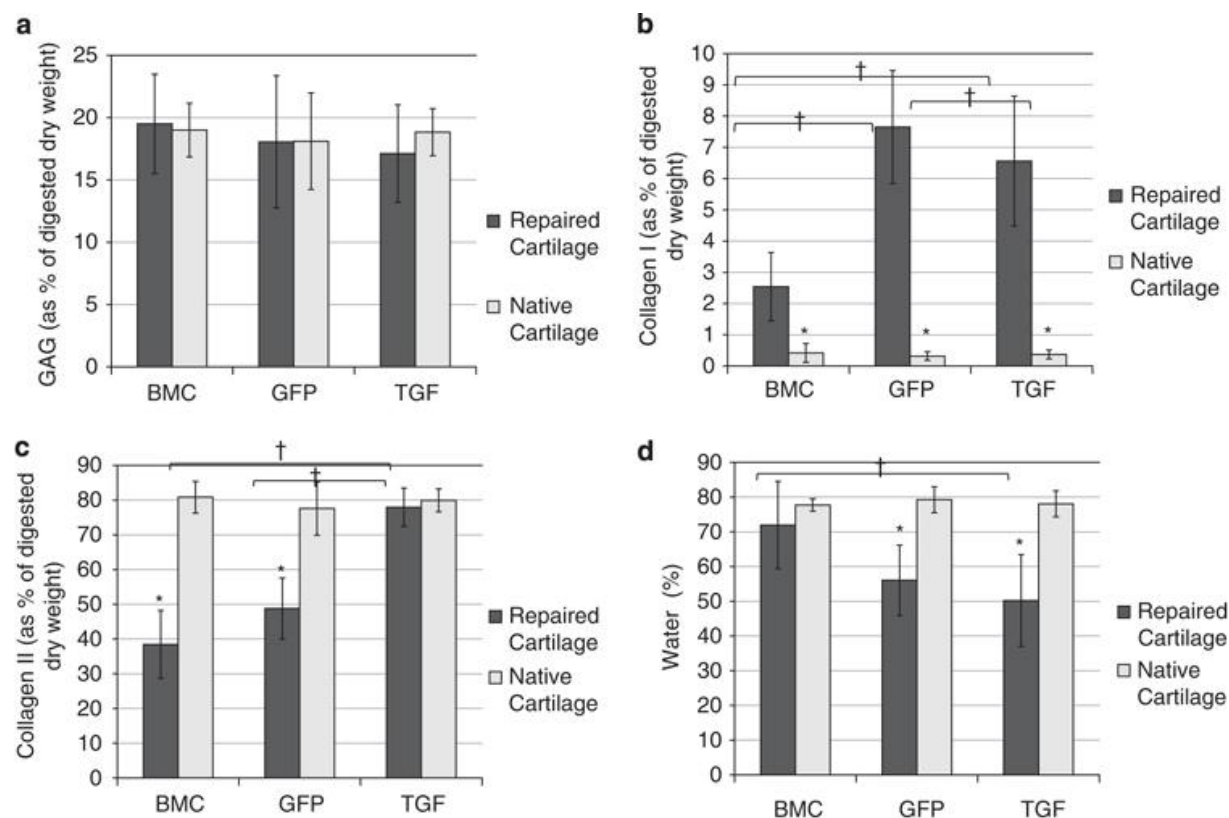
Figure **4.2: Biochemical analysis of repaired cartilage compared with native cartilage**. (**a**) GAG. (**b**) Collagen I. (**c**) Collagen II. (**d**) Water. *Two-tailed paired *t*-test: comparison of repaired and native cartilage (*P*<0.05). †One-way ANOVA with Tukey *post hoc* test: comparison of treatment groups (*P*<0.05).

The collagen type I content was found to be significantly higher in all treatment groups when compared with native cartilage (*P*<0.050 for all comparisons, paired samples *t*-test; Figure 4.1b). The three treatment groups also significantly differed in collagen type I content ($F_{2,19}$=13.9, *P*<0.001, one-way ANOVA; Figure 4.2b). Specifically, the collagen type I content in BMC group was significantly lower from that detected in GFP- and TGF-treated groups, respectively (*P*<0.001 and *P*=0.001, respectively, Tukey *post hoc* test), whereas there was no difference among GFP and TGF groups (*P*=0.482, Tukey *post hoc* test).

The collagen type II content was significantly lower in BMC and GFP treatment groups when compared with native cartilage (Figure 4.2c). There was no difference between the GFP and BMC groups (*P*=0.079, Tukey *post hoc* test). Collagen type II content in the TGF group was significantly higher ($F_{2,19}$=56.2, *P*<0.001, one-way ANOVA; Figure 4.2c) than that detected in GFP- and BMC-treated groups (*P*<0.001 for both, Tukey *post hoc* test).

When compared with native cartilage, water content in the repaired tissue was significantly lower in the TGF and GFP groups (*P*<0.001 and *P*=0.005, respectively, paired samples *t*-test;

Figure 4.2d), whereas the water content of the TGF group was significantly lower than those detected in the GFP ($F_{2,19}$=5.9, *P*=0.01, one-way ANOVA; Figure 4.1d) and BMC groups (*P*=0.008, Tukey *post hoc* test).

Biomechanical properties

Cartilage stiffness at micrometer scale

Dynamic elastic modulus |*E**| values for native articular cartilage and reparative cartilage obtained after treatment with gene plugs are shown in Figure 2. The measurements were obtained with a microspherical tip, nominal radius of 7.5 μm, and they reflect structural changes at the micrometer scale. |*E**|$_{micro}$ values gradually increased from native cartilage to the TFG-, BMC- and GFP-treated groups (Figure 3a). |*E**|$_{micro}$ was significantly higher in all repair groups when compared with native cartilage (BMC *P*<0.001, GFP *P*=0.003, TGF *P*<0.001, respectively, paired samples *t*-test). Treatment groups significantly differed in |*E**|$_{micro}$ ($F_{2,19}$=5.3, *P*=0.015; one-way ANOVA). |*E**|$_{micro}$ from the TGF group was significantly lower than that detected in the GFP group (*P*=0.014, Tukey *post hoc* test). Values from the TGF group also appeared lower compared with those of the BMC group, but no statistically significant difference was observed.
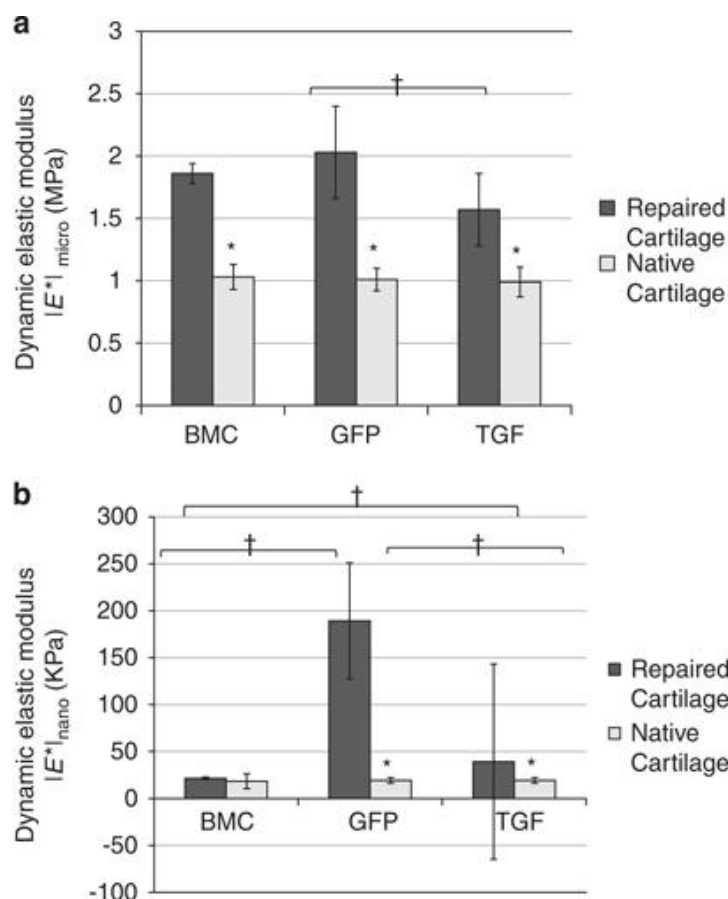
Figure 4.3: (a) Micrometer measurements. Dynamic elastic modulus |*E**|micro of native articular cartilage and repair tissue of the BMC, GFP and TGF group. Average microstiffness (M±s.d.) increased from native cartilage to GFP-treated group: |*E**|$_{micro}$=1.025±0.098 (native cartilage), |*E**|$_{micro}$=1.577±0.285 (TGF), |*E**|$_{micro}$=1.863±0.079 (BMC), |*E**|$_{micro}$=2.025±0.371 (GFP). *Two-tailed paired *t*-test comparison of repaired versus native cartilage (*P*<0.05). [†]One-way ANOVA with Tukey *post hoc* test comparison of repaired cartilage between treatment groups (*P*<0.05). **(b) Nanometer measurements.** Dynamic elastic modulus |*E**|$_{nano}$ of native articular cartilage and repair tissue of the BMC, GFP and TGF group. |*E**|$_{nano}$ =19.28±3 (native cartilage), |*E**|$_{nano}$=21.54±1.24 (BMC), |*E**|$_{nano}$=39.26±104.56 (TGF), |*E**|$_{nano}$=189.21±39.26 (GFP). *Two-tailed paired *t*-test comparison of repaired and native cartilage (*P*<0.05). [†]One-way ANOVA with Tukey *post hoc* test comparison of treatment groups (*P*<0.05).

There was a moderately positive association of $|E^*|_{micro}$ with water and a moderately negative association with collagen type II, but no correlation with GAG and collagen type I content (Table 4.2).

Table 4.2: Associations between dynamic elastic modulus measured on micrometer and nanometer scale and biochemical parameters (GAG, collagen I, collagen II, and water)

	Association [Spearman's ρ(p)]	
	/E*/ *micro*	**/E*/** *nano*
GAG	−0.35 (0.108)	−0.24 (0.288)
Collagen I	−0.08 (0.710)	0.80 (<0.001)[a]
Collagen II	−0.56 (0.007)[a]	0.29 (0.191)
Water	0.44 (0.038)[b]	−0.46 (0.033)[b]

 Abbreviation: GAG, glycosaminoglycan.
[a] Association is significant at the 0.01 level (two-tailed).
[b] Association is significant at the 0.05 level (two-tailed).

Cartilage stiffness at nanometer scale

Dynamic elastic modulus $|E^*|$ values for native articular cartilage and reparative cartilage are presented in Figure 4.3b. The measurements were obtained with sharp pyramidal tip, nominal radius of 20 nm, and they reflect structural changes at the nanometer scale. Obtained $|E^*|_{nano}$ values suggested that the BMC-treated group had very similar stiffness to native cartilage (P=0.345, paired samples t-test), but that stiffness was higher in TGF- and GFP-treated groups (P=0.028 and P=0.005, respectively, paired samples t-test; Figure 4.3b). Furthermore, statistically significant differences in $|E^*|_{nano}$ were found between treatment groups (P<0.001, Kruskall–Wallis test). Stiffness was significantly higher in the GFP control group than in the TGF group (P=0.007, Mann–Whitney test), whereas BMC had lower $|E^*|_{nano}$ when compared with both GFP and TGF (P=0.001 and P=0.004, respectively, Mann–Whitney test).

There was a strong positive association of $|E^*|_{nano}$ with collagen I content and a moderate negative association with water content, but no correlation with GAG and collagen II content (Table 4.2).

Polymerase chain reaction analysis

To determine any expression levels from the gene transfer vectors within the synovial membrane 6 months after surgery, polymerase chain reaction (PCR) was performed using

primer sets recognizing the cytomegalovirus (CMV) promoter as well as sheep β-actin. The analysis included five groups of specimens according to treatment, namely TGF-β1 vector-treated, GFP vector-treated as a transduction control, bone marrow treated, empty defect group and controls from contralateral knee. PCR analysis of the synovial tissue revealed no presence of the CMV promoter in any of the treatment groups or the control group 180 days after implantation. Expression of the β-actin gene was detected in all of the analysed samples.

4.4 Discussion

It is well known that the healing of focal lesions in adult articular cartilage is very limited and, over time, they may progress to osteoarthritis. Articular cartilage damage is a growing health care problem and a recent study showed that approximately two thirds of patients undergoing knee arthroscopies have been diagnosed with cartilage lesions[23]. On the other hand, the growing armamentarium of novel biological methods and technologies offer scientists and clinicians powerful tools for developing effective new methods in treating damaged cartilage. The cornerstones on which a successful tissue engineering-based strategy will likely be built include an adequate supply of repair cells, sufficient induction of those cells by growth factor signalling, and a biocompatible scaffold conducive to the repair process [24].

The approach to focal cartilage defect repair described in this study uses vector-laden coagulated bone marrow aspirates for gene delivery to the defect site. Aspirated autologous bone marrow contains progenitor cells, the matrix is completely natural and native to the host, and the constitutive fibrin fibres adhere the whole construct to the surface of the defect. Preliminary *in vitro* and *in vivo* studies on small animals showed that clotted mixtures of adenoviral suspensions with fresh aspirated bone marrow resulted in levels of transgenic expression in direct proportion to the density of nucleated cells within the clot [15]. This study is a step forward towards a clinical application of these gene plugs to treat local cartilage lesions. The whole study was conceived in a way to simulate potential clinical situation where one would have to treat isolated chondral defect situated on the load-bearing surface of the femoral condyle. Therefore, sheep were chosen for a large animal model. One drawback of the proposed model is the fact that sheep cartilage on the medial condyle is very thin. Ahern *et al.* [25] performed a detailed systematic review of preclinical animal models in single-site cartilage defect testing. According to their analysis, the ovine cartilage is variable in thickness and it measures from 0.40–1.68 mm. Minor variability in the obtained results

might be contributed to that fact, nevertheless, reproducible standardized chondral defects could be created in all animals, using an adapted punch-drill device. For implantation of the gene plugs, standard operation instruments were used. The proposed method proved to be a fairly straightforward technique for application in clinical settings. It is a single-step operation, which can be easily done by two surgeons within 30–45 min.

The use of TGF-β1-transduced BMCs for articular cartilage defects repair

Adult MSCs present a very interesting platform for the development of treatment strategies in orthopaedic tissue engineering. They can be obtained relatively easily from various tissue sources such as bone marrow, fat and muscle, and under appropriate conditions they have the capacity of differentiation into various mesenchymal lineages including bone and cartilage [5,26]. Numerous *in vitro* studies showed that primary MSCs undergo chondrogenic differentiation when cultured in the presence of specific media supplements, including dexamethasone and certain extracellular biological cues [27,28].

TGF-β1 has been used as a key inductor of chondrogenesis in many *in vivo* and *in vitro* studies, as it stimulates cell proliferation and synthesis of major components of ECM, GAG and collagen [29,30,31]. It was chosen for use in this study because it is one of the best characterized and most potent chondrogenic growth factors. The results of this study showed that all groups that underwent transplantation of BMCs have a high content of GAGs, but only the repair tissue from defects treated with TGF-β1 gene plugs had a very high content of collagen type II similar to native cartilage. The fact that only TGF-treated defects scored statistically higher in terms of columnar cellular distribution suggests that residing mesenchymal progenitors within the gene plug responded to the local expression of TGF-β1 in terms of chondrogenic differentiation, which ultimately resulted in higher ECM turnover and better quality of the cartilage repair. Guo *et al* [32] reported similar results in a rabbit model of full-thickness cartilage defects using an *ex vivo* approach and a chitosan scaffold. Another study by Pagnotto *et al.* [33] showed improved cartilage repair in osteochondral defects implanted with MSCs transduced with adeno-associated virus (AAV) carrying cDNA for TGF-β1. In their study, transgene expression slowly decreased from 100% at 2 weeks to 17% at 12 weeks, but it proved that gene therapy enables sustained delivery of the bioactive molecules for a period of time that is sufficient to induce and govern cellular response within the defect. Owing to its safe profile, AAV is considered to be the most suitable viral vector for human application, and is currently being tested in a phase I clinical trial [34].

Integration of newly formed cartilage with and neighbouring, undamaged tissue has always been a major issue in cartilage repair. Poor integration causes uneven distribution of mechanical loading, and predisposes the joint surface to the development of early degenerative changes. Although certain improvement in integration was observed in TGF-treated groups, the overall integration is far from being optimal.

Considering that a number of biological factors act in a highly coordinated manner during native tissue development, the use of a single factor to stimulate and regulate process of chondrogenic differentiation, while practical, has limitations with regard to the producing cartilage of optimal quality. Chondrogenesis is a finely regulated process, which includes numerous growth and transcription factors, and a combination of these might be more effective. For example, synergistic effects on chondrogenesis have been reported for TGF-β1 when co-administered with IGF-1 [35]. Steinert *et al.* [36] recently used an aggregate culture system to study effects of co-expression of TGF-β1, IGF-1 and BMP-2 on MSCs. Their results showed larger aggregates, higher levels of GAG synthesis and greater expression of cartilage specific marker genes by adding different combinations of growth factors. Furthermore, it is known that TGF stimulation of MSCs promotes hypertrophy and the increased expression of collagen type I and X. However, Kafienah *et al.* [37] have shown that including parathyroid hormone-related protein downregulates collagen type I and X in cartilage tissue engineered from MSCs. It should be also noted that some transcription factors such as Sox-9 (which is known to be essential for the full expression of chondrocyte phenotype) and Wnt are not chondrogenic itself, but can make cells more responsive to growth factors and other chondrogenic stimuli. Along these lines, to optimize the proposed method, delivery of multiple genes might be more reliable option, and further studies are needed to pinpoint the exact protocol in terms of concentration and temporal sequence of delivery of chosen genes.

Another important drawback to our study was the fact that we were not able to control weight-loading conditions in the operated animals. Inconsistencies in repair quality within the treatment groups could be attributed to the influence of the weight-loading conditions of the joint immediately after the surgical procedure. In human patients, proper rehabilitation protocols are crucial to optimize the results of bone marrow stimulating as well as cell-based techniques, including postoperative continuous passive motion exercises along with crutch-assisted restrictions of weight-bearing up to 6–8 weeks [38,39]. Practical limitations

prevented postoperative ambulation restrictions, possibly allowing detrimental shear forces on the construct and leading to a reduced quality of produced matrix. These limitations might be reflected in the fact that TGF-treated groups had good concentrations of GAGs and collagen II, but very high content of collagen I and low content of water.

Determining biomechanical properties of cartilage repair tissues by indentation-type atomic force microscopy

Biochemical and histological parameters provide information regarding the amount and spatial distribution of the major components comprising repaired cartilage. However, only biomechanical analysis can assess the load-bearing capabilities of the cartilage and therefore biomechanical parameters reflect the functionality of the repaired tissue. To determine load-bearing capabilities of examined tissue, indentation-type atomic force microscopy (IT AFM) was used to determine *stiffness*—a mechanical parameter that describes the relation between an applied, nondestructive load and resultant viscoelastic deformation of cartilage tissue. Furthermore, biomechanical data with biochemical content was correlated.

Hyaline cartilage is highly specialized tissue with unique three-dimensional structure, which allows it to behave mechanically as a viscoelastic solid [40]. This reflects the unique ultrastructure of cartilage ECM, which is composed of proteoglycans embedded into a network of different types of collagen fibrils. Under cyclic loading, the applied stress and resulting strain are not in phase. To determine stiffness of the cartilage, compressive force is applied and the ratio of stress to strain, the dynamic elastic modulus $|E^*|$, is calculated. Several studies describe the use of probes of varying shape for indentation testing of cartilage where data are typically assessed at millimeter scale. However, this is insufficient to detect local mechanical property variations of the examined tissue that reflect differences in cartilage structural organization at the molecular level [41,42].

To overcome these limitations, Stolz *et al.* [22] proposed a novel, AFM-based approach they termed IT AFM. Their protocol enabled absolute measurements of the dynamic elastic modulus $|E^*|$ at two different length scales of tissue organization—micrometer and nanometer. This is technically possible because two different probe types are used for these measurements: the microspherical tips for micrometerscale measurements, and sharp pyramidal tips for nanometerscale measurements. In our study, dynamic elastic modulus $|E^*|_{nano}$ of the native sheep cartilage is ~0.02 MPa, and $|E^*|_{micro}$ is ~1 MPa, which is in agreement with studies performed on human cartilage, where stiffness values averages

around 0.015 and 2.6 MPa, respectively, for healthy individuals without OA [43,44]. According to Stolz *et al.*, this 100-fold modulus difference between micrometer and nanometer scale is a result of assessing different levels of cartilage hierarchical organization. On the micrometer scale, articular cartilage behaves as relatively amorphous material, whereas at the nanometer scale, ultrastructural differences are resolved.

Microstiffness values were lowest for native cartilage and gradually rose from TGF- and BMC- to GFP-treated groups, respectively (Figure 4.2). This would suggest that the repair tissue of the TGF-treated group is qualitatively superior to the other two groups showing biomechanical properties close to native cartilage. However, nanoscale measurement showed that the BMC-treated group has very similar nanostiffness to that of native cartilage, and the stiffness values of the TGF- and GFP-treated groups are much higher (Figure 4.3). We hypothesized that this observation could reflect different amounts and spatial orientation of newly synthesized extracellular components and/or water content within the repair tissue in the last two groups. To test this hypothesis, correlation analysis was performed, which showed that the dynamic elastic modulus $|E^*|_{micro}$ correlated moderately positively with water and moderately negatively with collagen type II, but not with GAG and collagen type I content (Table 4.2). At the same time, $|E^*|_{nano}$ correlates strongly positive with collagen type I and moderately negative with water, but not with GAG and collagen type II content (Table 4.2). At the micrometer level, biomechanical properties of cartilage repair tissue are only moderately correlated with the biochemical content. This observation leads us to conclusion that, at micrometer level of tissue organization, it is not possible to determine contribution of individual ECM components to biomechanical properties of repaired cartilage. However, at the nanometer level, dynamic elastic modulus correlates with collagen I content, which is barely present in native cartilage. A sharp AFM tip has nominal radius of 20 nm that is smaller than an individual collagen fibril, which typically measures around 50 nm.[22] Although microspherical tip is too big to detect subtle differences in orientation and amount of collagen fibrils, sharp pyramidal tip can discriminate such differences, resulting in higher stiffness values.

Presence of adenoviral vector in the surrounding synovial lining

The use of viral-based gene therapy is controversial with regards to safety. Although very effective in terms of gene transfer and expression, viral vectors induce immune response and their presence in the surrounding tissue may result with detrimental side effects. For example,

TGF-β1 administered into the joint in sufficient concentrations can lead to chondrophyte formation at the joint margins, which at later stages calcify and become real osteophytes [45]. One of the major goals of this study was to determine whether there is any residual presence of virus within the synovium. After killing the animals, joints were inspected for any signs of osteophyte formation and/or arthrofibrosis, but none was detected. Although PCR analysis of the synovial lining tissue could not detect the residual presence of transgene in any of the experimental groups, suggesting that the virus is well contained within the clot, this information should be taken cautiously. Given what is known about the immune response to adenovirus and adenovirally modified cells, it is possible that any modified cells within the synovial tissue were cleared after 6 months. Future studies should use additional procedures, such as measure of elevated cytokines from lavage fluid during the first weeks following surgery, as a more sensitive indication of undesired side effects within the joint. The next generation of improved gene vehicles, such as those based on recombinant AAV (rAAV), might be more suitable for cartilage repair than the first generation adenoviral vectors used in this study. In comparison to adenovirus, rAAV is less immunogenic, and the reduced risk of adverse reactions is a substantial advantage favouring the use of this class of vector [20].

In conclusion, this study systematically explored the benefits and pitfalls of the novel technique to treat local cartilage defects by using gene plugs in clinical settings. In contrast to more complex approaches in tissue engineering, we advocate the use of simpler methods that harness the intrinsic regenerative potential of endogenous tissues, using biological stimuli to initiate and promote natural healing *in situ*. This concept has been termed *facilitated endogenous repair* by Evans *et al.* [46] and the ultimate goal is to enable clinicians to use tissue engineering that is not only successful but also cheap, safe and clinically expeditious. The proposed method is a single-step procedure that can be easily implemented in standard clinical settings, avoids the usual drawbacks associated with gene therapy because it is administered locally, and excludes the expensive *in vitro* production of autologous and engineered tissues.

4.5 Materials and Methods

Vector construction

The first generation recombinant vectors used in this study originated form replication-deficient type 5 adenovirus lacking E1 and E3 loci (Ad.).16 Vectors directing overexpression of TGF-β1 (Ad.TGF-β1) and Ad.GFP—each driven by the CMV promoter—were

constructed by Cre-lox recombination using the system of Hardy et al.17 These adenoviral vectors were propagated in 293-CRE8 cells and purified on three successive CsCl2 density gradients between 1.2 and 1.4 g ml−1. Following dialysis in 10 mM Tris-HCL, pH 7.8, 150 mM NaCl, 10 mM MgCl2 and 4% sucrose, the preparations were aliquotted and stored at −80 °C. Viral titers were estimated by optical density and standard plaque assay.

Animals

Twenty-eight skeletally mature sheep (female, 1−3 years old) were used for this study. The sheep were randomly assigned to one of the four groups. In the BMC group (*n*=6), the sheep were implanted with untreated autologous BMC that was aspirated from iliac crest of respective animal. In the GFP group (*n*=6), autologous BMCs genetically modified with Ad.GFP were implanted in sheep as a vector control. In the TGF-β1-treated (TGF) group (*n*=10), autologous BMCs genetically modified Ad.TGF-β1 were implanted in the sheep. In the negative control (CON) group (*n*=6), defects were left empty. Native cartilage from the contralateral knee was harvested from each animal and compared with the repair tissue of the defect sites. The experimental protocol was approved by the local Animal Experiment Ethical Committee.

Anaesthesia protocol

The sheep were operated on under general anaesthesia and aseptic conditions. The premedication was performed with 0.1 mg kg−1 of intramuscular xylazine (Xylapan, Vetoquinol, Bern, Switzerland) and cephalic vein was prepared for administration of drugs. Induction of anaesthesia was performed intravenously with 2.5% solution of thiopentale sodium (Thiopental, Nycomed, Ismaning, Germany) in a dose 5 mg kg−1 and small boluses of drug were administered until the jaws were relaxed for endotracheal intubation. Cefuroxime (Ketocef, Pliva, Zagreb, Croatia) was administered perioperatively. Carprofen (Rymadil, Pfizer Animal Healthcare, Exton, PA, USA) was administered postoperatively in a dose of 2 mg kg−1.

Surgical procedure

Medial parapatellar arthrotomy was performed on the right knee of each animal, and both condyles were exposed. A standardized partial-thickness chondral defect of 6.2 mm in diameter (Figures 4a and b) was made on the weight-bearing surface of the medial condyle

using a punch-drill device adapted from mosaicplasty instrumentation (Smith & Nephew Inc., Andover, MA, USA). Special care was taken not to damage the subchondral bone, as well as to create sharp edges at the border of the defects that were perpendicular to the joint surface. Defects were then treated as described below.
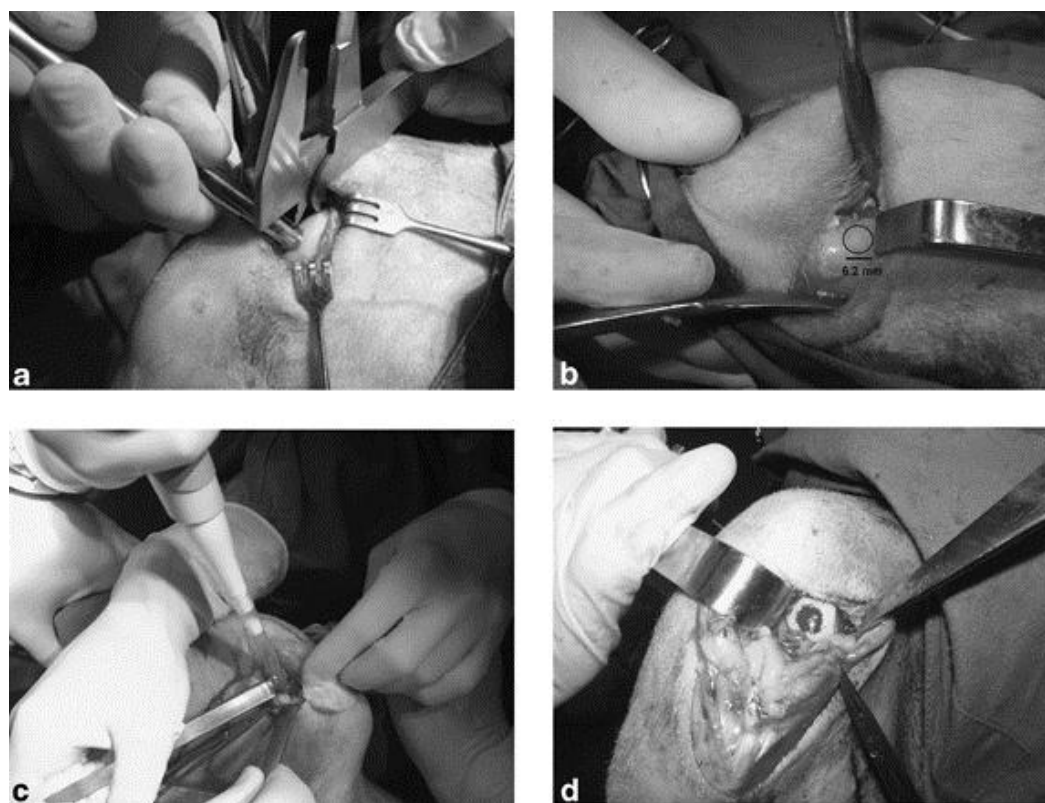
Figure 4.4 Implantation of a gene plug. (**a**) An adaptation of standardized mosaciplasty instrumentation was used to create a chondral defect on the weight-bearing surface of the medial condyle in sheep. (**b**) Care was taken not to penetrate the subchondral plate. The defect measured 6.2 mm in diameter. (**c**) Pressfit implantation of the bone marrow construct into the defect. (**d**) The plug is stable and well placed within the defect. The joint is rinsed with saline and ready to be closed.

Press-fit implantation of gene plugs and native bone marrow plugs into the defects

Under sterile surgical conditions, 3 ml of bone marrow was aspirated form the right iliac crest of an anaesthetized sheep using a TrapsystemSet (H-S Medical Inc., Boca Raton, FL, USA) and a 16-g needle. Using a 1-ml micropipette, aliquots of 250 µl were rapidly mixed with 25 µl suspension of 1×1010 viral particles of Ad.GFP or Ad.TGF-β1. The mixtures were pipetted into the defects and immediately covered with a paper to build a chamber and allow coagulation in situ for 5 min. The paper was then removed, and the implants were rinsed with saline solution and checked for stability by repetitive flexion and extension of the knee. The joint was closed by suturing in two layers (Figures 4.4c and d).

Gene transfer to BMCs for in vitro culture

A portion of bone marrow aspirate obtained from iliac crest (as described in previous paragraph) was used to generate genetically modified BMCs for in vitro culture. Using a 1-ml micropipette, aliquots of 250 μl of bone marrow aspirate were rapidly mixed with 25 μl suspension of 1×1010 viral particles of Ad.GFP. Following coagulation, the BMCs were removed from the vessel, and placed in individual wells of 24-well plates with 0.5 ml of DMEM with 10% FBS and 1% penicillin/streptomycin. Media were replaced every 3 days. Clots were maintained in this manner for 21 days until analysed with fluorescence microscopy. Native BMCs were used as negative controls. This parallel set of in vitro cultures served as indirect proof of transgenic expression within the transplanted gene plugs.

Harvesting the samples

Six months after surgery, all sheep were killed by intravenous injection of an overdose of barbiturate. The medial condyle containing the cartilage defect was removed and divided into two halves using a cooled saw: one being used for histology and one for biochemistry and biomechanical testing. Undamaged articular cartilage was taken from the medial condyle of the contralateral knee joint for comparison with treated condyles. The specimens for histology, biochemical and biomechanical analysis were prepared as described below. Synovial lining specimens were also taken from each joint and stored in liquid nitrogen for PCR analysis.

Morphologic analysis—histology

The osteochondral samples fixed for histology were decalcified in 10% ethylenediaminetetraacetic acid. The samples were dehydrated in alcohol, embedded in paraffin and sectioned at 5 μm. Sections were stained with haematoxylin and eosin to evaluate morphology, and safranin-O to assess proteoglycan distribution in the pericellular matrix. Slides were examined by two blinded observers using light microscopy and graded semiquantitatively using the ICRS Visual Histological Assessment Scale [18]. The scoring system was based on articular surface morphology, matrix composition, cellular distribution, cell population viability, subchondral bone morphology and cartilage mineralization.

Quantitative biochemical characterization

Samples were frozen and stored at $-80\,°C$ until ready for analysis. Wet and dry weights of the cartilage or repair tissue were determined before and after freeze drying. The samples were then solubilized using digestion with trypsin and processed for complete biochemical analysis, as described by Dickinson et al [19].

Each sample was milled in liquid nitrogen using a stainless steel percussion mortar and pestle, to obtain a fine particulate, and weighed after freeze drying to obtain the dry weight. Bovine pancreatic trypsin was prepared at $2\,mg\,ml{-}1$ in Tris buffer (pH 7.5) containing 1 mM iodoacetamide, 1 mM ethylenediaminetetraacetic acid and $10\,mg\,ml{-}1$ pepstatin A (all from Sigma-Aldrich, St Louis, MO, USA). An initial incubation for 15 h at $37\,°C$ with 250 ml trypsin was followed by further 2 h incubation at $65\,°C$ after the addition of a further 250 ml of the freshly prepared proteinase. All samples were boiled for 15 min at the end of incubation to destroy any remaining enzyme activity.

Type I collagen

The digests were assayed using inhibition enzyme-linked immunosorbent assay using a rabbit antipeptide antibody to type I collagen, as described earlier [19].

Type II collagen

The digests were assayed using inhibition enzyme-linked immunosorbent assay using a mouse immunoglobulin G monoclonal antibody to denatured type II collagen, COL2–3/4 m, as described earlier, but modified for use on 384-well plates to allow the use of a smaller volume of sample than is required for a 96-well plate [20].

Glycosaminoglycans

A previously described colorimetric assay for GAG was modified for use on 384-well plates to allow the use of a smaller volume of sample than is required for a 96-well plate [19,21].

Water content

The percentage of water was calculated by subtracting the dry weight of the sample and dividing the difference by the wet weight.

PCR analysis

To detect the presence of adenoviral genome in the synovial lining, PCR analysis was performed. Synovial membranes of the joints were digested with proteinase K for 4 h at 37 °C. Total DNA was then extracted using a DNeasy Tissue kit (Qiagen, Valencia, CA, USA), following the manufacturer's instructions. Amplification of the CMV promoter sequence within the vectors as well as the sheep β-actin gene was performed using the following primers: CMV forward 5′-TCATATGCCAAGTACGCCCCC-3′, reverse 5′-TGGGGCGGAGTTGTTACGAC-3′; β-actin forward 5′CATGCCATCCTGCGTCTGGACC-3′, β-actin reverse 5′ TACTCCTGCTTGCTGATCCACATCTGC-3′. Amplification products were visualized on agarose gel with ethidium bromide.

Biomechanical properties

Biomechanical properties of the repair tissue compared with regular cartilage from the contralateral knee was assessed by IT AFM of 2 mm diameter samples, harvested using a skin biopsy punch and scalpel. Care was taken to include the full thickness of the repair tissue but to exclude any subchondral bone. The specimens were then stored in the cold room at 4° Celsius in PBS supplemented with protease inhibitor cocktail (Complete, Boehringer Mannheim, Germany).

Mechanical properties (that is, stiffness) of articular cartilage and repair tissue were determined by measurements of |E*|, the dynamic elastic modulus of articular cartilage, at two different length scales of tissue organization: micrometer (|E*|micro) and nanometer (|E*|nano). Preparation of the cartilage samples, data acquisition and processing was done as described by Stolz et al.[22] Briefly, spherical tips with radius of 7.5 μm (SPI Supplies, West Chester, PA, USA) were mounted onto the end of rectangular tipples silicon nitride cantilevers having nominal spring constants of 0.35 N m−1 (MicroMasch, San Jose, CA, USA) and used for micrometer-scale experiments. For nanometer-scale experiments, square-based pyramidal silicon-nitride tips with a nominal tip radius of 20 nm were used on V-shaped 200-mm-long silicon nitride cantilevers with a nominal spring constant of 0.06 N m−1 (Veeco Instruments Inc., Plainview, NJ, USA). The IT AFM was operated in the force-volume mode, where the load–displacement curves were recorded at five different sites on the sample surface at a frequency of 3 Hz with scan areas of 0×0 μm and 10×10 μm. Data sets recorded at any given sample site consisted of 256 load–displacement curves (each curve

consisting of 512 data points), which were analyzed to compute the dynamic elastic modulus |E*|.

Statistics

A Kolmogorov–Smirnov test was used to test distributions of biochemical (GAG, collagen I, collagen II and water) and biomechanical data (|E*|micro and |E*|nano) for normality. Distributions were normal for all data sets except for |E*|nano. Therefore, parametric tests were used to analyse all biochemical and biomechanical data, whereas elastic modulus data were analysed by nonparametric testing. Biochemical and biomechanical properties of repaired cartilage were expressed as the mean (M) ± s.d. As the contralateral knee in each animal served as its own control, a two-tailed paired samples t-test was used to compare treatment versus control groups. Data from each test subsets were compared by one-way ANOVA with Tukey post hoc test where required. To analyse |E*|nano, results, we used Wilcoxon matched pairs test as a nonparametric equivalent of the paired samples t-test and Kruskal–Wallis and Mann–Whitney tests as equivalents of ANOVA and Tukey post hoc. Nonparametric tests were also used to analyse semiquantitative histological scores. Association between biomechanical properties and biochemical content were determined using Spearman correlation. Statistical significance was set at $P<0.05$. All analyses were performed using SPSS 17.0 for Windows (SPSS Inc., Chicago, IL, USA).

4.7 References

1. Saris DB, Vanlauwe J, Victor J, Haspl M, Bohnsack M, Fortems Y *et al.* Characterized chondrocyte implantation results in better structural repair when treating symptomatic cartilage defects of the knee in a randomized controlled trial versus microfracture. Am J Sports Med 2008; 36: 235–246.

2. Brittberg M, Lindahl A, Nilsson A, Ohlsson C, Isaksson O, Petrson L. Treatment of deep cartilage defects in the knee with autologous chondrocyte transplantation. N Engl J Med 1994; 331: 889–895|

3. Buckwalter JA, Brown TD. Joint injury, repair and remodeling: roles in post-traumatic osteoarthritis. Clin Orthop Relat Res 2004; 423: 7–16.

4. Ghivizzani SC, Oligino TJ, Robbins PD, Evans CH. Cartilage injury and repair. Phys Med Rehab Clin North Am 2000; 11: 289–307.

5. Pittenger MF, Mackay AM, Beck SC, Jaiswal RK, Douglas R, Mosca JD *et al.* Multilineage potential of adult human mesenchymal stem cells. Science 1999; 284: 143–147.

6. Glansbeek HL, van Beuningen HM, Vitters EL, van der Kraan PM, van den Berg WB. Stimulation of articular cartilage repair in established arthritis by local administration of transforming growth factor beta into murine knee joints. Lab Invest 1998; 78: 133–142.

7. Jelic M, Pecina M, Haspl M, Kos J, Taylor K, Maticic D *et al.* Regeneration of articular cartilage chondral defects by osteogenic protein-1 (bone morphogenetic protein-7) in sheep. Growth Factors 2001; 19: 101–113

8. Fortier LA, Mohammed HO, Lust G, Nixon AJ. Insulin-like growth factor I enhances cell-based repair of articular cartilage. J Bone Joint Surg Br 2002; 84-B: 95–108.

9. Kaps C, Bramlage C, Smolian H, Haisch A, Ungethüm U, Burmester GR *et al.* Bone morphogenetic proteins promote cartilage differentiation and protect engineered artificial cartilage from fibroblast invasion and destruction. Arthritis Rheum 2002; 46: 149–162.

10. Evans CH, Ghivizzani SC, Smith P, Shuler FD, Mi Z, Robbins PD. Using gene therapy to protect and restore cartilage. Clin Orthop Relat Res 2000; 379: 214–219.

11. Evans CH, Ghivizzani SC, Robbins PD. Orthopaedic gene therapy. Clin Orthop Relat Res 2004; 429: 316–329

12. Kang R, Marui T, Ghivizzani SC, Nita IM, Georgescu HI, Suh JK *et al. Ex vivo* gene transfer to chondrocytes in full-thickness articular cartilage defects: a feasibility study. Osteoarthr Cartil 1997; 5: 139–143.

13. Mason JM, Grande DA, Barcia M, Grant R, Pergolizzi RG, Breitbart AS. Expression of human bone morphogenetic protein 7 in primary rabbit periosteal cells: potential utility in gene therapy for osteochondral repair. Gene Ther 1998; 5: 1098–1104.

14. Safran MR, Kim H, Zaffagnini S. The use of scaffolds in the management of articular cartilage injury. J Am Acad Orthop Surg 2008; 16: 306–311.

15. Pascher A, Palmer GD, Steinert A, Oligino T, Gouze E, Gouze J-N *et al*. Gene delivery to cartilage defects using coagulated bone marrow aspirate. Gene Ther 2004; 11: 133–141.

16. Yeh P, Perricaudet M. Advances in adenoviral vectors: from genetic engineering to their biology. FASEB 1997; 11: 615–623.

17. Hardy S, Kitamura M, Harris-Stansil T, Dai Y, Phipps ML. Construction of adenovirus vectors through Cre-lox recombination. J Virol 1997; 71: 1842–1849.

18. Mainil-Varlet P, Aigner T, Brittberg M, Bullough P, Hollander A, Hunziker E *et al*. Histological assessment of cartilage repair. J Bone J Surg Am 2003; 85-A: 45–57.

19. Dickinson SC, Sims TJ, Pittarello L, Soranzo C, Pavesio A, Hollander AP. Quantitative outcome measures of cartilage repair in patients treated by tissue engineering. Tissue Eng 2005; 11: 277–287.

20. Cucchiarini M, Madry H, Ma C, Thurn T, Zurakowski D, Menger MD *et al*. Improved tissue repair in articular cartilage defects *in vivo* by rAAV-mediated overexpression of human fibroblast growth factor 2. Mol Ther 2005; 12: 229–238

21. Handley CJ, Buttle DJ. Assay of proteoglycan degradation. Methods Enzymol 1995; 248: 47–58.

22. Stolz M, Raiteri R, Daniels AU, Van Landingham MR, Baschong W, Aebi U. Dynamic elastic modulus of porcine articular cartilage determined at two different levels of tissue organization by indentation-type atomic force microscopy. Biophys J 2004; 86: 3269–3283

23. Aroen LS, Heir S, Alvik E, Ekeland A, Granlund OG, Engebretsen L. Articular cartilage lesions in 993 consecutive knee arthroscopies. Am J Sports Med 2004; 32: 211–215.

24. Freed LE, Guilak F, Guo EX, Gray ML, Tranquillo R, Holmes JW *et al*. Advanced tools for tissue engineering: scaffolds, bioreactors, and signaling. Tissue Eng 2006; 12: 3285–3305.

25. Ahern BJ, Parvizi J, Boston R, Schaer TP. Preclinical animal models in single site cartilage defect testing: a systematic review. Osteoarthr Cartil 2009; 17: 705–713

26. Caplan AI. Mesenchymal stem cells and gene therapy. Clin Orthop Relat Res 2000; 379: S67–S70.

27. Goldring MB, Tsuchimochi K, Ijiri K. The control of chondrogenesis. J Cell Biochem 2006; 97: 33–44|

28. Chen FH, Rousche KT, Tuan RS. Technology insight: adult stem cells in cartilage regeneration and tissue engineering. Nat Clin Pract Rheumatol 2006; 2: 373–382.

29. Tuli R, Tuli S, Nandi S, Huang X, Manner PA, Hozack WJ *et al*. Transforming growth factor-beta-mediated chondrogenesis of human mesenchymal progenitor cells involves N-cadherin and mitogen-activated protein kinase and Wnt signaling cross-talk. J Biol Chem 2003; 278: 412–427

30.   Palmer GD, Steinert A, Pascher A, Gouze E, Gouze J, Betz O *et al*. Gene-induced chondrogenesis of primary mesenchymal stem cells *in vitro*. Mol Ther 2005; 2: 219–228

31.   Lee KH, Song SU, Hwang TS, Yi Y, Oh IS, Lee JY *et al*. Regeneration of hyaline cartilage by cell-mediated gene therapy using transforming growth factor beta 1-producing fibroblasts. Hum Gene Ther 2001; 12: 1805–1813.

32.   Guo CA, Liu XG, Huo JZ, Jiang C, Wen XJ, Chen ZR. Novel gene-modified-tissue engineering of cartilage using stable transforming growth factor-beta1-transfected mesenchymal stem cells grown on chitosan scaffolds. J Biosci Bioeng 2007; 103: 547–556

33.   Pagnotto MR, Wang Z, Karpie JC, Feretti M, Xiao X, Chu CR. Adeno-associated viral gene transfer of transforming growth factor-ß1 to human mesenchymal stem cells improves cartilage repair. Gene Ther 2007; 14: 804–813.

34.   McPhee SW, Janson CG, Li C, Samulski RJ, Camp AS, Francis J *et al*. Immune response to AAV in phase I study for Canavan disease. J Gene Med 2006; 8: 577–588

35.   Yaeger PC, Masi TL, de Ortiz JL, Binette F, Tubo R, McPherson JM. Synergistic action of transforming-growth factor-beta and insulin-like growth factor-I induces expression of type II collagen and aggrecan genes in adult articular chondrocytes. Exp Cell Res 1997; 237: 318–325.

36.   Steinert AF, Palmer GD, Pilapil C, Ulrich N, Evans CH, Ghivizzani SC. Enhanced *in vitro* chondrogenesis of primary mesenchymal stem cells by combined gene transfer. Tissue Eng 2008; 14: 1–13.

37.   Kafienah W, Mistry S, Dickinson SC, Sims TJ, Learmonth I, Hollander AP. Three-dimensional cartilage tissue engineering using adult stem cells from osteoarthritis patients. Arthritis Rheumat 2007; 56: 177–187.

38.   Steadman JR, Briggs KK, Rodrigo JJ, Kocher MS, Gill TJ, Rodkey WG. Outcomes of microfracture for traumatic chondral defects of the knee: average 11-year follow-up. Arthroscopy 2003; 19: 477–484.

39.   Steadman JR, Rodkey WG, Rodrigo JJ. Microfracture: surgical technique and rehabilitation to treat chondral defects. Clin Orthop Relat Res 2001; 391 (Suppl): S362–S369

40.   Poole AR, Kojima T, Yasuda T, Mwale F, Kobayashi M, Laverty S. Composition and structure of articular cartilage: a template for tissue repair. Clin Orthop Relat Res 2001; 391 (Suppl): S26–S33.

41.   Appleyard RC, Swain MV, Khanna GA, Murrell GA. The accuracy and reliability of novel handheld dynamic indentation probe for analysing articular cartilage. Phys Med Biol 2001; 46: 541–550

42.   Lyyra T, Jurvelin J, Pitkanen U, Vaatainen U, Kiviranta I. Indentation instrument for the measurement of cartilage stiffness under arthroscopic control. Med Eng Phys 1995; 17: 395–399.

43.   Stolz M, Aebi U, Stoffler D. Developing scanning probe-based nanodevicesμ— stepping out of the laboratory into the clinic. Nanomedicine 2007; 3: 53–62.

44.   Swanepoel MW, Smeathers JE, Adams LM. The stiffness of human apophyseal articular cartilage as an indicator of joint loading. Proc Inst Mech Eng H (J Eng Med) 1994; 208: 33–43.

45.   Van Beuningen HM, van der Kraan PM, Arntz OJ, van den Berg WB. Transforming growth factor-β1 stimulates articular chondrocyte proteoglycan synthesis and induces osteophyte formation in the murine knee joint. Lab Invest 1994; 71: 279–290.

46.   Evans CH, Palmer GD, Pascher A, Porter RM, Kwong FN, Gouze E et al. Facilitated endogenous repair: making tissue engineering simple, practical and economical. Tissue Eng 2007; 8: 1987–1993.

Chapter 5

Anabolic and catabolic responses of human articular chondrocytes to varying oxygen percentages

Simon Ströbel, Marko Loparic, David Wendt, Andreas D Schenk, Christian Candrian, Raija LP Lindberg, Florina Moldovan, Andrea Barbero and Ivan Martin

5.1 Abstract

Introduction

Oxygen is a critical parameter proposed to modulate the functions of chondrocytes ex-vivo as well as in damaged joints. This article investigates the effect of low (more physiological) oxygen percentage on the biosynthetic and catabolic activity of human articular chondrocytes (HAC) at different phases of in vitro culture.

Methods

HAC expanded in monolayer were cultured in pellets for two weeks (Phase I) or up to an additional two weeks (Phase II). In each Phase, cells were exposed to 19% or 5% oxygen. Resulting tissues and culture media were assessed to determine amounts of produced/released proteoglycans and collagens, metalloproteinases (MMPs), collagen degradation products and collagen fibril organization using biochemical, (immuno)-histochemical, gene expression and scanning electron microscopy analyses. In specific experiments, the hypoxia-inducible factor-1α (HIF-1α) inhibitor cadmium chloride was supplemented in the culture medium to assess the involvement of this pathway.

Results

Independent from the oxygen percentage during expansion, HAC cultured at 5% O_2 (vs 19% O_2) during Phase I accumulated higher amounts of glycosaminoglycans and type II collagen and expressed reduced levels of MMP-1 and MMP-13 mRNA and protein. Switching to 19% oxygen during Phase II resulted in reduced synthesis of proteoglycan and collagen, increased release of MMPs, accumulation of type II collagen fragments and higher branching of collagen fibrils. In contrast, reducing O_2 during Phase II resulted in increased proteoglycan and type II collagen synthesis and reduced expression and release of MMP-13 mRNA and protein. Supplementation of cadmium chloride during differentiation culture at 5% O_2 drastically reduced the up-regulation of type II collagen and the down-regulation of MMP-1 mRNA.

Conclusions

The application of more physiologic oxygen percentage during specific phases of differentiation culture enhanced the biosynthetic activity and reduced the activity of catabolic enzymes implicated in cartilage breakdown. Modulation of the oxygen percentage during HAC culture may be used to study pathophysiological events occurring in osteoarthritis and to enhance properties of in vitro engineered cartilaginous tissues.

5.2 Introduction

Homeostasis of normal cartilage in adults represents a delicate balance between the synthesis and the degradation of extracellular matrix components to maintain the functional integrity of the joint. In elderly individuals, together with changes in proliferation activity, energy metabolism and response to growth factors [1], chondrocytes become less resistant to extrinsic stress. This in turn causes a disturbance of tissue homeostasis and thus the risk of degenerative pathologies of osteoarthritic nature [2]. In particular the oxidative stress is proposed to play a key role in cartilage degeneration.

Oxygen is a critical parameter proposed to modulate chondrocyte metabolic activity [3]. Indeed, articular cartilage is generally exposed to a finely regulated gradient of relatively low oxygen percentages (from about 10% at the surface to about 1% in the deepest layers) [4], which is essential for maintenance of specialized tissue function [5]. During the onset of cartilage degeneration, possibly due to surface fibrillation and/or microfractures of the subchondral bone, such gradients have been proposed to break down [6], thus contributing to the progression of the disease.

The influence of various oxygen percentages on chondrocyte function has been investigated in a broad variety of models, differing with respect to (i) the cell source used (species: bovine, chicken, rodents, human, and anatomical locations of cell harvesting: knee, hip, interphalangeal joint, nose), (ii) the characteristic of the donor (age, stage of cartilage degeneration), (iii) the oxygen percentage applied (from less then 1% to more than 60%), (iv) the hydrodynamic culture conditions (static culture or mixing within bioreactors), and (v) the stage of cell differentiation (cells in native tissue, de-differentiated cells, re-differentiating expanded cells in pellets, alginate gels, or different types of porous scaffolds). It is thus not surprising that the data reported in literature on the influence of oxygen percentage on chondrocyte behavior are rather controversial [3]. For instance, as compared to culture under normoxic conditions (18 to 21% oxygen), culture at more physiological, low oxygen percentages (1 to 8%) has been reported to increase [7-10], decrease [11,12] or have no effect on the chondrocyte proliferation rate [6,13-15]. Moreover, the expression of cartilage specific genes and/or the extent of matrix protein synthesis/deposition was reported to be up-regulated [6-9,12,15-22], down-regulated [10,23-26] or not modulated at all [6,9] by culture under more physiological oxygen percentages.

Importantly, in addition to the still controversial findings, in the above mentioned studies the effect of oxygen percentage on chondrocytes has mainly been investigated with regard to the cell biosynthetic activity, without considering and exploring chondrocyte catabolic processes.

We thus aimed our study at investigating the effect of a low (more physiological) oxygen percentage both on the cartilage tissue forming capacity of human articular chondrocytes (HAC), and on their pro-catabolic, matrix degradative activity. In particular, we hypothesized that culture at a more physiological oxygen percentage has a dual role in the chondrocyte metabolism, by enhancing their biosynthetic activity and at the same time reducing the expression of matrix degradative enzymes. To test these hypotheses, HAC were exposed to normoxic conditions (19%) or to a low oxygen percentage (5%) during culture in two simple and widely used model systems (that is, monolayer expansion or differentiation in micromass pellets), as well as at different phases of tissue development (that is., during de-novo tissue formation or in pre-formed tissues). We further investigated whether the applied oxygen percentage influences the structural organization of the collagen fibrils produced by HAC and whether those features have a pathophysiological counterpart in healthy and osteoarthritic cartilage tissue. Finally, in order to address whether the metabolic effects of HAC culture at low oxygen percentage involve signaling through the hypoxia-inducible factor-1α (HIF-1α) pathway, some cultures were supplemented with the specific inhibitor cadmium chloride.

5.3 Materials and Methods

Cartilage samples collection

Macroscopically normal human articular cartilage samples (Mankin Score: 2 to 3) were obtained post mortem (within 24 hours after death) from the knee joints of a total of six donors with no clinical history of joint disorders (mean age: 56 years, range: 43 to 65 years), after informed consent by relatives and in accordance with the local ethics committee (University Hospital Basel, Switzerland). Cells from different donors were used for independent experimental runs. Osteoarthritic cartilage tissues (Mankin Score: 6 to 7) harvested from three patients undergoing total or partial knee replacement (female:male = 2:1, mean age: 67 years, range 65 to 71 years) were used as controls for degenerated structural organization of collagen fibrils.

Chondrocyte isolation and expansion

Cartilage tissues were minced in small pieces and digested with 0.15% type II collagenase (10 ml solution/g tissue) for 22 hours. The isolated human articular chondrocytes (HAC) were expanded for two passages with Dulbecco's Eagle's Medium (DMEM) containing 4.5 mg/ml D-glucose, 0.1 mM nonessential amino acids, 1 mM sodium pyruvate, 100 mM HEPES buffer, 100 U/ml penicillin, 100 μg/ml streptomycin and 0.29 mg/ml L-glutamate

supplemented with 10% of foetal bovine serum (complete medium) and 1 ng/ml of Transforming Growth Factor β1 (TGFβ-1), 5 ng/ml of Fibroblast Growth Factor 2, and 10 ng/mL of Platelet-Derived Growth Factor-BB (all from R&D Systems, Minneapolis, MN, USA) (expansion medium) [27] in a humidified incubator (37°C/5% CO_2) at either normoxic condition (19% O_2) or low, more physiological oxygen tension (5% O_2). Expansion medium was equilibrated under 5% and 19% O_2 for at least six hours before each media change. Expanded cells were subsequently cultivated in pellets as described below.

3D pellet cultures

The chondrogenic capacity of expanded HAC was investigated in pellet cultures under the two oxygen conditions (19% O_2 and 5% O_2) used for the expansion. Chondrocytes were re-suspended in complete medium supplemented with 10 μg/ml insulin (ACTRAPID HM), 0.1 mM ascorbic acid 2-phosphate (SIGMA, San Gallen, Switzerland), 10 ng/mL Transforming Growth Factor-β3 (Novartis, Basel, Switzerland) (chondrogenic medium) [27]. Chondrogenic medium was equilibrated under 5% and 19% O_2 for at least six hours before each media change.

Pellets generated by cells from two donors after two weeks of culture under the two oxygen percentages (19% O_2 or 5% O_2) (Phase I) were further cultured for up to two weeks (Phase II) in chondrogenic medium at the same or at interchanged oxygen percentages (that is, from 5% to 19% O_2 or from 19% to 5% O_2) (Figure 5.1). For the HIF-1α inhibition experiments, pellets generated by cells from three donors after two weeks of culture at 19% O_2 were subsequently exposed to 5% O_2 and cultured for six hours or three days in chondrogenic medium supplemented with 5 μM cadmium chloride ($CdCl_2$, SIGMA) [28].

Resulting tissues were analyzed histologically, immunohistochemically, biochemically and via scanning electronic microscopy to determine the quality of generated tissue, anabolic and catabolic cell functions and collagen fibril organization.
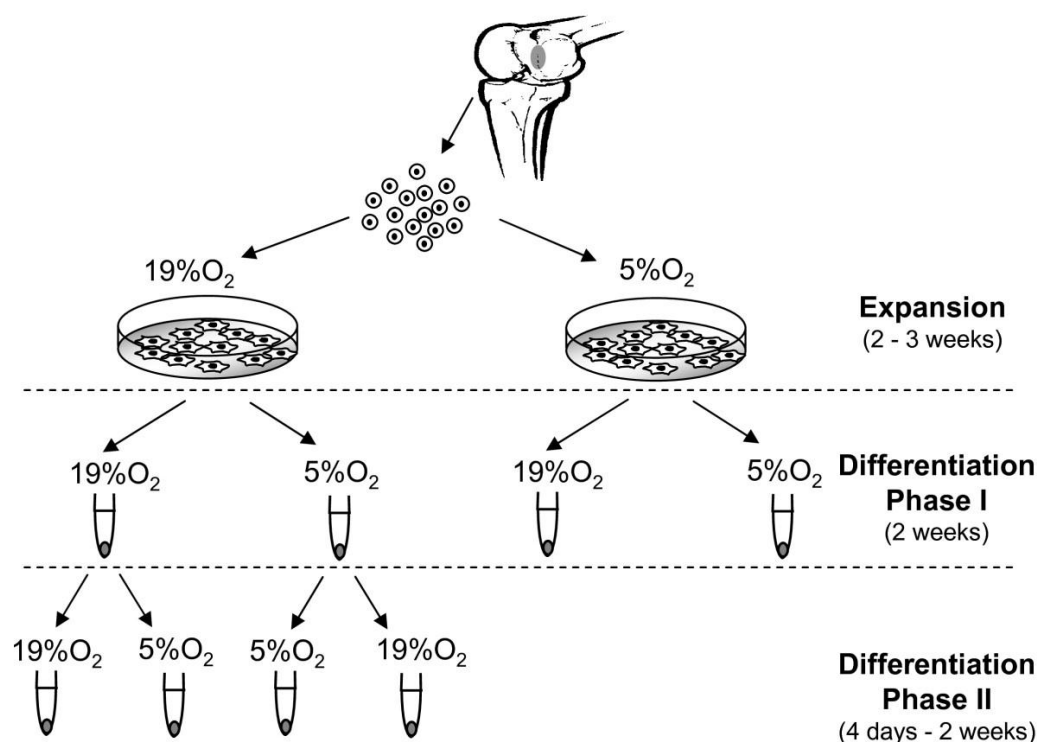
Figure 5,1: Experimental design. Human articular cartilage were cultured in monolayer (Expansion) under 5% and 19% oxygen percentages. Cells were then cultured for two weeks again under the two oxygen percentages (Differentiation Phase I). Pellets generated at 5% and 19% oxygen were further cultured at the same conditions or at interchanged oxygen percentages (Differentiation Phase II).

Pellet characterization

Biochemical analyses

For the determination of the glycosaminoglycan (GAG) and DNA contents, pellets were digested with protease K (0.5 ml of 1 mg/ml protease K in 50 mM Tris with 1 mM EDTA, 1 mM iodoacetamide, and 10 µg/ml pepstatin-A for 15 hours at 56°C) as previously described [29]. GAG contents of pellets were measured spectrophotometrically using the dimethylmethylene blue (DMMB) assay [30]. The DNA amount was measured spectrofluorometrically using the CyQUANT® Kit (Molecular Probes, Eugene, OR, USA) following the kit's instruction. GAG contents were reported as µg GAG/µg DNA.

Measurement of $[^{35}S]SO_4$ and $[^3H]$proline incorporation

The proteoglycan and collagen synthesis of pellets were measured by assessing the incorporation of $(^{35}S)SO_4$ and (^3H)proline for a period of 24 h as described previously [31]. Briefly, pellets were incubated in the presence of both $(^{35}S)SO_4$ (1 µCi/culture) to label proteoglycans and (^3H)proline (1.5 µCi/culture) to label collagen. For the assessment of the

released ECM fraction, radiolabeled proteoglycan and collagen were precipitated overnight at 4°C using respectively 100% ethanol and 70% ammonium sulphate and subsequently, resuspended in 4 M guanidine hydrochloride or 10% sodium dodecyl sulphate in Tris buffer (0.1 M, pH 7.0) respectively for proteoglycan and collagen. For the assessment of the incorporated ECM fraction, tissue pellets were digested with protease K as previously described. The incorporation of $(^{35}S)SO_4$ and (^3H)proline in culture pellet and in conditioned medium was measured in a Packard β-liquid scintillation counter with scintillation fluid (Ultima Gold, Perkin Elmer, Schwerzenbach, Switzerland). The amount of synthesised molecules was normalized to the DNA content of the tissue.

Histological and immunohistochemical analyses

Pellets were fixed in 4% formalin, embedded in paraffin and cross-sectioned (5 μm thick sections). The sections were stained with Safranin O for sulfated GAG and processed for immunohistochemistry to visualize type II collagen (II-II6B3, Hybridoma Bank, University of Iowa, Iowa City, IA, USA), as described in Grogan et al. [32] and type II collagen fragments according to Roy-Beaudry et al. [33].

Electronic microscopy (SEM)

Images obtained from both scanning electron microscopy (SEM) and transmission electron microscopy (TEM) were used for the structural analysis of collagen fibrils. Pellet samples were glued onto a Teflon disc with a five-minute curing epoxy glue (Devcon Epoxy, ITW Brands, Wood Dale, IL, USA). After which, the mounted specimens were placed in a vibratory microtome (VT 1000 E, Leica, Heidelberg, Germany) to trim off the outermost, approximately 150 μm thick cartilage layer parallel to the support surface to minimize inhomogenities across the surface among samples. The surface layer of the adult healthy and OA cartilage was examined without any modification. The samples were then prepared for SEM and TEM analysis as previously described [34]. For TEM analysis, the samples were further homogenised into small pieces in order to isolate single collagen fibrils.

Image analysis

Quantitative data on the collagen fibril organization were obtained using the Image Processing Library & Toolbox (IPLT) image analysis software package (Basel, Switzerland) [35]. A Canny edge detection algorithm [36], followed by a skeletonization algorithm [37] was applied to identify the collagen fibrils. The skeletonized data were subjected to an

algorithm identifying the end points and intersections of the skeleton. Using this information, the individual line segments were identified and analyzed. Finally, the following parameters were determined from each pellet condition: (i) the bending ratio, calculated as the mean-squared end-to-end distance divided by the mean-squared contour length and (ii) the persistence length, calculated using a previously described model [38]. Both these parameters were required to correlate the linearity of the fibrils and length before branching of each individual fibril to its mechanical properties, respectively [39].

Total RNA extraction and cDNA synthesis

Total RNA of pellets was extracted using Trizol (Life Technologies, Basel, Switzerland) and the standard single-step acid-phenol guanidinium method. RNA was treated with DNAseI using the DNA-free™ Kit (Ambion, Austin, Texas) and quantified spectrometrically. cDNA was generated from 3 μg of RNA by using 500 μg/ml random hexamers (Promega AG Dübendorf, Switzerland) and 1 μl of 50 U/ml Stratascript™ reverse transcriptase (Stratagene, Amsterdam, NL), in the presence of dNTPs. Real-time RT-PCR reactions were performed and monitored using the ABI Prism 7700 Sequence Detection System (Perkin-Elmer/Applied Biosystems, Rotkreuz, Switzerland). Cycle temperatures and times as well as primers and probes used for the reference gene (18-S rRNA) and the genes of interest (collagen type II and aggrecan) were as previously described [40]. Assays on-Demand (Applied Biosystem) were used to measure the expression of MMP-1 (Hs00233958_m1), MMP-2 (Hs00234422_m1), MMP-9 (Hs00234579_m1) and MMP-13 (Hs00233992_m1). For each cDNA sample, the threshold cycle (Ct) value of each target sequence was subtracted to the Ct value of 18-S rRNA, to derive ΔCt. The level of gene expression was calculated as $2^{\Delta Ct}$. Each sample was assessed at least in duplicate for each gene of interest.

Quantification of released matrix metalloproteinases

Matrix metalloproteinases (MMP) were quantified in media collected from cultured pellets by using the MultiAnalyte Profiling MMP base Kit (Fluorokine® MAP: LMP000) complemented with the specific MMPs (MMP-1: LMP901; MMP-3: LMP513; MMP-9: LMP911; MMP-13: LMP511, R&D Systems, Minneapolis, MN, USA). The assay was performed on a Luminex 100™ analyzer (Austin, Texas, USA) following the manufacturer's instructions. The amount of released MMPs was normalized to the DNA content of the tissue.

Statistical analysis

For each analysis, triplicate pellets for each condition and donor were assessed. Statistical evaluation was performed using SPSS software version 7.5 software (SPSS, Sigma Stat, Erkrath, Germany). Values are presented as mean ± standard deviation (SD). Differences between groups were assessed by Mann Whitney tests. Differences in the persistence length and bending ratio of collagen fibrils from different conditions were assessed by one-way analysis of variance (ANOVA) with Bonferroni post hoc test. Values of $P < 0.05$ were considered statistically significant.

5.4 Results

**Chondrogenic differentiation of HAC cultured under different oxygen percentages**

HAC were initially cultured in monolayer with expansion medium at 5% or 19% O_2 and subsequently re-differentiated in three-dimensional pellets at the two different oxygen percentages (Phase I) (See Figure 5.1 for the experimental design). HAC proliferated at comparable rates (less than 5% variation in the number of doublings/day; data not shown) at the two oxygen conditions. Cells expanded at either oxygen percentage and subsequently differentiated at 19% O_2 produced tissues faintly stained for GAG and type II collagen (Figures 5.2A, I and 2II and 5.2B, I and 2II). Instead, reducing oxygen percentage during differentiation enhanced the amount of cartilaginous matrix accumulation, as evidenced by a qualitative increased size of the generated tissues (Figure 5.2A, low magnification), an increased intensity of Safranin O and type II collagen stain (Figure 5.2A, B) and a statistically significant higher amount of GAG (3.4- and 3.1-fold for HAC expanded at 19% or 5% O_2 respectively) (Figure 5.2C). Due to the fact that expansion at 5% O_2 did not influence the extent of HAC differentiation, further assessments were only performed with cells expanded at 19% O_2. In agreement with the histological and biochemical results, the RT-PCR analysis confirmed statistically significant higher expression of the cartilage specific genes type II collagen (86.6-fold) and aggrecan (8.5-fold) at 5% O_2 than at 19% O_2 after the Phase I differentiation culture (Figure 5.2D, E).
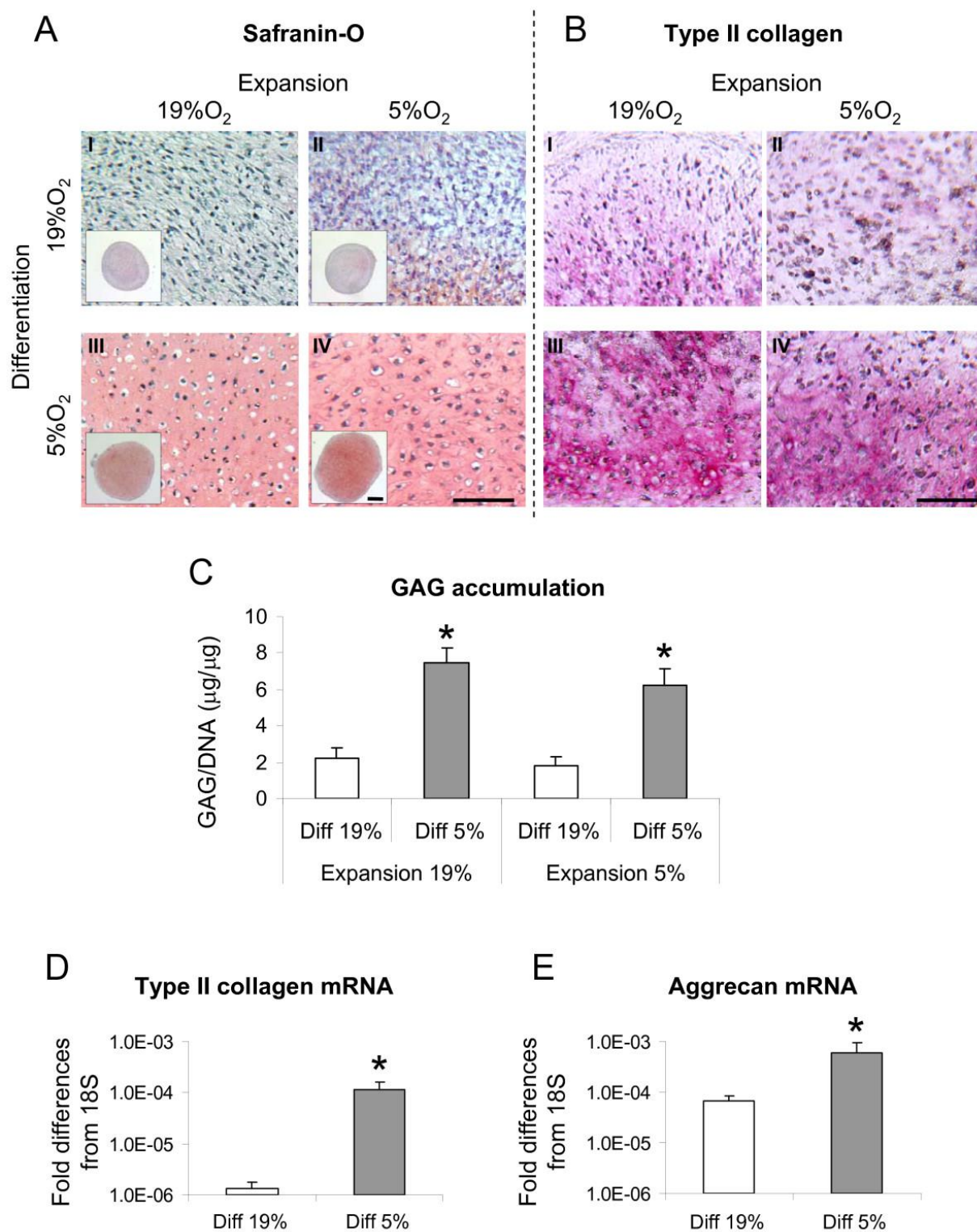
Figure 5.2: **Anabolic response of HAC to different oxygen percentages during the expansion and differentiation Phase I**. **(A - B)** Safranin O and type II collagen immunohistochemical stainings of representative tissues generated by human articular chondrocytes (HAC) expanded at 19% **(I and III)** or 5% **(II and IV)** oxygen and further cultured in pellets at 19% **(I and II)** or 5% **(III and IV)** oxygen. Bar = 100 μm. **(C)** Quantification of glycosaminoglycans (GAG) accumulated normalized to the amount of DNA. **(D - E)** Real time reverse transcription-polymerase chain reaction analysis of the expression of type II collagen and aggrecan mRNA by HAC cultured in pellets at 19% and 5% O_2. Levels are expressed as fold of difference from ribosomal 18S. For the gene expression analysis only expansion at 19% O_2 was considered. Values are mean $\pm$ SD of measurements obtained from three independent experiments. * = significantly different from the 19% O_2.

Expression of catabolic mediators

We then investigated the possible role of oxygen percentage in modulating the expression of catabolic mediators. Analysis of specific matrix metalloproteinases (that is, MMP-1, MMP-2, MMP-9 and MMP-13) by RT-PCR indicated that low oxygen percentage applied during the Phase I differentiation culture selectively down-regulated MMP-1 and MMP-13 mRNA expression (7.7- and 3.5-fold, respectively). MMP-2 mRNA was highly expressed and not modulated by the oxygen percentage. The expression of MMP-9 mRNA remained unaffected and was at the limit of detection at both oxygen percentages (Figure 5.3A).
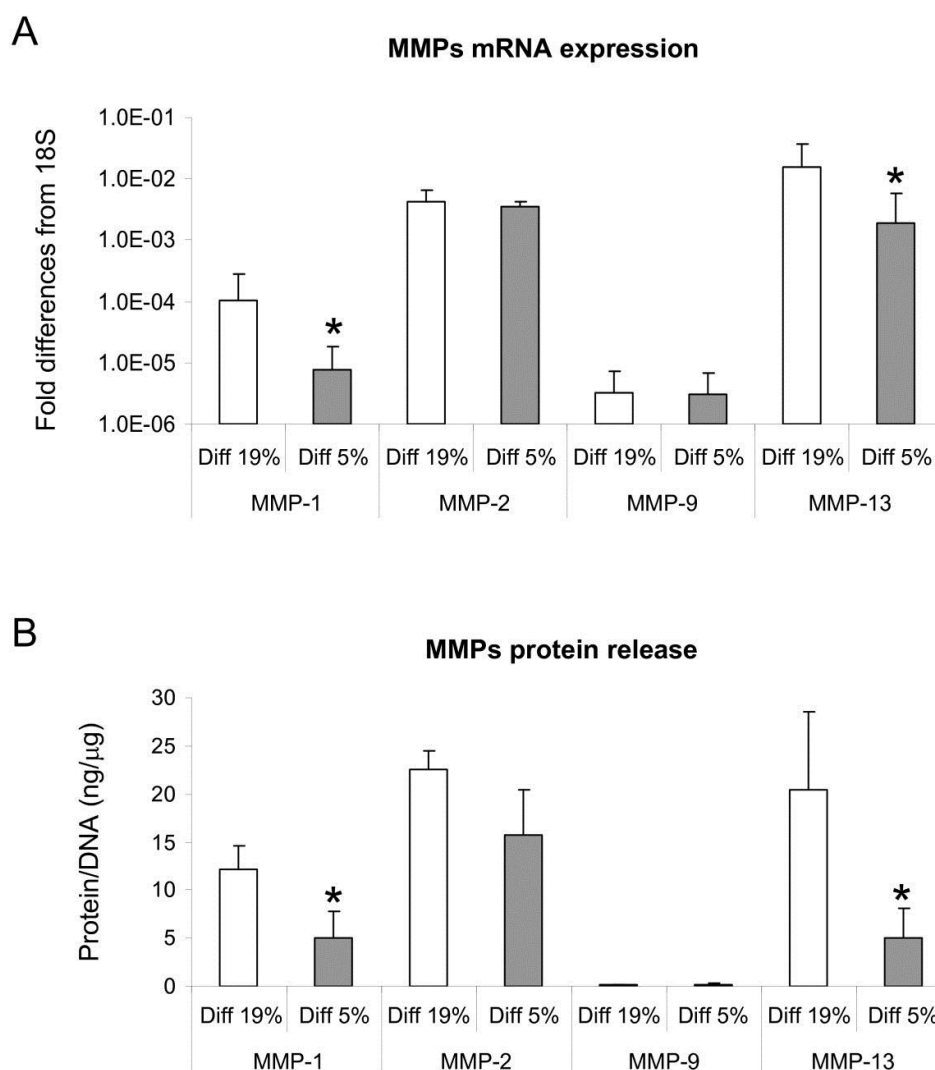
Figure 5.3: Quantification of MMPs produced by HAC cultured at different oxygen percentages during the Phase I. (A) Real time reverse transcription-polymerase chain reaction analysis of the expression of MMP-1, -2, -9, -13 mRNA by human articular chondrocytes (HAC) cultured in pellets at 19% and 5% O_2. Levels are expressed as fold of difference from ribosomal 18S. (B) Quantification of MMP-1, -2, -9, -13 released in the culture medium. Levels are normalized to the amount of DNA measured in relative pellets. Values are mean ± SD of measurements obtained from three independent experiments. * = significantly different from the 19% O_2. The protein levels of MMP-1, -2, -9, -13 were assessed in the supernatant of pellet cultures at the end of Phase I. Consistent with the mRNA results, the amounts of MMP-1 and -13 released were reduced in the pellets cultured at 5% O_2 as compared to those cultured at 19% O_2 (8.2- and 11.3-fold respectively). The protein expression levels of MMP-2 and -9 remained similar at the different oxygen percentages (Figure 5.3B).

Effect of oxygen percentage on HAC anabolic and catabolic activity in pre-formed cartilaginous tissues

We next investigated the influence of oxygen in anabolic (synthesis and accumulation of cartilaginous matrix proteins) and catabolic (MMPs expression, activity and degradation products) processes of pre-formed tissues. Pellets generated after two weeks of culture at 19% O_2 or 5% O_2 (Phase I) were subsequently cultured up to an additional two weeks (Phase II) at the same or at interchanged oxygen percentages (Figure 5.1).

Accumulation and synthesis of cartilaginous matrix proteins

In agreement with the above described results, pellets cultured for four weeks (two weeks of Phase I and two weeks of Phase II) at 5% O_2 were more strongly stained for Safranin O and type II collagen, and accumulated larger amounts of GAG (4.0-fold) as compared to those cultured for the same time at 19% O_2 (Figure 5.4A, B, C). Reducing oxygen percentage during Phase II for pellets cultured at 19% during Phase I resulted in an improved quality of the cartilaginous tissues, as assessed by an increased accumulation of cartilaginous matrix positive for GAG and type II collagen (Figure 5.4A, B) and by a higher GAG content (3.3-fold) (Figure 5.4C). Conversely, increasing oxygen percentage during Phase II for pellets cultured at 5% during Phase I resulted in a reduced accumulation of cartilaginous matrix (Figure 5.4A, B) and GAG content (1.9-fold) (Figure 5.4C).

Results from the radiolabelling experiments indicated that similar amounts of total collagen and proteoglycan (that is, released + accumulated) were synthesized by pellets cultured for 18 days (two weeks of Phase I and four days of Phase II) at the two oxygen percentages. However, as compared to 19% oxygen (Phase I and Phase II), the released fractions of these newly synthesized macromolecules by pellets cultured at 5% O_2 (Phase I and Phase II) were markedly and statistically significantly lower (2.0- and 2.9-fold respectively for collagen and proteoglycan), while the accumulated fractions were higher (2.1- and 6.6-fold respectively for collagen and proteoglycan). Consistent with the biochemical results, the culture at 5% O_2 during Phase II of tissues pre-formed at 19% O_2 during Phase I resulted in an augmented synthesis of collagen and proteoglycan (respectively by 2.7- and 1.4-fold). In particular, the increased synthesis of the newly synthesized macromolecules was mainly reflected by an augmented accumulation (up to 5.9-fold).
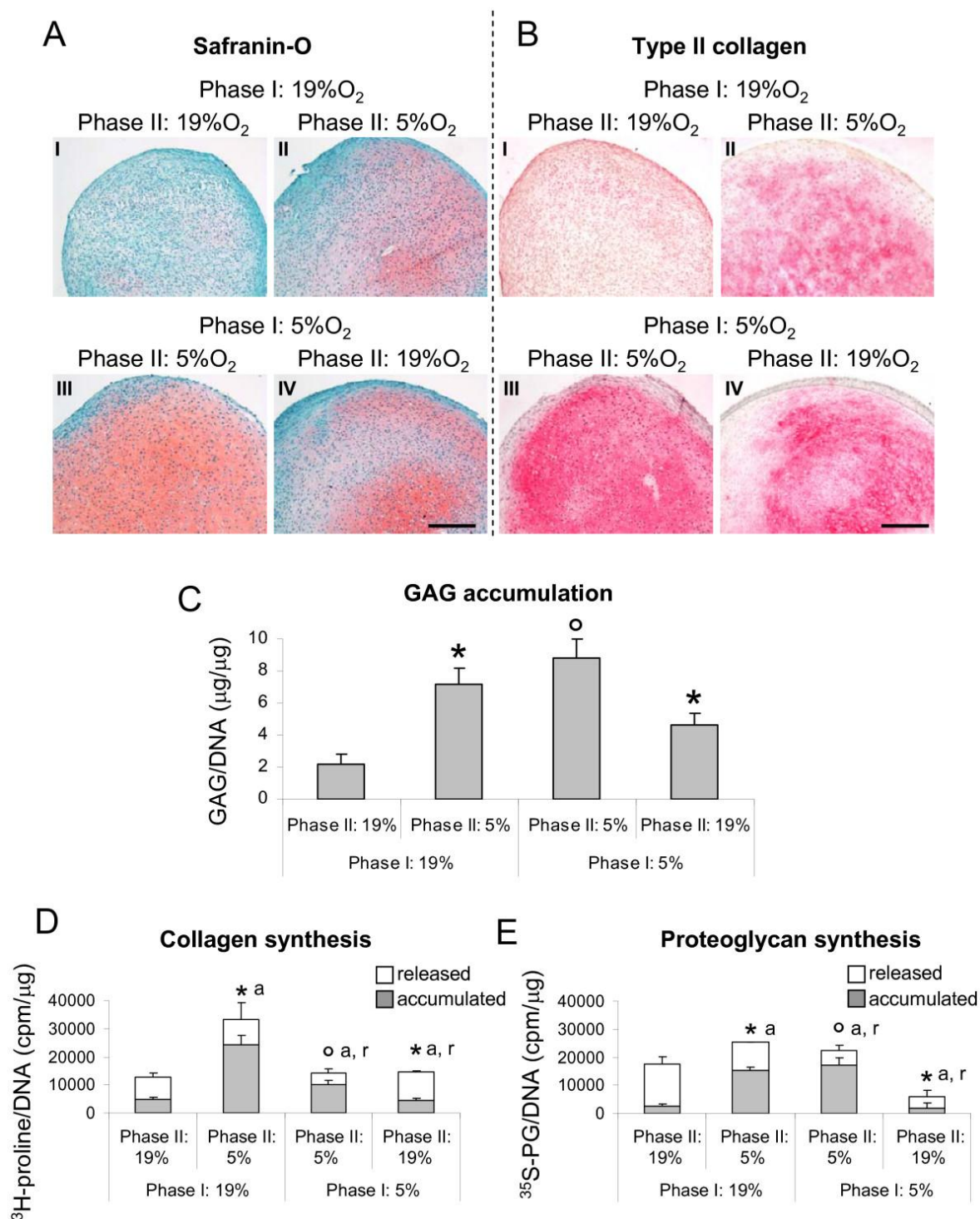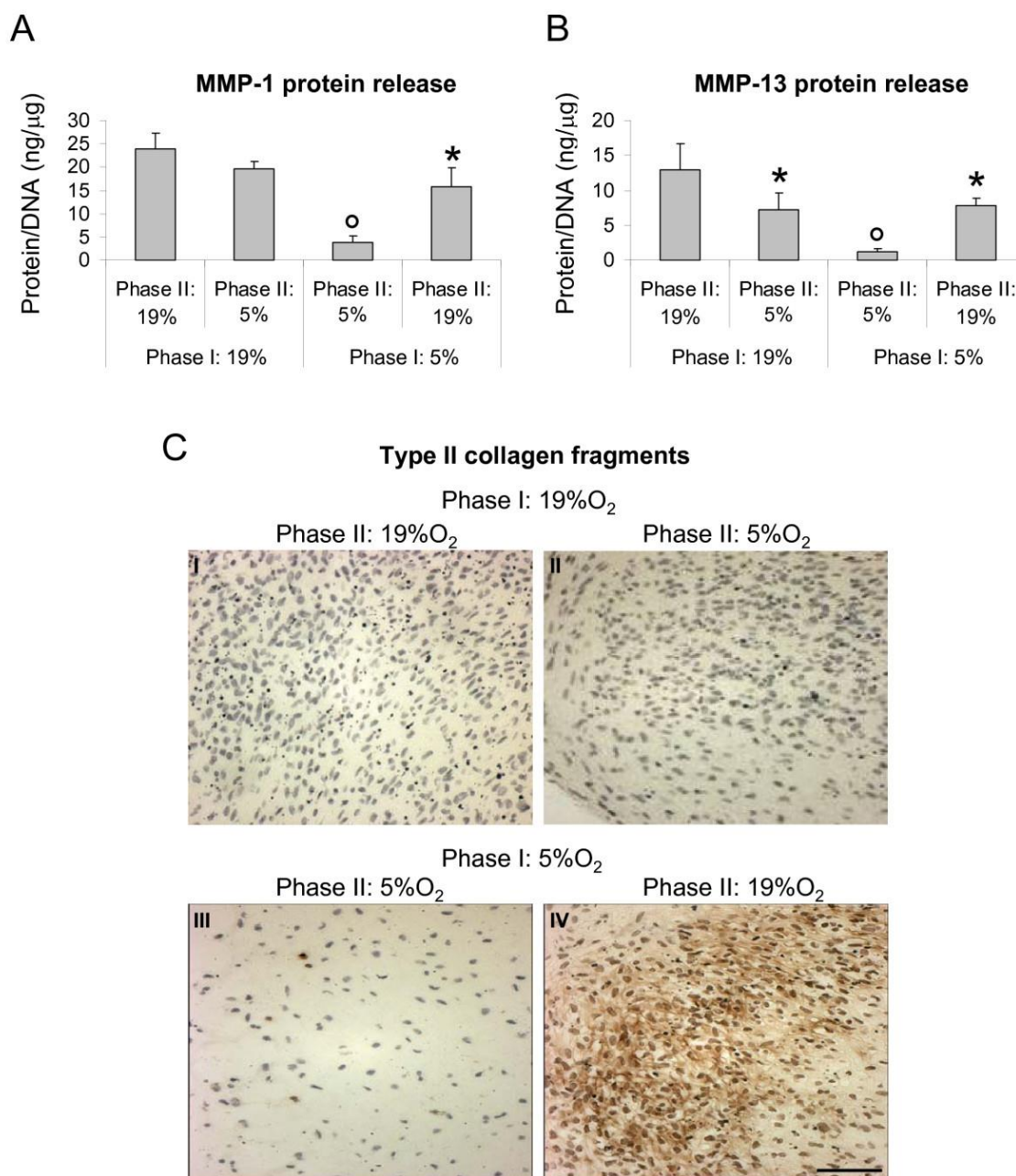
Figure 5.4: **Anabolic response of HAC to different oxygen percentages during differentiation Phase I and II**. (A - B) Safranin O and type II collagen stainings of representative tissues generated by human articular chondrocytes (HAC) cultured in pellets for two weeks (Phase I) at 19% (I and II) or 5% (III and IV) oxygen and further cultured for two additionally weeks (Phase II) at 19% (I and III) or 5% (II and IV) oxygen. Bar = 100 μm. (C) Quantification of glycosaminoglycans (GAG) accumulated in pellets cultured as described in (A - B) normalized to the amount of DNA. (D - E) Amounts of newly synthesized collagen (D) and proteoglycan (E) measured in pellets cultured for 18 days (two weeks of Phase I and four days of Phase II). The upper and lower parts of the columns represent the released and accumulated fractions respectively. Values are mean ± SD of measurements obtained from two independent experiments. * = significantly different from the group cultured with the same oxygen percentage in Phase I but with different oxygen tension in Phase II; ° = significantly different from the group cultured entirely at 19% O_2; a = accumulated, r = released.

Instead, the culture at 19% O_2 during Phase II of tissues pre-formed at 5% O_2 during Phase I differently modulated the synthesis of the two extracellular matrix molecules: while a decreased accumulation (2.3-fold) and an increased released (2.6-fold) was measured for collagen, only a reduction of the accumulated fraction was demonstrated for proteoglycan (8.6-fold) (Figure 4D, E).

MMPs production and activity

Pellets cultured for four weeks (two weeks of Phase I and two weeks of Phase II) at 5% O_2 released lower amounts of MMP-1 and -13 (6.1- and 10.1-fold respectively) as compared to those cultured for the same time at 19% O_2. Culture at 5% O_2 during Phase II of tissues pre-formed at 19% O_2 during Phase I resulted in reduced production of both MMPs, though only MMP-13 by statistically significant levels (by 1.8-fold). Instead, culture at 19% O_2 during Phase II of pellets pre-formed at 5% O_2 during Phase I resulted in increased release of both MMP-1 and MMP-13 (4.0- and 6.2-fold respectively) (Figure 5A, B).

Figure 5.5: Catabolic response of HAC to different oxygen percentages during differentiation Phase I and II. (A - B) Quantification of MMP-1 (A) and MMP-13 (B) released in the medium by human articular chondrocytes (HAC) cultured in pellets for four weeks (two weeks of Phase I and two weeks of Phase II). Levels are normalized to the amount of DNA measured in relative pellets. Values are mean ± SD of measurements obtained from two independent experiments. * = significantly different from the group cultured with the same oxygen percentage in Phase I but with different oxygen tension in Phase II; ° = significantly different from the group cultured entirely at 19% O_2 (Phase I and Phase II). (C) Immunohistochemical detection of type II collagen fragments of pellets cultured under conditions described in (A - B). Bar = 100 μm.

In order to assess whether the observed increased production of MMPs corresponded to an increased proteinase activity, pellets cultured for a total of four weeks at the different oxygen percentages were assessed immunohistochemically to detect the presence of type II collagen C-telopeptides, derived by MMP-1 and -13 collagenolytic activity [33]. Analyses indicated

that only the pellets formed at 5% O_2 during Phase I and subsequently cultured at 19% O_2 during Phase II were intensely stained for the type II collagen fragments (Figure 5.5C).

Collagen fibril organization

To determine whether increasing oxygen percentage during cultivation Phase II of tissues pre-formed at 5% O_2 would change the structure and arrangement of the collagen fibril network, pellets were qualitatively and quantitatively assessed via EM. Images indicated that the collagen fibrils of pellets cultured at 5% O_2 during Phase I and then for two weeks at 19% O_2 during Phase II were less linear than those of pellets cultured for four weeks at 5% O_2. Interestingly, a similar trend was also observed in the OA cartilage as compared to healthy cartilage samples (Figure 5.6A, B). In pellets, the collagen network was comprised of single fibrils with diameters ranging from 20 to 30 nm. In healthy adult cartilage, the network contained bundled and twisted collagen fibrils three- to four-fold larger in diameter. Quantitative image analysis indicated that increasing the oxygen percentage during Phase II resulted in a significant reduction of persistence length as well as bending ratio (47.9% and 10.5% respectively). Interestingly, both parameters were higher in healthy as compared to OA tissues (30.0% and 6.6% respectively for persistence length and bending ratio). Considerable decrease in persistence length and bending ratio would indicate softening and gradual deterioration of cartilage physiological function [39].

SEM images

Collagen structure
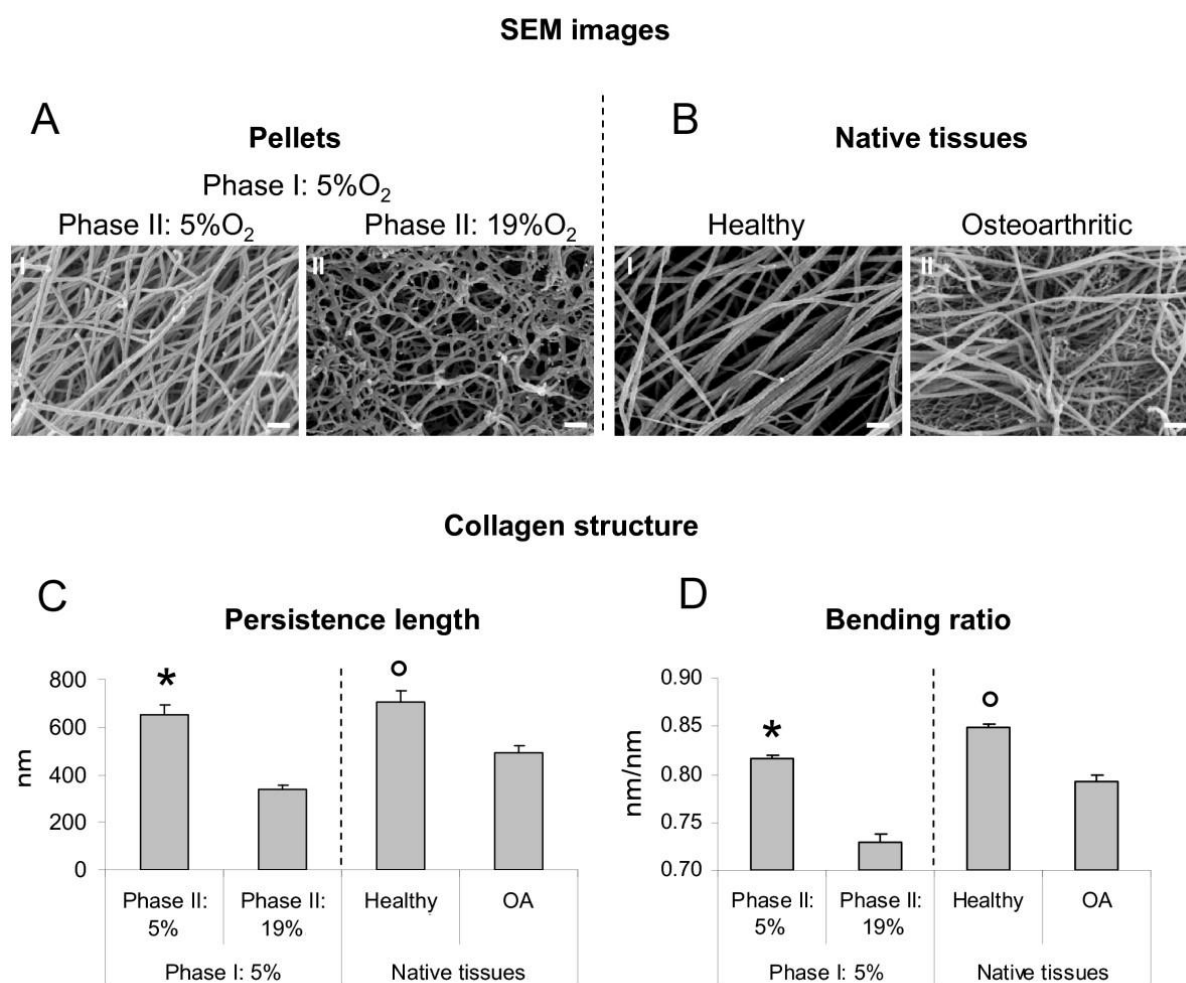
Figure 5.6: SEM images and structural analysis of extracellular collagen-fibrils from engineered, healthy and osteoarthritic cartilage samples. Representative scanning electron microscopy (SEM) images of (A) tissues generated by culturing human articular chondrocytes in pellets for four weeks (two weeks of Phase I and two weeks of Phase II) or (B) native human tissue biopsies from healthy or osteoarthritic (OA) cartilage. (C) Persistence length and (D) bending ratio assessment of the extracellular fibril network of engineered and native tissues. * = significant different from 19% O_2; ° = significant different from OA tissues.

Response to low oxygen under $CdCl_2$-treatment

To determine whether the observed pro-anabolic and anti-catabolic effects of low oxygen percentage are mediated by HIF-1α, HAC from three donors were pre-cultured in pellets during Phase I at 19% O_2. During the subsequent culture Phase II, the pre-cultured pellets were maintained at 19% O_2 or exposed to 5% O_2, with or without treatment with $CdCl_2$ for six hours or three days (Figure 5.7A). Following culture at low oxygen percentage, type II collagen mRNA was up-regulated to a higher extent after six hours (up to 33.0-fold; Figure 5.7B) than after three days (data not shown), while MMP-1 mRNA was down-regulated to a higher extent after three days (up to 65.5-fold; Figure 5.7C) than after six hours (data not shown). Supplementation of $CdCl_2$ during this culture phase almost abrogated the

aforementioned low O_2-mediated effects, so that the expression of type II collagen and MMP-1 mRNA reached levels comparable to those of cells cultured at 19% O_2 for the corresponding times (Figure 5.7B, C).
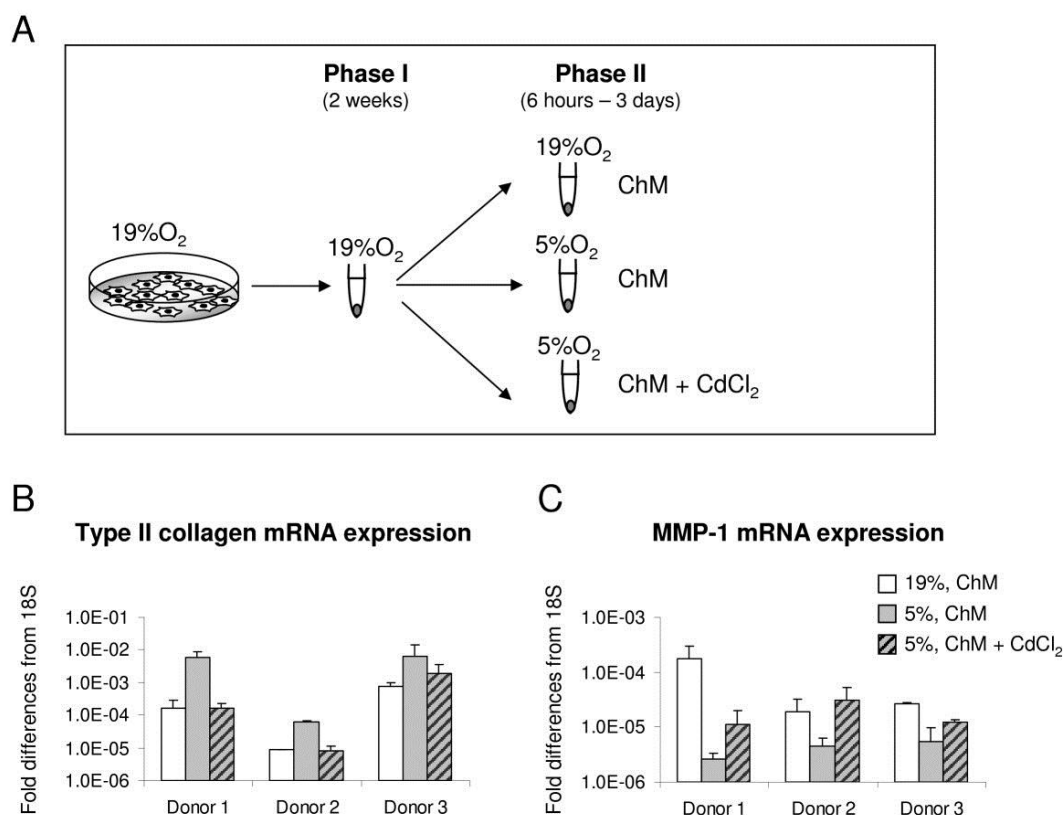
Figure 5.7: Effects inhibition of HIF-1α on anabolic and catabolic gene regulation at low oxygen percentage. (A) Experimental design: human articular chondrocytes from three donors were cultured as pellets in chondrogenic medium (ChM) at 19% O_2 (Phase I) and subsequently maintained at the same oxygen percentage or exposed to 5% O_2 in the absence or presence of 5 μM CdCl$_2$ for six hours or three days (Phase II). Real time reverse transcription-polymerase chain reaction analysis of type II collagen mRNA expression after six hours (B) and of MMP-1 mRNA expression after three days (C). Levels are expressed as fold of difference from ribosomal 18S. Values for each donor are mean ± SD of measurements obtained from three independent pellets.

5.5 Discussion

In this study we found that culture at low, more physiological (5%) oxygen percentage has a dual role in HAC metabolism, namely to enhance the proteoglycan and collagen synthesis and at the same time to reduce the activity of two key catabolic enzymes involved in cartilage breakdown (that is, MMP-1 and MMP-13). As a consequence, HAC exposure to 19% oxygen reduced the de novo formation of cartilage tissue and induced degradation of pre-deposited collagen fibrils, leading to structural features similar to those found in osteoarthritic tissue. Interestingly, HAC appeared to be highly sensitive to the oxygen percentage applied during

differentiation culture in pellets, but not during expansion in monolayers. The anti-anabolic and pro-catabolic effects mediated by low oxygen percentage were HIF1α-dependent, as assessed by specific inhibition of this factor by $CdCl_2$ treatment.

The application of 5% oxygen percentage during the HAC monolayer expansion did not influence the proliferation rate and chondrogenic capacity of HAC. This is in contrast with results reported by Egli et al. [7], indicating that bovine articular chondrocytes expanded under hypoxic conditions generated tissues with higher amounts of cartilaginous matrix as compared to those expanded under normoxic conditions. The discrepancy between our results and those generated by Egli et al. [7] can be related to the different type of cells used (human vs bovine), the stage of cell de-differentiation (second passaged vs first passaged cells) and/or the specific oxygen percentage tested (5% vs 1.5%). Indeed, HAC culture at lower than 5% oxygen during expansion may lead to a benefit in their redifferentiation capacity, and remains to be investigated.

The influence of oxygen percentage during the de-novo tissue formation was evaluated by culturing HAC in micromass pellets, a model commonly used to investigate in vitro cartilage development. Our results indicate that the application of 5% as compared to 19% oxygen percentage critically enhanced the chondrogenic capacity of HAC, as assessed by a greater accumulation of GAG and type II collagen. Similar responses to reduced oxygen percentage have been reported [9] using human nasal chondrocytes statically cultured in pellets for three days and subsequently transferred to a dynamic bioreactor system. We also investigated whether culture of chondrocytes at low oxygen percentage modulated the production of specific metalloproteinases involved in the degradation of extracellular matrix proteins. We observed that the expression of MMP-1 and MMP-13, both at mRNA and protein levels, was reduced in cells cultured at 5% as compared to 19% oxygen. Interestingly, MMP-1 (or collagenase-1) and/or MMP-13 (or collagenase-3) are among the enzymes expressed by human chondrocytes in degenerative pathologies of cartilage, namely osteoarthritis and rheumatoid arthritis [41] and are thus thought to play a critical role in cartilage destruction. In particular, it has been shown that both MMPs are involved in the initial phase of type II collagen breakdown [42,43], and MMP-13 is the collagenase with highest affinity for type II collagen [44]. However, the expression of other MMPs or degradative enzymes (for example, aggrecanases) not included in our study might also be regulated by culture at low oxygen tension.

Our results prompted us to hypothesize that different oxygen percentages could regulate not only cartilage generation, but also its further maturation and stability. We thus exposed

tissues formed at the different oxygen percentages for two weeks (Phase I) to interchanged oxygen percentages in a subsequent culture phase (Phase II). Results obtained from the radiolabelling experiments indicated that the exposure of tissues to 5% oxygen during Phase II induced higher synthesis and accumulation of collagen and proteoglycan. It remains to be assessed whether low oxygen percentages also enhance expression of molecules involved in stabilization of the newly synthesized extracellular matrix components (for example, decorin, fibromodulin, link protein, type IX collagen) [45]. Importantly, the presence of type II collagen cleavage products, indicative of MMP activity, was immunohistochemically detected [33] only in the pellets pre-formed at 5% oxygen (Phase I) and subsequently cultured for additional two weeks at 19% oxygen (Phase II). These results, together with the observed enhanced expression of MMP-1 and -13 at 19% oxygen, strongly indicate a direct involvement of oxygen in regulating the MMP-mediated breakdown of cartilaginous tissues. The result that pellets entirely cultured at 19% O_2 negatively stained for type II collagen fragments could be explained by the insufficient accumulation of the MMP substrate (that is, type II collagen) during the initial cultivation Phase I.

The presence of type II collagen fragments correlated well with the branched/tangled collagen fibril organization and decreased values of bending ratio and persistence length in pellets exposed to 19% oxygen. This could possibly result from an increased enzymatic cleavage of the extracellular matrix molecules by specific MMPs. Conclusively, increased activity of catabolic enzymes is affecting the collagen fibril network that exhibits lower values of bending ratio and persistence length. Based on this correlation, both parameters could potentially represent valuable markers for determining the degree of collagen deterioration. Exposure of cartilage tissues formed at physiological oxygen percentages to higher oxygen levels resembled degradation events occurring during the progression of OA, where, following initial pathologic events, the normal oxygen gradients break down [6]. Therefore, our tissue engineering model would be instrumental to investigation of the evolution of cartilage damage following alteration of the oxygen levels and to assess the effect of possible therapeutic targets.

The observed pro-anabolic and anti-catabolic effects of low oxygen culture were mediated by the hypoxia inducible signaling pathway, since reduction of the oxygen percentage did not regulate type II collagen and MMP-1 mRNA expression in the presence of the HIF-1α inhibitor cadmium chloride ($CdCl_2$) [28]. While the importance of HIF-1α in modulating the expression/synthesis of cartilage-specific genes was recently addressed [28-46], the involvement of this factor in the oxygen-dependent modulation of catabolic genes, recently

reported for porcine pulmonary artery endothelial and smooth muscle cells [47], has not been previously postulated for HAC.

5.6 Conclusions

The present study demonstrates that low oxygen percentage applied during the differentiation phases of human articular chondrocyte culture enhances cell biosynthetic activity as well as reduces the activity of catabolic enzymes known to play key roles in the breakdown of cartilage matrix during degenerative pathologies. These findings indicate that regulation of oxygen percentages during in vitro culture could be used to improve the generation of functional cartilage substitutes, and thus prompt the development of tools enabling accurate control of oxygen levels for tissues of clinically relevant size [48]. Moreover, modulation of oxygen tension in cultured HAC may be used as a tool to model and study in vitro pathophysiological events occurring in osteoarthritis. Finally, following such investigations, the identification of innovative strategies to maintain local in vivo oxygen percentages to defined levels could represent a powerful tool for preventing the progression of degenerative cartilage diseases.

Abbreviations

ANOVA: analysis of variance; cDNA: complementary deoxyribonucleic acid; CO_2: carbon dioxide; Ct: threshold cycle; DMEM: Dulbecco's modified Eagle's medium; DMMB: dimethylmethylene blue; dNTP: deoxyribonucleotide; ECM: extracellular matrix; EDTA: ethylenediaminetetraacetic acid; EM: electronic microscopy; GAG: glycosaminoglycans; HAC: human articular chondrocytes; HEPES: 4-(2-hydroxyethyl)-1-piperazineethanesulfonic acid; HIF-1α: hypoxia-inducible factor-1alpha; IPLT: Image Processing Library & Toolbox; MMP: metalloproteinase; mRNA: messenger ribonucleic acid; O_2: oxygen; OA: osteoarthritis; PBS: phosphate buffered saline; RNA: ribonucleic acid; rRNA: ribosomal ribonucleic acid; RT-PCR: reverse-transcriptase polymerase chain reaction; SD: standard deviation; SEM: scanning electron microscopy; TEM: transmission electron microscopy; TGFβ1: transforming growth factor beta-1.

Authors` contributions

SS participated in study conception and design, acquisition of data (biochemistry, histology, immunohistochemistry for type II collagen, RT-PCR analysis and cell culture), in the study design, in the interpretation of data and drafting the manuscript. ML participated in acquisition of the data (scanning electronic microscopy and image analysis) and in the interpretation of data. DW participated in study conception in the study design and revised the manuscript. ADS participated in analysis (image analysis). CC participated in study conception and provided the patient biopsies and their clinical data. RLPL participated in the development of the Luminex assays. FM participated in the acquisition of data (immunohistochemistry for type II collagen fragments) and revised the manuscript. AB and IM were responsible for study design, supervision of the experiments, interpretation of data and participated in writing the manuscript. All authors read and approved the final manuscript.

5.8 References

1.   Martin JA, Brown T, Heiner A, Buckwalter JA: Post-traumatic osteoarthritis: the role of accelerated chondrocyte senescence. Biorheology 2004, 41:479-491.

2.   Martin JA, Buckwalter JA: Roles of articular cartilage aging and chondrocyte senescence in the pathogenesis of osteoarthritis. Iowa Orthop J 2001, 21:1-7.

3.   Malda J, Martens DE, Tramper J, van Blitterswijk CA, Riesle J: Cartilage tissue engineering: controversy in the effect of oxygen. Crit Rev Biotechnol 2003, 23:175-194.

4.   Silver IA: Measurement of pH and ionic composition of pericellular sites. Philos Trans R Soc Lond B Biol Sci 1975, 271:261-272.

5.   Gonsalves M, Barker AL, Macpherson JV, Unwin PR, O'Hare D, Winlove CP: Scanning electrochemical microscopy as a local probe of oxygen permeability in cartilage. Biophys J 2000, 78:1578-1588.

6.   Grimshaw MJ, Mason RM: Bovine articular chondrocyte function in vitro depends upon oxygen tension. Osteoarthritis Cartilage 2000, 8:386-392.

7.   Egli RJ, Bastian JD, Ganz R, Hofstetter W, Leunig M: Hypoxic expansion promotes the chondrogenic potential of articular chondrocytes. J Orthop Res 2008, 26:977-985.

8.   Hansen U, Schunke M, Domm C, Ioannidis N, Hassenpflug J, Gehrke T, Kurz B: Combination of reduced oxygen tension and intermittent hydrostatic pressure: a useful tool in articular cartilage tissue engineering. J Biomech 2001, 34:941-949.

9.   Malda J, van Blitterswijk CA, van Geffen M, Martens DE, Tramper J, Riesle J: Low oxygen tension stimulates the redifferentiation of dedifferentiated adult human nasal chondrocytes. Osteoarthritis Cartilage 2004, 12:306-313.

10.   Nevo Z, Beit-Or A, Eilam Y: Slowing down aging of cultured embryonal chick chondrocytes by maintenance under lowered oxygen tension. Mech Ageing Dev 1988, 45:157-165.

11.   Lane JM, Brighton CT, Menkowitz BJ: Anaerobic and aerobic metabolism in articular cartilage. J Rheumatol 1977, 4:334-342.

12.   Murphy CL, Sambanis A: Effect of oxygen tension and alginate encapsulation on restoration of the differentiated phenotype of passaged chondrocytes. Tissue Eng 2001, 7:791-803.

13.   Malda J, van den Brink P, Meeuwse P, Grojec M, Martens DE, Tramper J, Riesle J, van Blitterswijk CA: Effect of oxygen tension on adult articular chondrocytes in microcarrier bioreactor culture. Tissue Eng 2004, 10:987-994.

14.   Marcus RE: The effect of low oxygen concentration on growth, glycolysis, and sulfate incorporation by articular chondrocytes in monolayer culture. Arthritis Rheum 1973, 16:646-656.

15. Saini S, Wick TM: Effect of low oxygen tension on tissue-engineered cartilage construct development in the concentric cylinder bioreactor. Tissue Eng 2004, 10:825-832.

16. Domm C, Schunke M, Christesen K, Kurz B: Redifferentiation of dedifferentiated bovine articular chondrocytes in alginate culture under low oxygen tension. Osteoarthritis Cartilage 2002, 10:13-22.

17. Kurz B, Domm C, Jin M, Sellckau R, Schunke M: Tissue engineering of articular cartilage under the influence of collagen I/III membranes and low oxygen tension. Tissue Eng 2004, 10:1277-1286.

18. Martinez I, Elvenes J, Olsen R, Bertheussen K, Johansen O: Redifferentiation of in vitro expanded adult articular chondrocytes by combining the hanging-drop cultivation method with hypoxic environment. Cell Transplant 2008, 17:987-996.

19. Murphy CL, Sambanis A: Effect of oxygen tension on chondrocyte extracellular matrix accumulation. Connect Tissue Res 2001, 42:87-96.

20. Murphy CL, Polak JM: Control of human articular chondrocyte differentiation by reduced oxygen tension. J Cell Physiol 2004, 199:451-459.

21. Nevo Z, Horwitz AL, Dorfmann A: Synthesis of chondromucoprotein by chondrocytes in suspension culture. Dev Biol 1972, 28:219-228.

22. Scherer K, Schunke M, Sellckau R, Hassenpflug J, Kurz B: The influence of oxygen and hydrostatic pressure on articular chondrocytes and adherent bone marrow cells in vitro. Biorheology 2004, 41:323-333.

23. Brighton CT, Lane JM, Koh JK: In vitro rabbit articular cartilage organ model. II. 35S incorporation in various oxygen tensions. Arthritis Rheum 1974, 17:245-252.

24. Clark CC, Tolin BS, Brighton CT: The effect of oxygen tension on proteoglycan synthesis and aggregation in mammalian growth plate chondrocytes. J Orthop Res 1991, 9:477-484.

25. Obradovic B, Carrier RL, Vunjak-Novakovic G, Freed LE: Gas exchange is essential for bioreactor cultivation of tissue engineered cartilage. Biotechnol Bioeng 1999, 63:197-205.

26. Ysart GE, Mason RM: Responses of articular cartilage explant cultures to different oxygen tensions. Biochim Biophys Acta 1994, 1221:15-20.

27. Barbero A, Grogan S, Schafer D, Heberer M, Mainil-Varlet P, Martin I: Age related changes in human articular chondrocyte yield, proliferation and post-expansion chondrogenic capacity. Osteoarthritis Cartilage 2004; 12:476-484.

28. Duval E, Leclercq S, Elissalde JM, Demoor M, Galéra P: Hypoxia-inducible factor-a inhibits the fibroblast-like markers type I and type III collagen during hypoxia-induced chondrocyte redifferentiation: Hypoxia not only induces type II collagen and aggrecan, but it also inhibits type I and type III collagen in the hypoxia-inducible factor 1a-dependent redifferentiation of chondrocytes. Arthritis Rheum 2009, 60:3038-3048.

29. Hollander AP, Heathfield TF, Webber C, Iwata Y, Bourne R, Rorabeck C, Poole AR: Increased damage to type II collagen in osteoarthritic articular cartilage detected by a new immunoassay. J Clin Invest 1994, 93:1722-1732.

30. Farndale RW, Buttle DJ, Barrett AJ: Improved quantitation and discrimination of sulphated glycosaminoglycans by use of dimethylmethylene blue. Biochim Biophys Acta 1986, 883:173-177.

31. Waldman SD, Couto DC, Grynpas MD, Pilliar RM, Kandel RA: A single application of cyclic loading can accelerate matrix deposition and enhance the properties of tissue-engineered cartilage. Osteoarthritis Cartilage 2006; 14:323-330.

32. Grogan SP, Rieser F, Winkelmann V, Berardi S, Mainil-Varlet P: A static, closed and scaffold-free bioreactor system that permits chondrogenesis in vitro. Osteoarthritis Cartilage 2003, 11:403-411.

33. Roy-Beaudry M, Martel-Pelletier J, Pelletier JP, M'Barek KN, Christgau S, Shipkolye F, Moldovan F: Endothelin 1 promotes osteoarthritic cartilage degradation via matrix metalloprotease 1 and matrix metalloprotease 13 induction. Arthritis Rheum 2003; 48:2855-2864.

34. Stolz M, Gottardi R, Raiteri R, Miot S, Martin I, Imer R, Staufer U, Raducanu A, Duggelin M, Baschong W, Daniels AU, Friederich NF, Aszodi A, Aebi U: Early detection of aging cartilage and osteoarthritis in mice and patient samples using atomic force microscopy. Nat Nanotechnol 2009, 4:186-192.

35. Philippsen A, Schenk AD, Signorelli GA, Mariani V, Berneche S, Engel A: Collaborative EM image processing with the IPLT image processing library and toolbox. J Struct Biol 2007, 157:28-37.

36. Canny JF: A computational approach to edge detection. IEEE Trans Pattern Anal Mach Intell 1986, 8:679-698.

37. Gonzalez RC, Woods RE: Digital Image Processing. 3rd edition. Prentice Hall, Inc., USA; 2007.

38. Hagerman PJ: Flexibility of DNA. Annu Rev Biophys Biophys Chem 1988, **17:**265-286.

39. Raub CB, Unruh J, Suresh V, Krasieva T, Lindmo T, Gratton E, Tromberg BJ, George SC: Image correlation spectroscopy of multiphoton images correlates with collagen mechanical properties. Biophys J 2008, 94**:**2361-2373.

40. Jakob M, Demarteau O, Schafer D, Hintermann B, Dick W, Heberer M, Martin I: Specific growth factors during the expansion and redifferentiation of adult human articular chondrocytes enhance chondrogenesis and cartilaginous tissue formation in vitro. J Cell Biochem 2001, 81:368-377.

41. Burrage PS, Mix KS, Brinckerhoff CE: Matrix metalloproteinases: role in arthritis. Front Biosci 2006, 11:529-543.

42.   Dahlberg L, Billinghurst RC, Manner P, Nelson F, Webb G, Ionescu M, Reiner A, Tanzer M, Zukor D, Chen J, van Wart HE, Poole AR: Selective enhancement of collagenase-mediated cleavage of resident type II collagen in cultured osteoarthritic cartilage and arrest with a synthetic inhibitor that spares collagenase 1 (matrix metalloproteinase 1). Arthritis Rheum 2000, 43:673-682.

43.   Wu W, Billinghurst RC, Pidoux I, Antoniou J, Zukor D, Tanzer M, Poole AR: Sites of collagenase cleavage and denaturation of type II collagen in aging and osteoarthritic articular cartilage and their relationship to the distribution of matrix metalloproteinase 1 and matrix metalloproteinase 13. Arthritis Rheum 2002, 46:2087-2094.

44.   Reboul P, Pelletier JP, Tardif G, Cloutier JM, Martel-Pelletier J: The new collagenase, collagenase-3, is expressed and synthesized by human chondrocytes but not by synoviocytes. A role in osteoarthritis. J Clin Invest 1996, 97:2011-2019.

45.   Poole AR, Kojima T, Yasuda T, Mwale F, Kobayashi M, Laverty S: Composition and structure of articular cartilage: a template for tissue repair. Clin Orthop Relat Res 2001, 391(Supp l):26-33.

46.   Pfander D, Cramer T, Schipani E, Johnson RS: HIF-1alpha controls extracellular matrix synthesis by epiphyseal chondrocytes. J Cell Sci 2003, 116:1819-1826.

47.   Ye H, Zheng Y, Ma W, Ke D, Jin X, Liu, Wang D: Hypoxia down-regulates secretion of MMP-2, MMP-9 in porcine pulmonary artery endothelial and smooth muscle cells and the role of HIF-1. J Huazhong Univ Sci Technolog Med Sci 2005, 25:382-384.

48.   Wendt D, Stroebel S, Jakob M, John GT, Martin I: Uniform tissues engineered by seeding and culturing cells in 3D scaffolds under perfusion at defined oxygen tensions. Biorheology 2006, 43:481-488.

Chapter 6

Stretching, unfolding and deforming protein filaments adsorbed at solid-liquid interfaces using the tip of an Atomic-Force Microscope

Douglas B. Staple, Marko Loparic, Hans Jürgen Kreuzer, and Laurent Kreplak

6.1 Abstract

Cells move by actively remodeling a dense network of protein filaments. Here we analyze the force response of various filaments in a simplified experimental setup, where single filaments are moved with an atomic-force microscope (AFM) tip against surface friction, with the AFM operating in the torsional mode. Our experimental findings are well explained within a simple model based on Newtonian mechanics: we observe force plateaus, which are the signature of the sequential stretching of single repeat units, followed ultimately by deformation of the whole polymer shape.

6.2 Introduction, results, discussion

During tissue morphogenesis, mammalian cells move within an extracellular matrix composed of cross-linked collagen fibrils [1]. The traction force enabling cell movement, typically several nN per μm^2 [2], is localized at discrete sites called focal adhesions [3]. Such localized forces are sufficient to induce major rearrangements of the fibrillar elements [1,4]. These substrate changes are readily observable by atomic-force microscopy (AFM) of fibroblasts moving on glass coated with collagen fibrils: single fibrils appear bent, oriented in the direction of the closest cell adhesion site [5]. Here we develop a simplified experimental setup for analyzing the frictional and elastic response of fibrils: A single protein filament or fibril is adsorbed on a substrate and moved by an AFM tip perpendicular to the AFM cantilever axis and at a constant velocity [6]. The AFM cantilever twists substantially, generating force and moving the polymer forward [7]. Past studies addressing polymers on surfaces have classified adsorption regimes and behavior in the standard AFM geometry (retracting from the surface) [8]. Here we concentrate on the essential physics of manipulating molecules in the interfacial plane. We choose as model systems desmin intermediate filaments (IFs) and collagen fibrils; both adopt roughly linear configurations when adsorbed on mica (Fig. 6.1). The response of these two types of filaments to the AFM were qualitatively different: collagen fibrils were moved by the cantilever, elongated and bent into a continuous cusp shape [Fig. 6.1(b), arrow 1], while desmin filaments (and bundles of collagen fibrils) were locally stretched until broken, see Fig. 6.1(b) (arrow 2) and Fig. 6.2(a). These elongations imply that fibrils were locally stretched up to 3.5 and 1.3 times their original length, for desmin IFs and bundles of collagen fibrils, respectively. For both systems the stretching involved a few repeat units; however, for desmin this amounts to a length of ~150 nm [Fig. 6.2(a)], whereas for the collagen bundles the deformed region was micrometers long [Fig. 6.1(b)]. To quantify these observations we show in Fig. 6.2(c) the

force versus cantilever displacement curves for a desmin filament. Such curves always show an initial linear region (in all of $n = 60$ experiments), a force plateau, and a subsequent nonlinear increase in force [7]. In some experiments we observed two consecutive force plateaus, as shown in Fig. 6.2(c). Similar force curves with multiple steps were also observed for desmin filaments reassembled from a one-to-one mixture of wild-type desmin and a point mutant D399Y [9]; see Fig. 6.2(d). Because the torsional force constant of the AFM tips had to be relatively large to sustain forces up to $f \approx 4$ nN, the resulting force fluctuations $\delta f = (k_c\, k_b\, T)^{\frac{1}{2}} \approx 100$ pN are substantial, and must be filtered from the raw data; here we accomplish this filtering using a running-average over 5 nm. The local stretching of filaments shown in Figs. 6.1 and 6.2 is an unexpected result considering their properties in solution. In solution fibrils appear rodlike on the µm scale, and these rodlike configurations are maintained during adsorption, as shown in Fig. 6.1(a). When stretched on the surface, however, these filaments form sharp ''corners'' and stretching continues in relatively straight subsegments [Fig. 1(a), arrow 2].
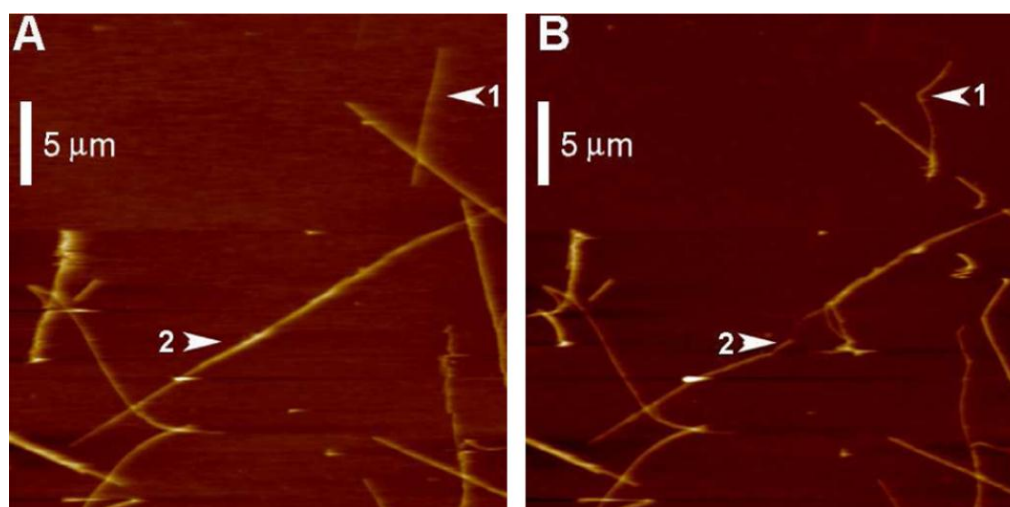
Figure 6.1:. Manipulation of collagen fibrils adsorbed to mica, pretreated with 1 M MgCl$_2$ and immersed in PBS. Panels (a) and (b) were imaged prior to and after manipulation, respectively. Arrowheads identify two manipulations yielding a bent fibril with a cusped shape (1) and a stretched and broken bundle of fibrils (2).

This implies that fibrils behave structurally different under these conditions; here the shape of the molecule is dominated by tension, rather than by bending rigidity as for solvated fibrils. In order to quantify these observations, we model filaments on surfaces as single or continuous-multistate wormlike chains (WLCs) subject to surface friction and external force. The fact that the filaments can be ''stretched'' implies that they have an effective contour length L_c longer than the end-to-end length with which they are adsorbed to the surface (L_0). Furthermore, because we are stretching a small number of repeat units, we must account for

the discreteness of the chain. To accomplish this we describe individual repeat units separately, using a WLC model for each segment. These separate WLCs are connected end-to-end to form the complete filament. Here we will refer to the individual WLCs as ''linkers'' and to the composite chain as a ''discretely connected wormlike chain'' (DC-WLC) [see Fig. 2(b)].
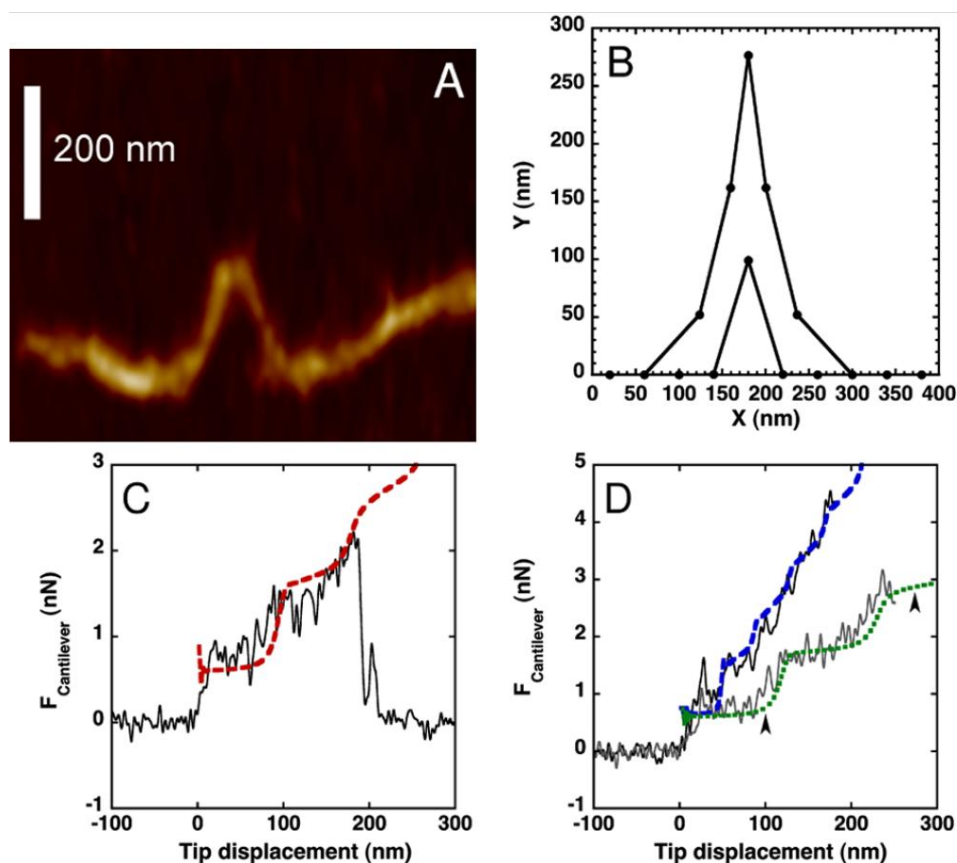

Figure 6.2: (a) AFM image of single wild-type desmin filaments obtained after manipulation (adsorbed to mica and immersed in 25 mM Tris-HCl, 100 mM NaCl, pH 7.5). (b) Shape of a DC-WLC manipulated by a point probe at its middle for two cantilever displacements. (Dots represent beads and lines represent linkers.) Parameters: $v = 50$ nm/s (as in experiment), $L_p = 0.4$ nm, $L_c = 3200$ nm, $L_0 = 1000$ nm, $N = 25$ beads, and $N v = 0.3$ N s/m. (c) Force versus displacement curves corresponding to panel A. Theoretical fit (broken line): $L_c = 2200$ nm, $N = 20$, others as in panel (b). (d) Force versus displacement curves of desmin filaments containing an equal amount of wild-type proteins and mutant D399Y proteins [9] with theoretical fits. Arrowheads indicate tip displacements corresponding to the shapes presented in panel (b). Parameters (dotted curve): as in panel B; broken curve: $L_p = 2$ nm, $L_c = 1600$ nm.

To simplify the inclusion of friction within a Langevin approach, we couple these massless linkers using beads with the mass m of a filament repeat unit. (In practice the mass of the beads does not affect the results, as we are in the low Reynolds number limit.) This model is akin to the Rouse model, where we use WLC linkers instead of harmonic springs to account for the large effective extensibility of the chain ($L_0 < L_c$). In summary, the filaments are modeled by N beads, connected by massless WLC linkers. The motion of the polymer is

controlled by the tension along the chain, the friction force on the molecule, and the force applied at some point along the chain by the AFM cantilever [see the inset of Fig. 6.3(a)]. For the tension on the *i*th linker we take the approximate force-extension relation of the WLC [10]:

$$f_i^{(t)} = \frac{k_b T}{L_p} \left[\frac{1}{4(1 - x_i/L_b)^2} - \frac{1}{4} + \frac{x_i}{L_b} \right],\tag{1}$$

where *T* is the temperature, $L_b = L_c / N$ is the contour length between beads, and x_i is the distance separating beads *i* and *i* + 1.
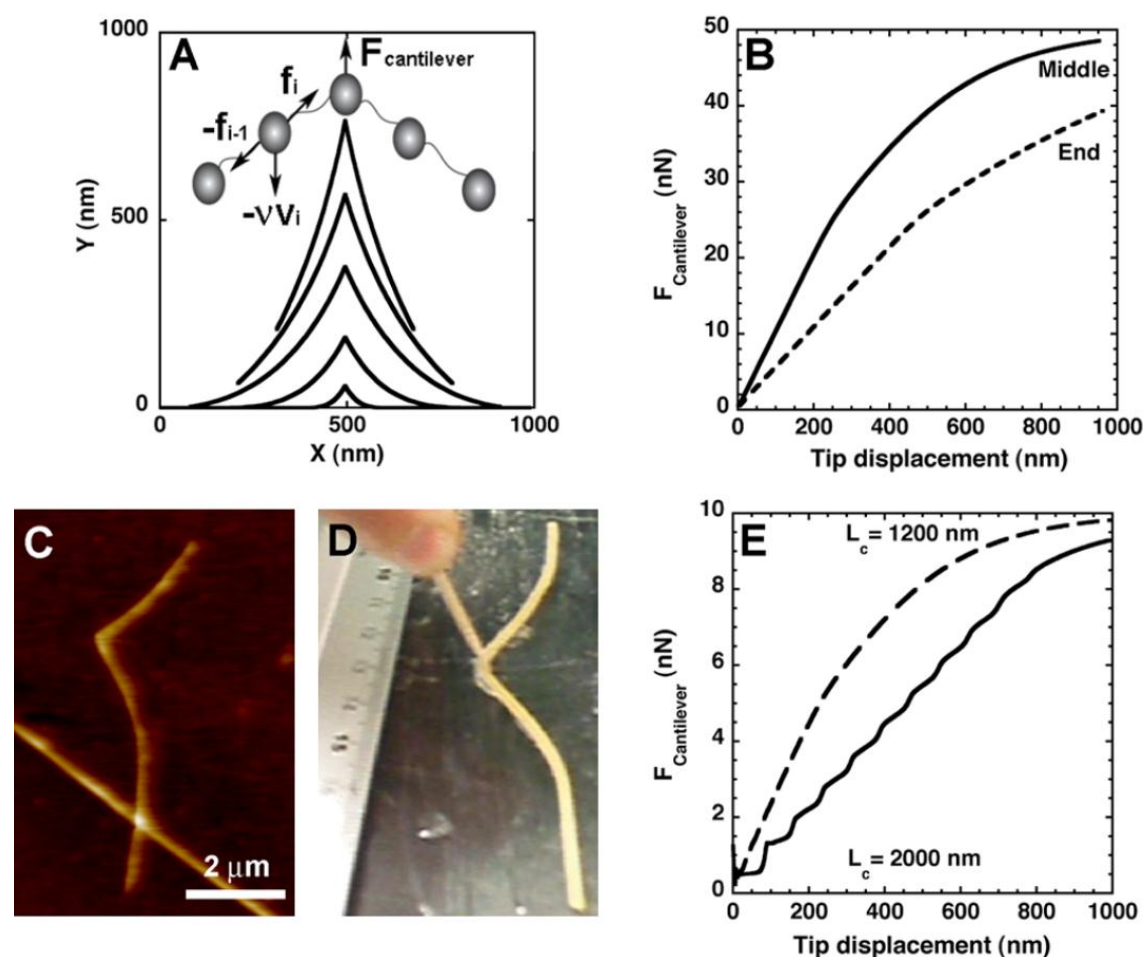

Figure 1 Theoretical and experimental models. (a) Shapes of a DC-WLC chain manipulated by a point probe. Parameters: $L_p = 1$ nm, $L_c = 1200$ nm, $N = 100$, N $v = 1$ Ns/m, others as in Fig. 2(b). Inset: Schematic of the DCWLC. (b) Force versus displacement curves for the same chain manipulated at its middle (solid line) and at one end (broken line). (c) AFM image of a collagen fibril after manipulation revealing a similar cusp shape. (d) A 12 cm long rubber band adsorbed to a glass plate coated with silicon grease (Corning) and manipulated at an average velocity of 3 mm/s. (e) Force versus displacement curves for two DC-WLC chains, with $L_c = 1200$ and 2000 nm for solid, dashed curves, respectively. [$N = 20$ beads; other parameters as in panel (a).]

The polymer remains in contact with the substrate during the whole experiment, and the ith monomer experiences a viscous drag or friction force, linear in the velocity of each monomer bead $\mathbf{f}_i^{(f)} = -v\,\mathbf{v}_i$, where v is the friction coefficient and v_i is the velocity of the *i*th bead.

In addition, the AFM tip exerts a force at a specific site of the chain, e.g., in the middle or at one end, $f_{i=a}^{(AFM)} = k_c\,(vt - y_i)$; here we take the force to be due to a harmonic cantilever moving at a constant velocity. These forces are inserted into the Langevin equations for the individual beads, with the cantilever fluctuations as the external noise. The shape of the polymer chain as a function of time is obtained as the average motion, equivalent to the solution of Newton's equations. The role of the fluctuations will be studied elsewhere after appropriate measurements have been performed. In our model the chain has an overall contour length L_c and is adsorbed to the substrate with an end-to-end length $L_0 < L_c$. Two cases are of interest: $L_c \sim L_0$, corresponding to collagen fibrils [11] and $\mathrm{Lc} \sim 2\text{--}3L_0$, corresponding to desmin IFs [6]; this second case also encompasses other biopolymers such as DNA [12], and fibrin [13]. If the chain has a limited extension ($\mathrm{L0} \sim \mathrm{Lc}$), or if the force necessary to extend the chain is small compared to the viscous drag $v\upsilon$, then the chain segments in the vicinity of the moving point probe extend first [Fig. 6.3(a)]. This process continues until all segments are under tension and gives rise to a linear force versus displacement curve [Fig. 6.3(b), solid line]. After all segments have extended close to their limit, the whole chain is set in motion [Fig. 6.3(a)] and the force converges asymptotically to $v\upsilon$. As expected, the force versus displacement curve depends on the position of the point probe along the polymers [Fig. 6.3(b), compare solid and broken lines]. The cusp shape of the chain is due to the incremental motion of chain segments nearest to the moving tip; this is observed both at the nano and macro scales, see Figs. 6.3(c) and 6.3(d). Indeed, we see the same cusped shape with rubber bands (mm scale) as with fibrils (μm scale). For quantitative agreement between the model and experimental data, the viscous drag coefficient v had to be between 10^{-3} and 10^{-1} Ns/m. Below 10^{-3} Ns/m the system is underdamped and strong oscillations occur; above 10^{-1} Ns/m the system is overdamped, and around 10^2 Ns/m the chain is stuck to the substrate. In order to relate the viscous drag coefficient to a bulk viscosity η, we use Stokes's relation, $v = 6\pi\eta a$, where a is the radius of the particle. This radius can take any value between 1 and 100 nm for biopolymers, so our range of v is equivalent to a bulk viscosity η between 10^3 and 10^7 Pa s, corresponding to peanut butter and pitch, respectively. Although the AFM experiments are performed in water (bulk viscosity 10^{-3} Pa s), the binding of the protein filaments to the substrate ions gives rise to an extremely

viscous interface. These numbers compare well with estimates based on the thermal activation model by Briscoe and Evans [14,15] and also with estimates based on the Tomlinson model [16]. Because the equivalent viscosity is so high, the repeat units of the chain are stuck in position if no force is applied by the point probe. This is in agreement with the AFM experiments, where no evidence of relaxation was detectable long after a given manipulation [7]. Even though we are studying a dynamic process, the large viscosity imposes a near-equilibrium stretching of the chain, validating the use of Eq. (1) to estimate the tensions at the linkers' ends. For desmin filaments the number of participating repeat units is small because each unit can extend to several times its original end-to-end length before the next repeat unit is affected. We can account for this in the model by setting N to a small number; in such a situation the stretching of individual repeat units is observable as steps in the force versus displacement curve, if the units are extensible enough [Fig. 6.3(e), compare $L_c = 1200$ nm and 2000 nm with 20 beads]. In addition, the deformation only affects the chain in the vicinity of the applied force, in stark contrast to the cusplike shape and in perfect agreement with experiment. (It should be noted that, when pulling in the center of a symmetric chain, one force step corresponds to two repeat units unfolding on opposite sides of the point probe.) So far, single force steps have been reported experimentally for desmin IFs [7] but not multiple ones. In these earlier experiments, the pieces of filament that were manipulated had an average length of only 80 ± 27 nm ($n = 60$) and the maximal tip displacement was on average 150 ± 41 nm ($n = 60$) [7]. Assuming in our model that each linker is 45–50 nm long and can extend to 160–180 nm maximum, the observation of more than one force step is indeed very unlikely. However, we did find, retrospectively, one force curve out of 60 measured in that study that displayed two force steps [7]. As further experimental evidence for the existence of multiple force steps in desmin filaments, we performed an additional $n = 90$ experiments on a population of desmin filaments reassembled from a one-to-one mixture in urea of wild-type desmin and a point mutant D399Y [9]. AFM measurements were performed exactly in the same conditions as wild-type desmin filaments [7]; the pieces of filament that were manipulated had an average length of 125 ± 37 nm (n ¼ 90), and the maximal tip displacement was on average 215 ± 73 nm ($n = 90$). As predicted by our model, we found samples with multiple force steps, as previously presented in Fig. 6.2(d). Such multiple steps were visible in a total of 11 out of $n = 90$ curves; even though each individual curve was distinct from the others, it was possible to fit each one by allowing variations in the number of beads N, the contour length of the linkers L_c, and the persistence length L_p. Since we have to change the chain parameters (N, L_c, L_p) to fit the experimental

data, desmin filaments cannot be well modeled by a single DC-WLC. This is due to the fact that desmin IFs have a hierarchical structure, with around 40 protein chains arranged in parallel in the cross-section of the filament [9]. The chains dimerize to form 45 nm long repeat units, which are double stranded α-helical coiled coils, and which can unfold upon stretching [17]. The unfolding of the coiled-coil essentially implies that the length of a repeat unit increases. Sliding between the chains can also occur, explaining the extreme extensibility of hese filaments [6]. Hence, the WLC linkers should be replaced by a more complex multistate polymer model. As a step in that direction we have implemented a continuous two-state model for the linkers [18]: we describe the linker as a double stranded α-helical coiled coil, 40 nm in length, composed of 0.15 nm long units that can unfold to 0.38 nm. The coiled-coil and unfolded polypeptides have persistence lengths of L_{p1} = 25 nm [17] and L_{p2} ¼ 0:4 nm, respectively. We assume a Gibbs free energy difference between the two states of ΔV = 250 meV and an interaction energy between the two states of 20 meV, with other parameters as in Fig. 6.2(b).
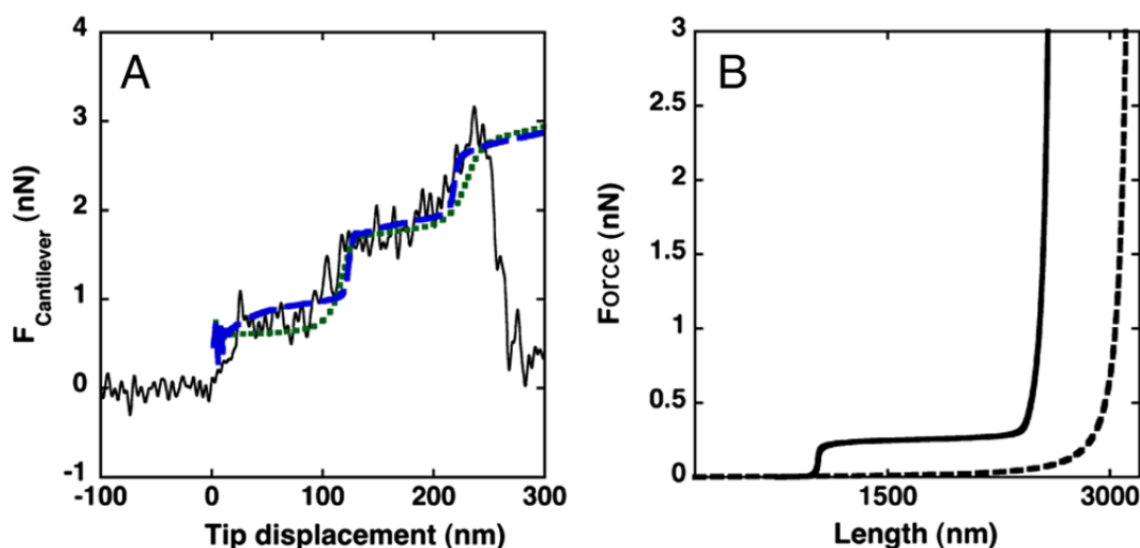
Figure 6.4: (a) Comparison of the DC-WLC fit of Fig. 2(d) (dotted line) with a two-state model fit (broken line) for the same experimental curve. (b) equilibrium stretching curves for the two models: two-state (solid line) and DC-WLC (dotted line).

In Fig. 6.4(a) we show again the experimental data and corresponding fit from Fig. 6.2(d) (green dotted curve), which we compare with a fit from the two-state model [6.4(a), blue dashed curve]. Note that our original fit based on the simpler DC-WLC model is already within the experimental error; additional experiments are necessary to resolve the difference between the two fits. Nevertheless, this example demonstrates the potential of the techniques

presented in this paper: Based on the fit parameters we can calculate the expected equilibrium force-extension relations in the standard AFM geometry (one end of the molecule tethered to the AFM tip); see Fig. 6.4(b). With the continuous two-state model we obtain a plateau force at 230 pN; this value is higher than the plateau forces measured for a single myosin coiled-coil [17], but desmin IFs consist, in cross-section, of around 20 coiled-coils wrapped around each other. Interestingly, assuming a filament diameter of 10 nm, the stress at the plateau is expected to be on the order of 3MPa, which is in excellent agreement with published values for macroscopic bundles of IFs [19].

6.3 Conclusion

In summary, AFM manipulation of protein filaments at solid-liquid interfaces yields information about their mechanical properties relevant for the understanding of cell motion. In this study the AFM is moved perpendicularly to its axis: torsional forces balance frictional and mechanical forces between the AFM tip and the molecule and surface. The mechanical properties of the stretched molecule are still visible in this geometry, and we obverse the sequential unfolding of single repeat units as force plateaus. Differences in the mechanical response for different filaments can be traced back to their characteristics, namely, their contour length, their persistence length, and their friction coefficient. We demonstrate these features within a simple mechanical model, which is sufficient to understand the current experimental data.

6.4 Acknowledgments

6.5 References

1.   Stopak, D., N.K. Wessells, and A.K. Harris, Morphogenetic rearrangement of injected collagen in developing chicken limb buds. Proc Natl Acad Sci U S A, 1985. 82(9): p. 2804-8.

2.   Sabass, B., et al., High resolution traction force microscopy based on experimental and computational advances. Biophys J, 2008. 94(1): p. 207-20.

3.   Kadler, K.E., A. Hill, and E.G. Canty-Laird, Collagen fibrillogenesis: fibronectin, integrins, and minor collagens as organizers and nucleators. Curr Opin Cell Biol, 2008. 20(5): p. 495-501.

4.   Wolf, K., et al., Compensation mechanism in tumor cell migration: mesenchymal-amoeboid transition after blocking of pericellular proteolysis. J Cell Biol, 2003. 160(2): p. 267-77.

5.   Friedrichs, J., et al., Cellular remodelling of individual collagen fibrils visualized by time-lapse AFM. J Mol Biol, 2007. 372(3): p. 594-607.

6.   Kreplak, L., et al., Exploring the mechanical behavior of single intermediate filaments. J Mol Biol, 2005. 354(3): p. 569-77.

7.   Kreplak, L., H. Herrmann, and U. Aebi, Tensile properties of single desmin intermediate filaments. Biophys J, 2008. 94(7): p. 2790-9.

8.   Serr, A. and R.R. Netz, Pulling adsorbed polymers from surfaces with the AFM: stick vs. slip, peeling vs. gliding. Europhysics Letters, 2006. 73(2): p. 292-298.

9.   Bar, H., et al., Impact of disease mutations on the desmin filament assembly process. Journal of Molecular Biology, 2006. 360(5): p. 1031-1042.

10.   Marko, J.F. and E.D. Siggia, Stretching DNA. Macromolecules, 1995. 28(26): p. 8759-8770.

11.   Lanir, Y., Structure-Strength Relations in Mammalian Tendon. Biophysical Journal, 1978. 24(2): p. 541-554.

12.   Bustamante, C., et al., Entropic Elasticity of Lambda-Phage DNA. Science, 1994. 265(5178): p. 1599-1600.

13.   Liu, W., et al., Fibrin fibers have extraordinary extensibility and elasticity. Science, 2006. 313(5787): p. 634.

14.   Briscoe, B.J. and D.C.B. Evans, The Shear Properties of Langmuir-Blodgett Layers. Proceedings of the Royal Society of London Series a-Mathematical Physical and Engineering Sciences, 1982. 380(1779): p. 389-&.

15.   Glosli, J.N. and G.M. Mcclelland, Molecular-Dynamics Study of Sliding Friction of Ordered Organic Monolayers. Physical Review Letters, 1993. 70(13): p. 1960-1963.

16.   Fusco, C. and A. Fasolino, Velocity dependence of atomic-scale friction: A comparative study of the one- and two-dimensional Tomlinson model. Physical Review B, 2005. 71(4): p. -.

17.   Schwaiger, I., et al., The myosin coiled-coil is a truly elastic protein structure. Nature Materials, 2002. 1(4): p. 232-235.

18.   Hanke, F. and H.J. Kreuzer, Conformational transitions in single polymer molecules modeled with a complete energy landscape: continuous two-state model. European Physical Journal E, 2007. 22(2): p. 163-169.

19.   Fudge, D.S., et al., The mechanical properties of hydrated intermediate filaments: Insights from hagfish slime threads. Biophysical Journal, 2003. 85(3): p. 2015-2027.

Chapter 7

Conclusions and perspectives

Micro- and nanomechanical analysis of articular cartilage by indentation-type atomic force microscopy – validation with a gel-microfiber composite

Standard methods used for assessing the properties of cartilage (e.g. histology, biochemistry etc.) provide valuable information about the concentration and zonal distribution of the specific components, but not about mechanical properties. Established mechanical testing techniques offer quantitative measurements of bulk mechanical properties that are not sufficient for the tissue engineering and diagnostic purposes where precise and detailed measurements are needed. Over the last decade, AFM has been established as a powerful tool for imaging, measuring and manipulating soft biological matter at all relevant scales of cell and tissue architecture [63, 64]. In 2004 Martin Stolz and Ueli Aebi [65] have shown that articular cartilage exhibits a scale dependent dynamic stiffness and opened new scientific horizons in understanding molecular origins of cartilage mechanics. In the later work they also reported that mechanical changes during development of OA in human cartilage and animal model were only detectable at the nanometer scale, but not at the micrometer- to millimeter scales [2, 3, 4]. However, in all previous studies there was no clear indication provided about the origin of bimodal stiffness distribution. Therefore, the main focus of our study was to find the direct correlation between specific components of articular cartilage and resulting peaks in stiffness distribution at the nanometer and micrometer scale. We discriminated contribution of PGs to cartilage stiffness by modulating ionic strength of the PGs structure which resulted in a shift of the "softer" peak while "stiffer" peak remained unchanged. This was the direct proof that the lower stiffness peak is mainly due to the PGs contribution while higher peak is corresponding to the collagen behavior. By reproducing bimodal distribution on the gel-microfiber composite comprised of PEG fibres embedded in the agarose gel we obtained a further confirmation of our hypothesis. In addition, we were able to correlate extensive crosliniking bonds between collagen fibrils with much higher bulk stiffness of the native cartilage when compared to the gel-microfiber composite where crosslinking was not formed. Similarly we measured much higher stiffness for PGs integrated in native cartilage comparing to stiffness obtained on the extracted PGs by Ortiz et. al [66]. Finally, results obtained in this study, document a high analytical potential of nanoscale assessment (Figure 7.1) of cartilage. Our future efforts will be focused on the detection of the early onset of the OA by measuring mechanical properties of cartilage and parallel correlate them with accumulation of potential biochemical markers (PGs, lubricin fragments and specific neoepitope like VDIPEN).
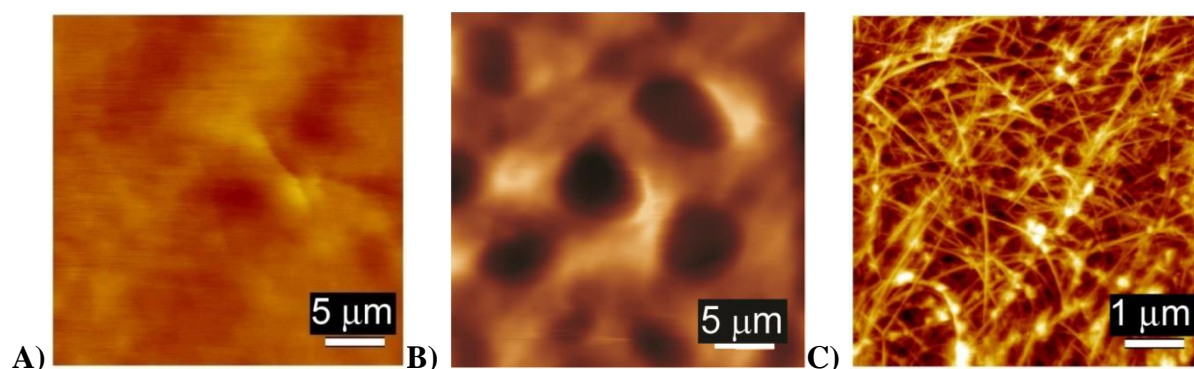
Figure 7.1 AFM image of native cartilage obtained with (A) micrometer sized tip diameter ~ 10µm, (B) sub-micrometer sized tip diameter ~ 0.9 µm, and (C) nanometer sized tip diameter ~ 20nm.

Sliding Motion Improves Surface Properties of Engineered Cartilage: Evaluation by Friction Force and Indentation-Type Atomic Force Microscopy

For treatment of cartilage defects it is of crucial importance to design and generate engineered cartilage with biochemical and biomechanical properties similar to authentic articular cartilage. The structure and mechanical properties of the superficial zone in AC play a critical role in frictionless gliding and weight bearing of the joints. However, surface characteristics are often either not addressed enough or completely ignored. Boundary lubrication has an important role in cartilage tribology and is primarily defined by the lubricin molecule. Use of the bioreactor system that stimulates cells with dynamic compression and sliding surface motion similar to natural joint movement enhanced lubricin synthesis and its accumulation on the surface. However, distinct properties of generated cartilage (too soft and small immature tissue) prevent to probe it with robust, standard friction testing devices. This has motivated us to introduce a friction force AFM method that overcomes these issues and provides accurate measurements of the boundary friction. Results confirmed our hypothesis that samples stimulated both axially and vertically produced the highest amounts of lubricin and exhibited the lowest friction. .Our findings demonstrate that mechanical stimulation similar to joint articulation resulted in superior cartilage surface properties and underlines the importance of a biomechanical stimulus similar to physiological articulation for the (re-)generation and maintenance of a functional AC surface. In addition, we propose the quantitative AFM-based analysis of graft material as a pre-requisite for evaluating the

functionality of engineered articular cartilage surfaces. Our future investigation will aim at studying the role of lubricin in the early onset of the OA.

Articular cartilage repair by genetically modified bone marrow aspirate in sheep

In this work we have systematically explored a novel, gene therapy based treatment for repairing cartilage defects. Such single-step procedure involves use of therapeutic gene transfer to stimulate chondrogenesis of mesenchymal progenitors harvested from the bone marrow. The motivation for using this approach comes from the need to surmount complex and time consuming *ex vivo* tissue engineering protocols. Obtained results show that mesenchymal progenitor's transduced with potent chondorgenic factor (TGF-β1) exhibit properties close to the native cartilage. Moreover, histological and biochemical parameters were correlated with the mechanical measurements both at the nanometer and micrometer scale. For example, higher collagen I content in GFP samples correspond to the highest stiffness value. This difference was clearly detected at the nanometer scale as the unimodal stiffness distribution (see Chapter 2) resulting from very dense collagen network and relatively low PG concentration. Importantly, with mechanical characterization of the native healthy cartilage we obtained detailed mechanical profile which needs to be achieved in order to generate optimally functional cartilage. As the next step it will be of high interest to monitor the stiffness profile of cartilage grafts where multiple genes will be used simultaneously in modulating chondrogenesis.

Anabolic and catabolic responses of human articular chondrocytes to varying oxygen percentages

Oxygen is widely recognized as a significant factor in chondrocytes metabolism. Aim of this study was to investigate the effect of physiological (hypoxic) oxygen culture condition on chondrocytes in tissue formation and degradation activity. Moreover, we examined the structural organization and mechanics of collagen fibrils synthesized in both hypoxic and normoxic oxygen conditions and made further comparison with the collagen extracted from healthy and OA cartilage. Interestingly, hypoxic conditions applied in the specific phase of chondrocytes differentiation strongly enhanced biosynthetic activity and suppressed degradation processes. In contrast, normoxic oxygen condition, almost identically to OA cartilage, stimulated degradation of the collagen network and formation of tangled collagen fibrils with very low stiffness properties. Striking similarity between tissue engineered

cartilage cultured under normoxic conditions and OA cartilage could provide a good *ex vivo* model for studying pathophysiological processes in OA. We will further use this model together with the state of the art collagen manipulation setup (Chapter 5) to gain more insight into the mechanical behavior of individual collagen fibrils under different anabolic and catabolic conditions.

Stretching, unfolding, and deforming protein filaments adsorbed at solid-liquid interfaces using the tip of an atomic-force microscope

Mechanical properties of collagen molecules at different levels of their assembly could play a role in the overall mechanical properties of cartilage. Moreover, collagen fibrils are forming dense meshwork in the extracellular matrix and thus have a significant impact on the chondrocytes migration. However, mechanical properties of collagen fibrils have only received attention in the last few years due to limitations in available techniques to examine them. In our study we present experimental and theoretical data on the stretching and unfolding of collagen and desmin intermediate filaments adsorbed to artificial surfaces. AFM manipulation on a surface immersed in liquid is relatively new and has previously defied quantitative analysis. By showing that the results of AFM experiments can be explained in terms of simple theoretical arguments, we make these experiments quantitative. Furthermore, our experimental results, combined with our theoretical model, demonstrate for the first time the forced stick-slip stretching of a single desmin filament and collagen fibril. Moreover, lateral manipulation allowed us to test filaments and fibrils trough the entire scale of deformation up to the breaking point which is a real advantage over other similar techniques. Another advantage is that by using AFM for we were able to test microfibrils of small diameter (~50nm) in near physiological buffer condition while most of the studies so far were preformed on air-dried fibrils. Due to above mentioned advantages our setup will be further used for studying mechanical properties of collagen fibrils extracted from cartilage at different stages of OA progression and from tissue engineered constructs and models for OA (Chapter 4).

Conclusions

The work presented in this thesis provides new insights into the mechanical behavior of the cartilaginous tissue and its main components at the nanometer scale. In particularly, we identified the key contributors to bimodal distribution. Lower stiffness peak was associated with PGs and higher with collagen contribution. Defined assessment of the PGs mechanics opened further possibilities to investigate their behavior in the native, diseased and engineered cartilage. Moreover, we identified lubricin as a critical molecule for tribological properties of cartilage. To achieve this we had to extend the operation range of the AFM, by developing the friction force mode for boundary lubrication assessment of tissue engineered cartilage. Then small collagen microfibrils (diameter ~50nm) caught our intention since they were present basically in all types of engineered cartilage but also in OA cartilage. Hence we wanted to measure their contribution to the cartilage mechanical properties. However, techniques that were available did not offer an accurate and reproducible characterization of collagen fibrils. Most of them were not even optimized for work in liquid environment which is prerequisite for measuring biological materials. All those issues motivated us to overcome obstacles and to develop lateral manipulation by AFM. With the new setup we are able for the first time to measure collagen molecules in near physiological conditions and test the full range of collagen deformation up to the breaking point.

Perspectives

Today, our AFM setup is optimally tuned for accurate assessment of compression, tension and friction properties of cartilage and similar soft tissues. New scientific data presented in this thesis underscore the importance of nanomechanics for cartilage function and are currently explored for early diagnostic of OA and quality control of tissue engineered cartilage. Now we focus on assessing the friction interactions between solid and soft matrix components, collagen and PGs respectively. Energy dissipated during this process is still not measured. Although based on theoretical approximation it accounts for substantial contribution in cartilage function and could provide significant contribution towards the better understanding of cartilage mechanics at the molecular level. Next the exploration of collagen nanomechanics at different stage of fibrillogenesis and assembly (e.g rope like, parallel, tangle) will have significant impact not only for cartilage tissue engineering but also

for synthetic material application. Last but not least, we want to focus on implementing hardware and software advancements for the development of easy to use and reliable tissue diagnostic tool. By combining state-of-the-art AFM techniques with cutting edge modelling and simulation in applied "Patient-specific MultiScale Modeling and Simulation of OSTEOarthritis" proposal (EU project – FP7), we want to provide a holistic understanding of the causes of OA across the different biological scales. This is expected to bring important answers and solutions towards the treatment and prevention of OA in the future.

References

1. Stolz, M., et al., Ex vivo measurement of the elasticity of extracellular matrix constituents by atomic force microscopy (AFM). Molecular Biology of the Cell, 1999. 10: p. 145a-145a.

2. Stolz, M., et al., Early detection of aging cartilage and osteoarthritis in mice and patient samples using atomic force microscopy. Nature Nanotechnology, 2009. 4(3): p. 186-192.

3. Stolz, M., et al., Dynamic elastic modulus of porcine articular cartilage determined at two different levels of tissue organization by indentation-type atomic force microscopy. Biophysical Journal, 2004. 86(5): p. 3269-3283.

4. Dean, D., et al., Compressive nanomechanics of opposing aggrecan macromolecules. Journal of Biomechanics, 2006. 39(14): p. 2555-2565.

5. Jay, G.D., et al., Prevention of cartilage degeneration and restoration of chondroprotection by lubricin tribosupplementation in the rat following ACL transection. Arthritis Rheum, 2010.

Acknowledgments

I would like to thank to prof. Ueli Aebi and Ivan Martin for recognizing my interminable motivation for scientific work and for giving me the opportunity to do my MD-PhD in their Labs.

I am very grateful to my thesis committee members, Prof. Niklaus F. Friederich who kindly agreed to become Co-Referee and prof. Anne Spang to accept the chairing of my PhD defense.

I would like to thank to Dr. Zora Housley-Markovic and Prof. Roderick Lim for proof read of my PhD thesis.

I am very grateful to Prof. Martin Stolz, Prof. Laurent Kreplak, Dr. Sybille Grad, Dr. Simon Stroebel, Marija Plodinec, Dr. Riccardo Gottardi, Prof. Roberto Raiteri, Dr. Andrea Barbero, Dr. Damir Hudetz, Dr. Andreas Schenk, Prof. Dan Daniels and Dr. Dieter Wirz for scientific support and fruitful collaborations!

Many thanks to my lab buddies; special thanks to Prof. Roderick Lim – Rodjo for his support and great scientific discussions in Sunny`s. Thanks also to the team: Janne Hyötylä, Dr. Larisa Kapinos, Dr. Unai Silvan, Raphael Wagner, Kai Schleicher, Orit Peleg, Rafael Schoch.

I would also like to thank to Dr. Markus Dürrenberger, Marcel Düggelin and Daniel Mathys for their help on the scanning electron microscope

Thanks also goes to all the current and alumni members of the Aebi lab: PD Dr. Cora-Ann Schoenenberger PD Dr. Birthe Fahrenkrog, Dr. Esther Owsianowski, Dr. Yvonne Lussi, Dr. David Walter, Dr. Teba Al Haboubi, Dr. Ulrich Schröder,

Thanks to Röbi Wyss, Ursula Sauder, Vesna Olivieri, Roland Buerki and Margit Jenny (computer support), Liselotte Walti for their technical support.

To my parents and grandparents, thank you so much for your unconditional support, understanding and encouragement throughout my MD-PhD.

CURRICULUM VITAE

MARKO LOPARIC

Department of Structural Biology
Maurice Mueller Institute
Faculty of Natural Sciences
University of Basel
Klingelbergstrasse 50-70, Basel, Switzerland
Phone number: 00 41 61 2672108
Fax: 00 41 61 2672109
e-mail: marko.loparic@unibas.ch

PERSONAL INFORMATION	**FAMILY ADDRESS**
Date of Birth: January 23, 1980	Mittlere strasse 75
Place of Birth: Cakovec, Croatia	4056 Basel, Switzerland
Citizenship: Croatian	Tel: 00 41 61 5341637
Marital status: married, one child	

EDUCATION

1986-1994 Elementary High School, Gorican, Croatia

1994-1998 Gymnasium Cakovec, Cakovec, Croatia

1998-2005 University of Zagreb, Medical School, Zagreb

2006-2007 Research assistant at the Departments of Surgery and of Biomedicine, University Hospital Basel, University of Basel, Switzerland

2007- 2010 MD-PhD student at the Biozentrum, Department of Structural Biology, University of Basel, Basel, Switzerland

FELLOWSHIPS

Awarded scholarship for talented students

HONOURS AND ACHIVEMENTS:

1998 - First place on the National competition for young students in biology with project: Determination and comparison of active substances in intensive cultured and natural chamomile

2003-2004 A student representative in the University Informatics Council

PUBLICATIONS:

Status of women in small academic medical communities: case study of the Zagreb University School of Medicine.

Danić A, Hadzibegović I, Loparić M.

Croat Med J. 2003 Feb;44(1):32-5

Stretching, unfolding, and deforming protein filaments adsorbed at solid-liquid interfaces using the tip of an atomic-force microscope.

Staple DB, Loparic M, Kreuzer HJ, Kreplak L.

Phys Rev Lett. 2009 Mar 27;102(12):128302. Epub 2009 Mar 27

Atomic-Force Microscopy for Biological Imaging and Mechanical Testing across Length Scales, in Live Cell Imaging

Plodinec M., Loparic M., Aebi U.

A Laboratory Manual 2nd ed. , D.L.S. Robert D. Goldman, Editor. 2010, Cold Spring Harbor Laboratory Press.

Anabolic and catabolic responses of human articular chondrocytes to varying oxygen percentages.

Stroebel S, Loparic M, Wendt D, Schenk AD, Candrian C, Lindberg RL, Moldovan F, Barbero A, Martin I.

Arthritis Res Ther. 2010 Mar 2;12(2):R34

Articular cartilage repair by genetically modified bone marrow aspirate in sheep.

Ivkovic A, Pascher A, Hudetz D, Maticic D, Jelic M, Dickinson S, Loparic M, Haspl M, Windhager R, Pecina M.

Gene Ther. 2010 Mar 11.

Micro- and nanomechanical analysis of articular cartilage by indentation-type atomic force microscopy – validation with a gelmicrofiber composite

Loparic M, Wirz D, Daniels AU, Raiteri R, VanLandingham MR, Guex G, Martin I, Aebi U and Stolz M

Biophysical Journal, 2010 June; 98; (Cover of Issue)

Sliding motion modulates stiffness and friction coefficient at the surface of tissue engineered cartilage.

Grad S*, Loparic M*, Peter R, Stolz M, Aebi U, Alini M.

*These authors contributed equally to the work

Osteoarthritis Cartilage. 2012 Apr;20(4):288-95. Epub 2012 Jan 10.

SCIENTIFIC MEETINGS

2006	Biovalley Science Days, Basel, Switzerland – poster presentation
	Biozentrum Symposium, Basel, Switzerland – poster presentation
2007	Current Issues in the Management of Knee Osteoarthritis, Scientific Symposium, Basel
	Biozentrum Symposium, Basel, Switzerland – poster presentation
2008	First European Conference on Nanomedicine, Basel, Switzerland – Poster presentation
	Symposium of Structural Biology and Biophysics, Biozentrum, Basel, Switzerland – poster presentation
	5th Basel International Knee Congress and Instructional Course, Basel, Switzerland – poster presentation
	Has been selected as one of the 100 students in both science and arts from across Europe to take part in the program "Roche Continents: Youth! Arts! Science!", Salzburg, Austria

Biozentrum symposium, Basel, Switzerland – poster presentation

EMPA PhD symposium, St. Gallen, Switzerland – poster presentation

2009   EUCOR meeting, Mulhouse, France - poster presentation

Swiss Nano2009, Basel, Switzerland - poster presentation

2009   Symposium Core Program Structural Biology and Biophysics, Basel,Switzerland - oral presentation

Biozentrum Symposium 2009, Biozentrum, Basel, Switzerland - poster presentation

2010   Orthopedic Research Society 56th Annual Meeting, New Orleans, USA – 2 posters presentations

Invited tutorial speaker on the 3D Anatomical Human Summer School (Marie Curie Research Training Network, EU FP6)**,** Chania, Greece

RESEARCH PROJECTS

Swiss Nanoscience Institute Basel; Module 1 Nanobiology - Endoscopic Nanotools for Diagnosis and Intervention – Functional characterization of tissue engineered cartilage by AFM

TEACHING EXPERIENCE

2007-2009 - Blockkurs: AFM in Biology II (winter and summer semester)

2008,2009 - Exercises: Methods in Structural Biology (winter semester)

LANGUAGES:

Fluent in English, understand German

COMPUTER SKILLS:

Labview, Adobe Illustrator, Microsoft Office, Photoshop, Visual Basic